FINAL REPORT

DOE Award Number**:**	DE-FG02-06ER64250
Recipient:	Altair Nanotechnologies, Inc.
Project Title:	Scientific Evaluation of Nanomaterials of TiO_2 and Related Derivatives in a Variety of Applications
Principal Investigator:	Bruce J. Sabacky, Ph.D. VP and Chief Technical Officer Altair Nanotechnologies, Inc. 204 Edison Way Reno, NV 89502
Teaming Members:	Rutgers University Western Michigan University University of California – Santa Barbara
Reporting Date:	September 30, 2008

FINAL REPORT

This final report for DOE Award # DE-FG02-06ER64250 is divided into four stand-alone sections – one section for each of the project objectives. Each section summarizes project activities and compares actual accomplishments with project goals for each objective.

Altair Nanotechnolgies, Inc. (Altair) has performed and hereby reports on research and development of novel nanomaterials for applications in 1) advanced power storage devices, 2) sensors for chemical, biological and radiological agents and on an 3) investigation into mechanisms of living cell-nanoparticle interactions that will allow predictions of health and safety issues and potentially result in novel agents for remediation of chemical and biological hazards.

The project was organized around four distinct objectives. Two of the objectives are focused on developments designed to dramatically improve the performance of rechargeable Li-Ion batteries. These efforts are based on extensions of Altair's proprietary TiO_2 nanoparticles and nanoparticle aggregates in the form of lithium titanate spinel, lithium manganates and lithium cobaltates.

A third objective leverages the core Altair nanomaterials technology to develop a unique (nanosensor) platform for the error-free, "lab on a chip" detection of chemical, biological and radiological agents for hazardous materials remediation and threat detection. The innovative approach taken by the Altair/Western Michigan team develops individual nanosensor elements built upon a construct that includes a target-specific receptor molecule coupled through a signal transducing nanomolecule to a gold, TiO_2 or SiO_2 nanoparticle coated with a high density of strongfluorescing molecules for signal amplification

The final objective focuses on interaction mechanisms between cells and nanoparticles with the goal of understanding how specific chemical and physical properties of these nanoparticles influence that interaction. The effort will examine a range of microbes that have environmental or societal importance.

Statement of Project Objectives

Objective 1. Design, synthesis and testing of Li-ion hosts for cathode service in inherently safe, long calendar life, long cycle life, high power, fast charge, secondary Li-ion batteries (Subcontract to Rutgers University).

Objective 2. Design Synthesis and Characterization of Nanosensors For Chemical Biological, and Radiological Agents (Subcontract to Western Michigan University).

Objective 3. Development, Testing and Demonstration of a High-Rate Low-Temperature Lithium-Ion Battery Platform.

Objective 4. Interactions of Engineered Nanoparticles with Environmentally- and Societally-Important Bacteria (Subcontract to The University of California - Santa Barbara).

FINAL REPORT – Objective # 1

Project Title**:** Design, synthesis and testing of Li-ion hosts for cathode service in inherently safe, long calendar life, long cycle life, high power, fast charge, secondary Li-ion batteries

Project PI(s): Timothy M. Spitler and Matthew Stewart

Teaming Member: Rutgers Energy Storage Research Group

Executive Summary:

In the Objective I program, Research was carried out that produce Li-ion cells with a nanostructured $Li_4Ti_5O_{12}$ containing negative electrode and cathodes which contained various Lithium Metal/mixed-metal oxide actives. We searched for the right cathodic active that maximizes the life of nLTO based energy storage devices and found that a patented formula by 3M ($LiNi_{1/3}Co_{1/3}Mn_{1/3}O_2$) provided the best possibilities. We searched for the right grain size or Surface Area of the 4V active that would provide matching cell rate performance when paired with 30 to 45m^2/g LTO and found that 10m^2/g NCM was adequate. We generated a series of electrolytes, tested those electrolytes and found that a 40% Acetonitrile + 60vol% 3-methoxypropionitrile solvent system that contained 1M-LiTFSI + 0.5M-$LiBF_4$ as dissolved salts was an excellent power cell electrolyte between 45degC and -40degC. If the CAN is removed and the solvent is pure 3-MPN an electrolyte that works well between 60degC and -40degC can be generated with a closed cup flash point of 79degC promoting improved safety. Further, the test cell was redesigned in an attempt to produce a testing matrix which did not limit the cell life or at least vastly extends the cell life so that active material life effects produced by this research were not masked by Li-ion cell life issues that had nothing to do with the active materials. This work was not completed in that cells with very high surface 4V actives (~10m^2/g) that allowed cycling for 6 months at 60degC were not generated. We believe we are close but the cell budget and time allowed for the research were not sufficient. Nice improvements were made from our starting point which was a cell that ballooned at 60degC and did not cycle well at -40degC

Comparison of Goals/ Objectives Met with Planned:

The established goals of Objective One as stated in our proposal follow. *"The work plan for Objective 1 was organized into 4 time-phased tasks, each of which contained a set or sets of experiments in a minimum and essential design. Often the Task sets are a "competition" that produces a winner, which is gated to the next set of experiments. A fast paced, industrial style research approach will be used in this work."*

a. ***Task I.*** **(July 1 to December 31, 2006; Altair and Rutgers*).*** *Produce and test an improved Cell Design that allows reliable use of thin composite electrode tapes (for power and fast charge) and easy/sure scale-up to very large format electrodes (necessary for 50 to 200 kWh battery backs); develop swell resistant polymers for high temperature (60^oC) cycle-life and calendar life; and develop suitable electrolytes for improved -40^oC to +60^oC operability. Multiple electrolyte systems, perforated Al-foil*

current collectors (e.g., of various thicknesses), and more swell resistant binder formulations (e.g. mixtures of PVDF and HFP, which are commercially available in industrial scale quantities) will be tested in an appropriate partial-factorial design of experiments (see the Addendum for more experimental detail). Specific performance change(s) will be referenced to a baseline cell generated in our NSF-SBIR Phase II program (see specifications for Cell #1 in Table I in the Addendum).

Though the overall objective of this program is to find a Cathode Active, a Li-Ion host, that will extend cell life of nLTO anode Li-ion cells, which are currently cathode active life limited, and improve the charge/discharge rate performance of nLTO anode Li-ion cells (leading to an anode rate limited design), which again are rate limited by the cathode active, our initial research in this Project is focused on generating a Li-ion cell, of the Bellcore type, which is not in itself limiting on cell rate and cell life. Material substitutions and improvements in the cell structure were limited to commercially available materials.

During the first 6 months of this program, a commercially available high molecular weight Homo-polymer of PVDF was found and substituted into the cell. This substitution was essential to allow high temperature testing without softening or dissolving of the polymer by the electrolyte within the cell. The initial polymer product used was Kynar 301F. Its molecular weight is >500. This polymer of polyvinyliden fluoride is barely soluble in Acetone and Propylene Carbonate (PC). The Acetone/PC mixture was in use in the original “Bellcore” recipe and was adequate for work with co-polymers of PVDF and HFP. Even higher molecular weight polymers are available commercially. These Ultra high molecular weight polymers (MW>1,000,000) like Kynar HSV 900 were even more challenging that 301F to work with due to difficult dissolution properties though less polymer content and/or higher bond strengths are achievable. Kynar 301F was purchased for $9/pound in a 100 pound barrel but is likely available in quantity buys at ~$5/lb. A method for producing a solution of 301F in Acetone plus Propylene Carbonate was developed by Aurelien Du Pasquier of the Rutgers ESRG and involved heating to 70degC after mixing the 301F in a solution Acetone and PC in a lab blender for 15 minutes. The PC to polymer ratio is typically 2.5/1 with acetone used as a diluent for viscosity control. The carbon black and the active is then added and mixed and again heated in flask with air gun till 70degC is reached. The slurry is then transferred to a homogenizer and dispersed until clean above 5 micron as determined on a Hegman gage. Since switching to the homopolymer class of Kynar products we had a consistent problem with delamination of the cells when tested at 60 to 65degC. Triethylphosphate (TEP) was found to be an excellent plasticizer for both 301F and HSV 900. TEP replaced the PC (propylene carbonate) originally used in that function in our tape casting slurry recipe. The ultrahigh MW polymer by Kynar (trade name HSV 900) was the best polymer for the ruggedized cell.

During the first 6-months in this program, the microporous separator was replaced with a tougher commercial material. This substitution solved the soft short problem and allowed production of cells with good charge retention, as required for calendar life studies. Charge loss of a few percent per month is ideal for the planned calendar life studies. The product is Tonen 16MMS which is made by ExxonMobil Chemical company in a wholly owned subsidiary, Tonen Chemical, located in Osaka, Japan. We purchased this material for $5/m^2 in 2-short rolls. It is likely available in large quantity contracts for ~$2/m^2. In all, 3-Tonen products, 2-Celgard products, and an experimental product by Porous Power were examined in cell. We had consistent problems getting

the required bonding of the polymer based electrode tapes to the 16MMS separator after our our switch to the Kynar 301F or HSV 900 polymer. This problem was likely solved by the use of TEP (as plasticizer) and some reformulation of the tape casting recipe. The final "trick" was to clamp the cell stack during drying at 80degC. Drying is done after leaching the plasticizer out of the composite electrodes with ether then acetone. Apparently cell shrinkage was initiating delamination during the drying process.

New electrolytes were formulated and tested. The original electrolyte was 2M-$LiBF_4$ in Acetonitrile (ACN), as is used commercially in "Super Capacitors". That electrolyte is known to be the most conductive of commercial systems. This electrolyte cased ballooning of the cells at 60degC due to the high vapor pressure of the electrolyte. We generated mixed nitrile, mixed "Lithium salt" formula's which have boiling points much higher that 80degC, which allows high temperature cycling, and have freezing points lower than old electrolyte which froze at -40degC. This best of these electrolyte is likely novel and has the formula 1-molar LiTFSI (Lithium trifluoro sulfonimide by 3M) and 0.5-molar $LiBF_4$ dissolved in 43-methoxypropionitrile. The close cup flash point of this new electrolyte was 79degC. We paid ~$1300/liter for this electrolyte or ~$1000/kg to Ferro Corporation, a USA corporation, who triple distilled the solvents and produced an electrolyte with <50ppm water content. Quantity pricing is not known. Our search work included 5-different solvent formulations (based on ACN and 3-MPN) each of which contained a couple of different "salts".

We obtained 2-Aluminum, perforated current collector feedstocks, to replace the expanded grid type originally in use. The expanded diamond grid was made by Dexmet, a USA Corporation. The Japanese sourced perforated foil was not available from a USA manufacturer. A sample of perforated-foil was provided to Rutgers by a Japanese company who would not sell to Altairnano. Via Predmaterials the perforated foil sample supplied is 30u thick, 30% hole and the holes are 0.5 mm in diameter. No USA manufacturers could be found that commercially produced 20u to 40u thick, perforated Al foil. While this difficult procurement task dragged on in this Project, we decided to make some bicells with the central electrode current collector being solid Aluminum foil as a preview of the connection advantage realizable from used of a flat surface to laminate to instead of the vertical surfaces in expanded al foil We did pick up some lower initial 10kHz impedance (about 2.5ohm-cm^2 instead of the usual 7.5 ohm-cm^2), by replacement of the expanded grid type current collector in the unimproved cell recipe, but the ohmic increases of the worked cell still occurred. Further testing, analysis, consultation lead us to conclude that the foil precoat was also a problem. In Li-ion cells the current collectors are coated about 1 mil (wet coat basis) thick with a carbonatious, conductive coating (black-paint). Cells eventually were produced with the Predmaterials perforated foil (imported from Japan) and provided adequate performance for this work in the improved cell recipe (5-ohm*cm^2 at 10-kHz instead of 10-ohm*cm^2)

Though not on our original list of materials of construction to improve in the test cell design, the current collector precoat formulation was added because of unacceptable and rapid increases in the high frequency impedance, likely based on Aluminum corrosion. The original precoat formulation was Dag-EB012 by Acheson Colloids out of Port Huron, Michigan. This aqueous solvent based, conductive coating is convenient and safe to use, dries at low temperature but, according to Acheson technical, is a first Generation product with life limited due to solvation of the binder by the electrolyte. Once the precoat binder is softened or dissolved, resultant oxidation

of the Aluminum current collectors causes ohmic-impedance growth in Li-ion cells. We purchased, as recommended by Acheson, 2-Dag products (EB815 and EB030) with polyamide-imid binder systems. Both products require 350degC bake on temperatures (for 2-minutes). Both are rated for 202degC where our EB012 had no temperature rating. Using a spray gun, ADP produced 5, 1'x1' pieces of EB-815 coated, perforated, Aluminum foil. This foil was tested in an improved cell. The results indicate we had adequate improvement in Ohmic impedance stability to allow test work to proceed. The Ohmic increase problem (sometimes referred to as electronic cell resistance) was solved at least for the 12 days of Ragonne, and cycle life testing. This is the first time we ever observed cell test results without Ohmic increases in high temperature cycle testing. During calendar life testing we found the EB815 coating failing (increasing ohmic) and we tried to the Dag-EB030 formulation to further toughen the current collector pre-coat. A doubling of the initial ohmic resistance occurred without elimination of the ohmic increase problem. A rugged coating for the current collectors, the best way of applying that coating, whether to etch or not to etch the aluminum current collectors before application are questions and problems that were not resolved by this program. These products were made in Japan at a subsidiary of Acheson which is owned by National Starch which is owned by ICI and are available commercially at $26/lb FOB Port Huron, Mi when purchased in 5-gallon containers.

The final change in design of the cell that was tested during the second 6-month period was the inclusion of a clamping device on the 2"x3" bicell. The clamping of the cell may have helped in some cases but did not prevent gassing of the separator and shutdown of the cell, only postponed it. The calmping was not help with the increasing ohmic resistance problem.

We had originally scheduled Objective I, Task I to be completed by December 31, 2006. This task must be completed before Task III and Task IV can begin and task II is finished. We ended up 6-months behind on completion of Task I.

b. ***Task II.*** **(July 1, 2006 to June 30, 2007; Altair).** *"Development and testing of less soluble, longer calendar life Li-ion hosts for cathode service in improved cell designs. We will be using "doped" compounds to promote less soluble ~4V Li-ion hosts suitable for cathode service against nano-structured aggregates of Li4Ti5O12 (nLTO) used in anodes in this work. These less soluble compounds are expected to promote better cycle life and longer calendar life. Since we are using nLTO based anodes we are free to use high excess capacity cathodes to "buy" longer life if required ("current commercial secondary Li-ion batteries" use graphite based anodes which have 0.3V redox potential versus Li0/Li+ and require excess capacity anodes to avoid formation of lithium metal in the anode and resultant catastrophic decomposition of the cell after Li metal plating of graphite). Two different grain sizes (0.25 micron and 0.5 micron) of three doped materials will be evaluated in the form of "Power Spheres", which are 1 micron to 10 micron high-porosity aggregates with uniform, well connected grains. These materials will be used in cathodes that have a capacity equal to that of the anode and twice that of the anode. The cathode active compounds are* $LiCo_{1/3}Ni_{1/3}Mn_{1/3}O_2$, $Li_1Co_{0.05}Mn_{1.90}O_4$, *and* $LiNi_{1/2}Mn_{3/2}O_4$. *The full testing protocol (see Tables II and III in the Addendum) comprises 4 weeks of testing on a given cell."*

The summary table TMS I, below, provides a concise listing of the Li-ion hosts produced by this program. Please not that the number of materials produced and tested was a substantial increase in the scope of these activities compared to what we stated in the application.

Table TMS I: Summary Table of Obj. I, Task II Products. As stated materials vs. as produced.

Compound (approximate Formulas)	Stated grain size goal (micron)	Stated SA-BET goal (m^2/g)	Stated Aggregate PSD goal (micron)	~Adjusted grain size (micron)	~Adjusted SA-BET (m^2/g)	~Adjusted Aggregate PSD (micron)	Feed Stock
$LiCo_{1/3}Ni_{1/3}Mn_{1/3}O_2$	0.25	5.3	1 to 10	0.133	9.8	1-20	L19056 by 3M
$LiCo_{1/3}Ni_{1/3}Mn_{1/3}O_2$	0.50	2.7	1 to 10	0.667	2.0	1-20	L19056 by 3M
$Li_1Co_{0.05}Mn_{1.90}O_4$	0.25	5.7	1 to 10	0.133	10.8	1-20	L410+L032 by Lico
$Li_1Co_{0.05}Mn_{1.90}O_4$	0.50	2.85	1 to 10	0.667	2.2	1-20	L410+L032 by Lico
$Li_1Co_{0.10}Mn_{1.80}O_4$	0.25	5.7	1 to 10	0.133	10.8	1-20	L410+L032 by Lico
$Li_1Co_{0.10}Mn_{1.80}O_4$	0.50	2.85	1 to 10	0.667	2.2	1-20	L410+L032 by Lico
$Li_1Co_{0.025}Mn_{1.95}O_4$	0.25	5.7	1 to 10	0.133	10.8	1-20	L410+L032 by Lico
$Li_1Co_{0.025}Mn_{1.95}O_4$	0.50	2.85	1 to 10	0.667	2.2	1-20	L410+L032 by Lico
$Li_{1.1}Mn_2O_4$	0.25	5.7	1 to 10	0.133	10.8	1-20	CMD+LiOH
$Li_{1.1}Mn_2O_4$	0.50	2.85	1 to 10	0.667	2.2	1-20	EMD+LiOH
$LiNi_{1/2}Mn_{3/2}O_4$	0.25	5.3	1 to 10	0.133	10.0	1-20	EMD+bNiCO3+LiOH
$LiNi_{1/2}Mn_{3/2}O_4$	0.50	2.7	1 to 10	0.667	2.0	1-20	EMD+bNiCO3+LiOH
$LiNi_{1/2}Mn_{3/2}O_4$	0.25	5.3	1 to 10	0.133	10.0	1-20	CMD+blk-NiO+LiOH
$LiNi_{1/2}Mn_{3/2}O_4$	0.50	2.7	1 to 10	0.667	2.0	1-20	CMD+blk-NiO+LiOH
$Li_{1.02}Ni_{0.44}Co_{0.29}Mn_{0.25}O_2$	0.25	5.3	1 to 10	0.10	15.5	1-20	L310 by Lico
$Li_{1.02}Ni_{0.44}Co_{0.29}Mn_{0.25}O_2$	0.50	2.7	1 to 10	0.5	2.5	1-20	L310 by Lico

In general the process used to reform purchase active's involved 3-major processing steps. A kg of the purchase material was slurried in water at 20wt% concentration. The slurry was circulated on a Draise DCP-12 bead mill till 60-80m^2/g SA-BET was reached. The milled slurry was then spray dried. The spray dried agglomerates were then thermally treated to promote grain growth and interconnection to produce the target SA-BET.

The active's made from scratch began with an aq. slurry of metal oxides and LiOH. This mixture was milled to 60-80m^2/g. The mill discharge was spray dried. The spray dryer discharge was then fired in furnace to form the desired compound. The formed active was then milled, spray-dried, and sintered in furnace to the desired SA-BET.

Some of the materials that were produced are imaged below.

Altair ID	Formula	BET surf. Area m^2/g	Theoretic capa. mAh/g
LTS1	$Li_4Ti_5O_{12}$	29.5	160
LCO2	$LiCoO_2$	2.2	140
NCM1	$Li_{1.02}Ni_{0.44}Co_{0.29}Mn_{0.25}O_2$	2.54	140
NCM2	$Li_{1.01}Ni_{0.45}Co_{0.3}Mn_{0.23}O_2$	15.5	140
NCM-3M	$Li_{1.04}Ni_{0.32}Co_{0.31}Mn_{0.33}O_2$	9.55	163
LCMS10-2	$LiCo_{0.1}Mn_{1.9}O_4$	9.62	110
LMS-8	$Li_{1.1}Mn_{1.9}O_4$	8.71	110

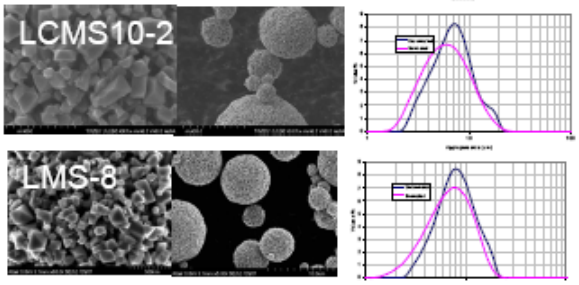

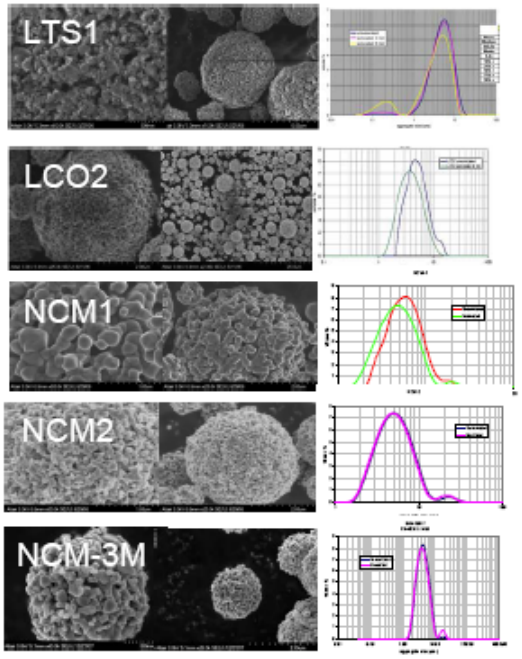

c. ***Task III*. (July 1, 2007 to March 31, 2008; Altair and Rutgers): "***Extended cycle life testing, calendar life testing and extrapolation/prediction of cycle life and calendar life. This work will take place in Year 2, and involves the exposure to various stresses or treatments of battery cells Altair Nanotechnologies, Inc. Confidential 5 built using the best cell "chemistry" derived in Task II and cell design obtained in Task I. In order to predict calendar life and cycle life performance over a full 6 years, cyclical stresses have to be monitored for a testing period of 7 to 9 months. The goals are: predicted 6-year minimum calendar life and predicted cycle life of greater than 6,000 cycles (Table IV in the Addendum has details of the long-term testing protocol)."*

Objective I Reports X, XI, XII and XIII focused on extended cycle life testing as well as calendar life testing.

Report DOE X was titled "Development of Calendar Test Cells: a 3 cell program" and was issued October 2007. This report was 14 pages in length. In this work we tried to finalize the cell design, electrolyte type and active materials to be used in a set to cells promoted to long term cycle life and calendar life testing.
Those cells included all our materials changes and assembly refinements.

Test bicells materials of construction and ingredients:

- Current collectors: Perforated aluminum foil that is 30 micron thick, 30% hole by area, the holes being 0.5 mm in diameter.
- Current collectors shall be etched using KOH, neutralized using DI water and dried using dry acetone before coating. Only freshly etched surfaces shall be spray coated.
- Current Collector Precoat: A bake on product by Acheson Colloids rated for 202degC service, Dag EB815, is applied by spray gun to a wet coat thickness of ~1 micron then dried and bakes per Acheson procedure.
- Separator: The microporous membrane is supplied by Tonen named 16MMS is made of PE and resembles a "felt" like structure. It is 30% porous with 30 micron pores.

- Polymer: A homopolymer of PVDF is used that is made by Kynar under the trademark HSV900. This is a linear chain homopolymer with am Ultra-high MW by Kynar. folk can't measure.
- Plasticizer: Triethylphosphate.
- Solvent: Acetone
- Anode carbon: Super P by Timcal having ~89m^2/g
- Cathode Carbon: An activated carbon by Timcal (E350G) having ~400m^2/g.
- Electrolyte**: 1M-LiTSFI + 0.5M-$LiBF_4$ in 60vol% 3-methoxypropionitrile and 40vol% Acetonitrile as solvent.**
- Actives**: ~45m^2/g LTO and ~10m^2/g $Li_{1.02}Ni_{0.44}Co_{0.29}Mn_{0.25}O_2$**

The testing protocol began with Ragonne testing to 100C rate followed by full DOD cycle testing at 20C rate. One thousand cycles at 25degc and at 60degC on each of the cells followed by -40degC cycle testing.

The Ragonne testing showed that the cells charged faster than they discharged indicating that the 10m^2/g NCM type used required higher SA to balance the charge/discharge rate profiles. We guess the 15m^2/g would be sufficient. The ability to charge these cells at 100C rate to about 60% capacity is rather spectacular.

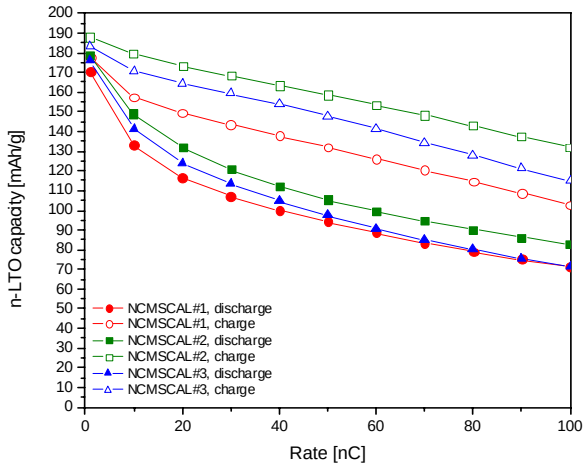

The Ragone data on the left includes test results on 3-bicells. The empty circle, triangle and square markers are of the cell capacity performance as a function of various charge rates from 1 to 100C with a consistent 1C rate discharge. The solid circle, triangle and square markers are of the cell rate capacity performance as a function of various discharge charge rates from 1 to 100C with a consistent 1C rate charge. We found it interesting that with NCM type cathode actives the cell charged faster that it discharge which is not true with LCO and LMO type cathode actives.

Electrochemical Impedance Scan data was produced on the fresh made cells (before charging), after initial charge, after Ragonne testing, after 1000 25degC 20C rate cycles, after 1000 60degC, 20C rate cycles and after the -40degC cycle testing at 1C rate. The cycle voltage range was 1.5 to 2.8 at 25 and -40degC while the voltage range was 1.8 to 2.8 during the 60degC testing. The data showed that the diffusion based impendaces were nicely stable but the electronic or ohmic based impedances or resistances steadily increased. This stead increase is almost certainly due to corrosion problems on the current collector. The active materials and the electrolyte looked good for long term calendar testing but the rate of corrosion of the current collector was too thigh to promote these cells to that test work.

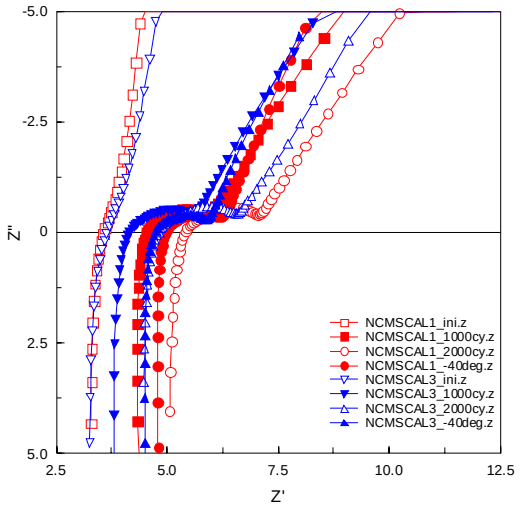

The EIS data of two of the cells is representative of all produced and is presented on the left. As the cycle testing took place at 20C rate it required about 8 days of the 2000 cycles, including the other testing the cells were only about 10days on test. The charge transfer semi-circles are small, well formed and stable as is the intercalation capacitance portion of the Nyquist plot. What steadily increased in this test work was the Ohmic resistances. That value should be very close to fixed during this 10-days of testing. The selected current collector coating or its method of application and curing, or the pretreatment of the current collector foil or some combination are inadequate to fix the ohmic impedance to ~3 Ohm-cm^2 for 10 days of testing, This problem negates our interest in taking these cells to 6 month calendar testing. The final cycle testing at -40degC showed no cell damage by EIS analysis. Nice cells but not good enough.

The cycle life testing showed gassing problems with the cell during 60degC cycling. When 4 bolt steel plates were tightened on the cells to provide 20PSI squeeze and the cells were degassed by syringe a more stable ending was observed in the detail plot on the right. Not good enough for the calendar testing. The gassing issue at 60degC indicates a passivation routine needs be developed that will limit side reactions and that a small voltage range needs be determined that limits gassing at 60degC or rather limits side reactions that generate the H2, CO2, alkanes and alkenes that the gass is made of mostly reduction of water and organics.

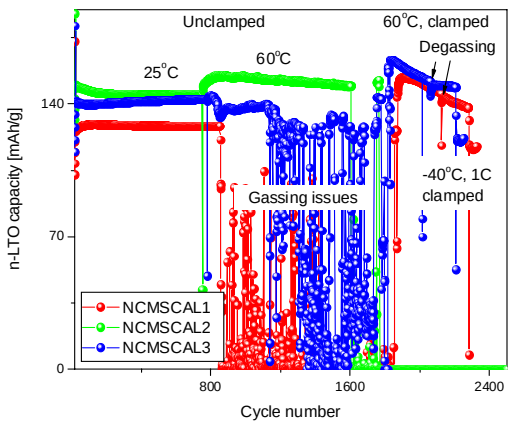

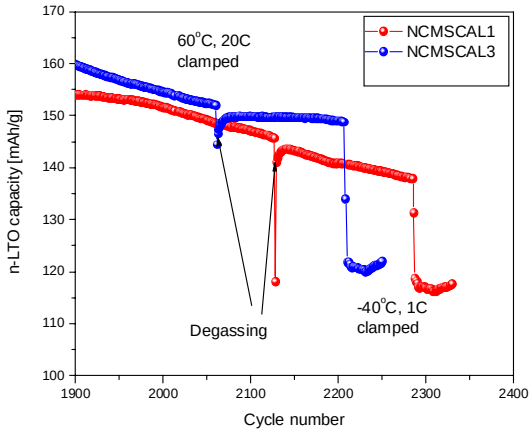

In Report XI we none the less proceeded with the Report X cells but upped the matching ratio and included clamping and degassing, hoping that this might be adequate. Report XI is dated 2/14/2008, titled "Calendar Life Testing of Improved cell using NCM and nLTO: a 3 cell program" and is 18 pages in length including the cover page.

"Report XI Experimental Design; A 3-cell program, using the totally improved cell including clamping after Ragonne testing and degassing. In this work we will produce 3-bicells using the Report X cell type. These bicells use NCM2 and LTS1 as actives. This work is expected to examine the decay of charge retention, 1 & 10C rate cycle capacity, and 0.02 Hz impedance of 3 identical cells as a function of time and exposure temperature. If the data produced is orderly enough then fit to the Arrhenius equation and extrapolation of life to 3 to 5 years will be generated.

TABLE TMS I: Experimental Design

Cell #	Anode Active* (nLTO recipe)	Anode D g-nLTO (g/in^2)	Cathode Active (NCM recipe)	Matching Ratio (g-nNCM/ g-nLTO)	70degC Drying (after ether leach)	120degC (overnight Vacuum dry)	Degas Routine	Clamping During Cycling & Calendar testing	TMR (Cathode cap. Anode cap.)
1	LTS1 ~45m^2/g	0.04	NCM-2 ~10m^2/g	1.8	CLAMP	CLAMP	After Ragonne & After 200 60degC Cycles at 20C rate	Yes	1.6
2	LTS1 ~45m^2/g	0.04	NCM-2 ~10m^2/g	1.8	CLAMP	CLAMP	After Ragonne & After 200 60degC Cycles at 20C rate	Yes	1.6
3	LTS1 ~45m^2/g	0.04	NCM-2 ~10m^2/g	1.8	CLAMP	CLAMP	After Ragonne & After 200 60degC Cycles at 20C rate	Yes	1.6

Please Note:

- The Anode in cells 1-3 is targeted at 0.04-gLTO/in^2. Therefore the cells contain ~0.28 g of LTO. The cells have ~40mAh capacity. The cell capacity is anode limited. At 4.8Ahr/m^2 capacity the cells are Power type cells.
- For calculation of the TMR's we used 160Ahr/Kg as the capacity of LTS1. For NCM-2 we used 140Ahr/kg as the capacity of these Li-ion hosts."
- The NCM-2 has the formula **$Li_{1.02}Ni_{0.44}Co_{0.29}Mn_{0.25}O_2$.**

Though the original program included 6 months of calendar testing by the time we got to this stage ther was only 4 months left in the program. We added some diagnostic work to this report in that we did derivative plots on the first 1C rate charge of fresh cells at 3-temperatures (25, 45, and 60degC) to search for side reaction voltages. This work pointed out the importance of adjusting the EOC and EOD voltage as a function of cell working temperature to avoid gas producing side reactions.

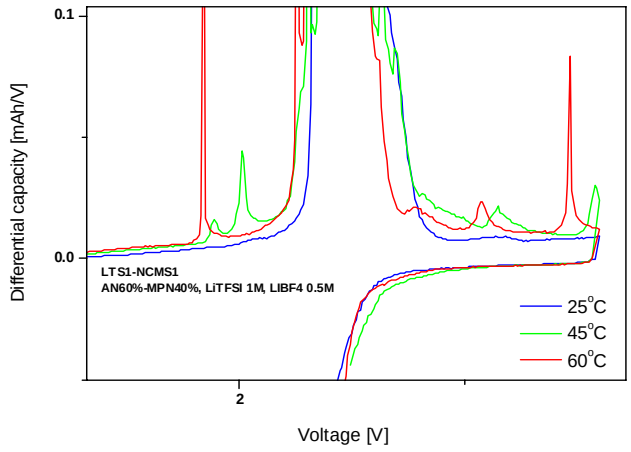

The differential plot at left clearly shows very strong side reaction occurring at ~1.9volts and 2.75volts when the fresh cell is initially cycled at 60degC. Please notice that at 25degC the cycle shows virtually no side reactions between 1.8 and 2.8 volts. Avoidance of these side reactions at high temperature cycling is a doable strategy. Also quenching of these side reactions through the development of

a passivation routine is likely a complementary strategy.

The number of cells was increased during this work from the original design agreement and we ended up producing 13 cells for testing. Three series of cells were built: The NCMSCAL were used for 70% SOC storage calendar testing, the A series was used for 1C-10C cycling, and the B and C series were used for 6C cycling.

Table II. Summary of the cells characteristics

Sample ID	LTO (mg)	LTO g/in^2	NCM g/in^2	Capacity (mAh)	MR	TMR*
NCMSCAL (3 cells)	206	0.033	0.04	24.6	2.63	2.36
Type A (3 cells)	168	0.035	0.034	26.9	2.04	1.78
Type B (3 cells)	168	0.035	0.032	26.9	1.92	1.68
Type C (4 cells)	192	0.04	0.031	30.7	1.63	1.42

*Calculations are based on 160 mAh/g LTO, 140 mAh/g NCMS.
MR = Matching Ratio (active cathode weight/ active anode weight)
TMR = Theoretic Matching Ratio (cathode capacity/ anode capacity)

The longest testing was done at 6C rate. Since only 72 cycles per day are produced at this rate, every 20 cycles represents 10 days of testing. The cycle number versus cell capacity diagram follows.

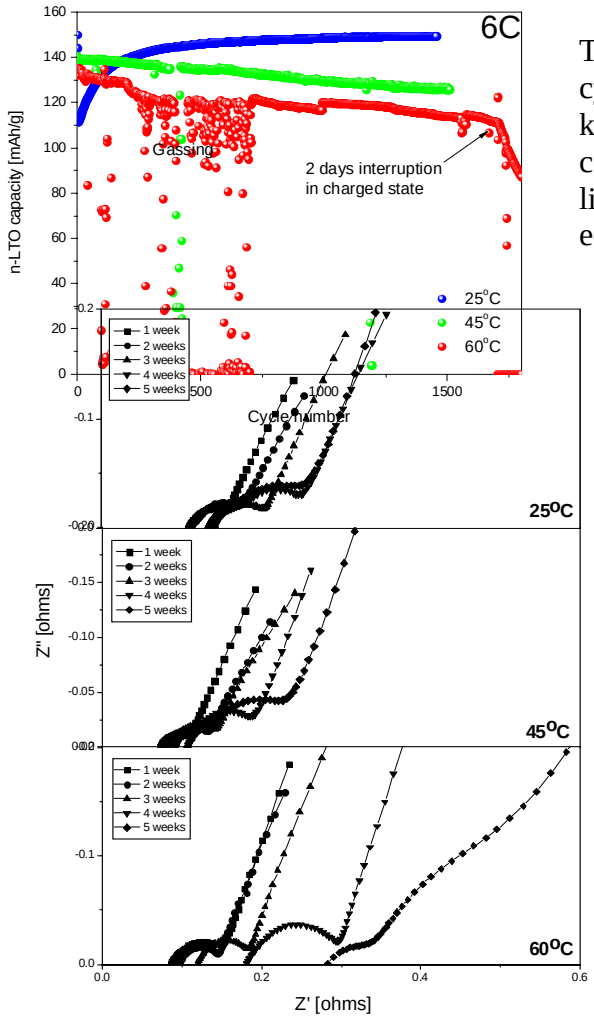

The steadily increasing cell capacity during 6C cycling at 25degC (blue line) may indicate some kind of formation or passivation is occurring in the cell. The capacity decay at 45degC cycling (green line) is orderly and allows the use of the Arrhenius equation. At 60degC the gassing issue is still present but the cell recovered. An accident left the 60degC test cell in full charge state and damaged the cell. Better, but not really good enough!

The Report XI EIS data provides additional information.

The longer cycling at slower rates revealed that the charge transfer semi-circle is not stable in all EIS plot to the left. The semi-

circle forms best at 60degC. As the surface of the NCM is not stable we either have the wrong NCM formulation or are in need of a high temperature passivation routine or both. At 60degC the Ohmic or electronic resistance of the cell triples in 5 weeks. The current collector is not stable. Work needs to be done here to solve this problem. His is label Figure 7 in Report XI and is referred to in the conclusions below.

The conclusion section of Report are included as very valid.

CONCLUSIONS of REPORT XI:

- The cells appear stable up to 45°C, but the electrolyte still generates gassing at 60°C which is responsible for the cells failure mode.
- The electrolyte side reactions are visible on the derivative of the first charging voltage profiles at 45 and 60°C.
- The activation energy for the capacity fade increases up to ~80 kJ/mol, then decreases, both at 1C and 6C cycling.
- Self-discharge was too high for two weeks storage testing.
- The activation energy for the impedance is in the range of 3kJ/mol for the HF impedance, and 32 kJ/mol for the interfacial impedance from two weeks 70% SOC storage data.
- Cells are still cycling at 25 and 45°C at 6C rate, with over 2,000 cycles, and over two months duration.
- The EIS data contained in Figure 7 charts the EIS of "identical" cells over 5 weeks of cycling at low, middle, and high temperature. The 60degC cell showed consistent and accelerating increase of the 10K Hz impedance. The major resistance components to high frequency impedance are the resistance of the electrolyte and the resistance of the current collector composite electrode interface. Our guess, from historic learning generated by this program, is that the failure of protective/conductive coating on the aluminum current collector is the likely source of this problem. We had selected and tested Acheson Colloids Dag EB815 as a tougher precoat for this work based on earlier experimentation. This is the most conductive (15-Ohms/sq.) of the tough, bake on coatings that Atchison offers. Dag EB030 is advertised as the toughest of their foil coatings for the price of 270-Ohms/suare.This less conductive coating is pure polyimide resin (instead of imid/amid mix) has a higher resin/graphite ratio and is touted as, acid, solvent and base resistant. This product should be tried! Additionally, a fluoro-polymer based coating is available this is flexible and inert to solvent, acid and base.
- The EIS data contained in Figure 7 charts the EIS of "identical" cells over 5 weeks of cycling at low, middle, and high temperature. At all three temperatures, the steady growth of the charge transfer semicircle diameter and by the 5th week the change of shape from a semicircle to a misshapen flat on the front side sind of semi circle indicate problems with the interface between the cathodic active and the cell binder and carbon. We suspect that this is indication of electrolyte problems. Could be salts or more likely the solvent mix, the ACN content of the solvent in particular. Cells should be produced that do not contain the ACN fraction of the solvent system but just pure 3-MPN (3-methoxypropionitrile).

The Report XII experimental design agreement was issued March 13, 2008. In this work 6-bicells were prepared. We switched the electrolyte to 1M-LITFSI + 0.5M-$LiBF_4$ in pure 3-MPN solvent. The acetonitrile was eliminated from the electrolyte to lower the vapor pressure and hopefully decrease the reactivity of the solvent portion of the electrolyte (decrease gassing). We dropped the SA of the LTO by switching to a 29.5m^2/g material produced by our production organization. We lowered the SA of the NCM to 2.5m^2/g from 10m^2/g but stayed with the $\mathbf{Li_{1.02}Ni_{0.44}Co_{0.29}Mn_{0.25}O_2}$ formula. The lowered SA of the actives might contribute to less gassing. None of these changes were effective in producing better cells. The work was terminated early.

Report XIII was issued May 25, 2008. The report was titled "*Testing at various temperatures of 5-high SA cathode actives in the ruggedized bicell*." Report XIII is 27 pages long. In this experimental design 5-different actives were tested in improved or ruggedized cell. The cells all used the pure 3-MPN electrolyte. The materials used were:

Table TMS II: listing of active ingredients.

Active (ID)	Compound (~Formulas)	Grain Size (ηm)	SA-BET (m^2/g)	Aggregate PSD for 99% (micron)	Feed Stock	~Capacity (Ah/kg)
ηLTO	$Li_4Ti_5O_{12}$	40	29.5	1-70	$Ti(OH)_4$, TiO_2 and $LiOH*H_2O$	160
NCM1	$Li_{1.02}Ni_{0.44}Co_{0.29}Mn_{0.25}O_2$	525	2.5	1-25	L310 by Lico	140
NCM2	$Li_{1.02}Ni_{0.44}Co_{0.29}Mn_{0.25}O_2$	80	15.5	1-25	L310 by Lico	140
NCM-3M	$Li_{1.04}Ni_{0.32}Co_{0.31}Mn_{0.33}O_2$	130	9.55	1-40	Std. product by 3M	160
LCMS10-2	$LiCo_{0.1}Mn_{1.9}O_4$	135	9.62	1-25	LiOH, $LiCoO_2$, MnO_2	120
LMS8	$Li_{1.1}Mn_{1.9}O_4$	164	8.71	1-25	$LiOH*H_20$, MnO_2	120

Ragonne test results follow:

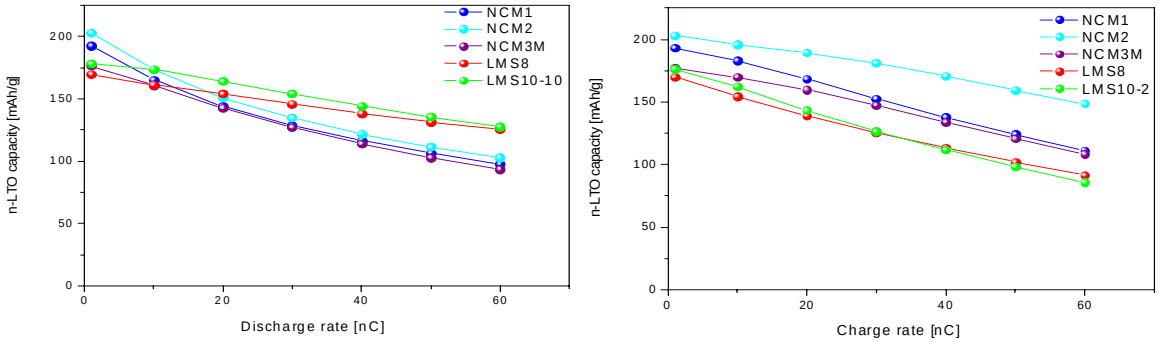

Cycle testing at 25, 45, and 60degC was performed. That is 1000 20C rate cycles at each temperature. One material produced EIS data that was clearly unequaled by the other material. The 3M patented formulation which was by our analysis $Li_{1.04}Ni_{0.32}$ $Co_{0.31}Mn_{0.33}O_2$ and produced the most stable EIS.

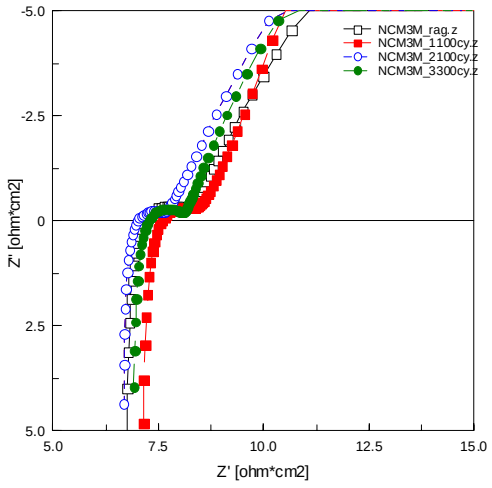

In Nyquist form that EIS data is presented in the image to the left. The ohmic was apparently stabilized by using a thick coating of the EB815 conductive and protective black paint that is on the Al current collectors. The last 1000 cycles which were run at 60degC are displayed in green dots. As the cycling was at 20C rate it took 10 days to get to 2400 cycles.

Additional cells were produced using the 3M-NCM formula reformed by Altairnano to ~10m^2/g and cycled at 60degC using a reduced voltage range as indicated.

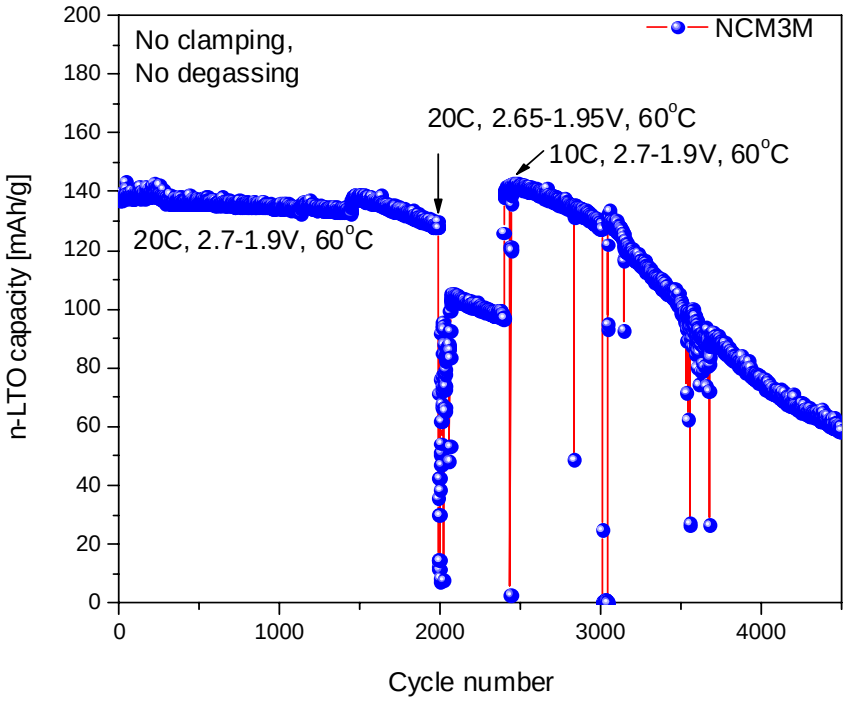

EIS data (below) and analysis in Nyquist format of the cell that produced the above cycling data showed that eventually the ohmic resistances did increase as did the charge transfer semicircle.

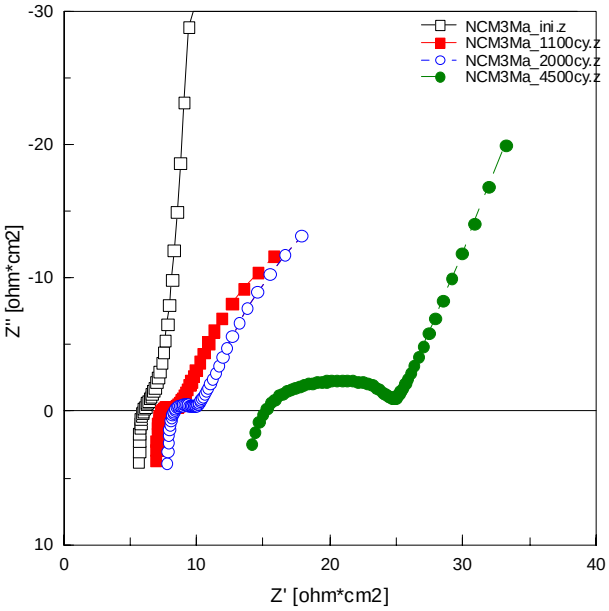

We believe we have finally found a 4V active formulation that allows for use in high SA forms. The conclusions to this work were:

- The EB815 Al coating is suitable for low impedance and elevated temperature operation but not good enough for years of calander life.
- The 3-MPN electrolyte does not cause any important decrease of the cells rate capability, and enables 60°C operation without gassing. It is a good alternative to acetonitrile based systems.
- Of all the cathodes studied, the $LiNi_xCo_yMn_zO_2$ layered compounds were the most stable. Especially the 3M $\mathbf{Li_{1.04}Ni_{0.32}Co_{0.31}Mn_{0.33}O_2}$ cathode gave the best results.
- Very stable cycling at 20C, 60°C for 1,500 cyles was obtained with this cathode by reducing the voltage operating window to 2.7-1.9 V.

- The ruggedized battery design and proper cathode selection have enabled 60°C operation with 10m^2/g BET specific surface area cathodes.
- Better electrolyte selection and **formation routine** may further improve these results.

Report XIII was the last work done on this grant. Out of time and out of cells

c. ***Task IV*. (April 1, 2008 to June 31, 2008; Altair and Rutgers***) Demonstration of Scale-up by producing and testing four 4" by 6" bicells. This represents a 4-fold scale up of the cell technology from the 2" by 3" test cells developed in Year 1 (Tasks I and II) under this grant. Cell testing shall be performed on these cells as the testing protocols used earlier in Task II."*

Task IV was not arrived at. The monies allocated to this activity were converted to additional 2"x3" cells that were used in various experimental work.

Summary of Project Activities:

In essence this program was a search for a 4V Li-ion host formulation that would pair in performance with nanostructured tetra-lithium-titanate. LTO has extreme life capability and in nano form it has been reported to cycle millions of times in hybrid capacitance devices. When nanostructured LTO is substituted for graphite in the negative electrode of a lithium ion cell the rate capability, the temperature limits for operation, the cycle life, and the calendar life of the cell are all limited by either the positive electrode active or that active in combination with the electrolyte in use. Altairnano has material technology that allows reforming of existing 4V actives or scratch production of 4V actives with SA-BET's fully adjustable from 1 to 40m^2/g. This allowed us to search for the right SA-BET or grains size that would match the rate performance of ~30m^2/g nLTO by Altairnano. We also searched for an improved electrolyte that would promote high rate charging and discharging and allow cell operation between -40 and 60degC.

The test bed for the various electrolytes and high SA 4V actives were 2"by3" Bellcore type bicells. This cell had to be ruggedized to allow for 60degC test work. This involved a search for and testing of various high temperature tolerant PVDF type polymers. A new separator that stopped the soft short problem typical of the old PVDF coated Celgard type. A new current collector was needed to replace the expanded grid type that was in use. The new current collector must allow for better bonding and the use of thin tape type composite electrodes necessary for high power (60 to 100c rate charges and discharges). A new plasticizer for the higher molecular weight polymer had to be found because the homopolymer class of PVDF's is more difficult to put into solution. We also needed to improve the currently collector coating, a protective and conductive coating by finding one that allow 60degC test work without dissolving in the electrolyte.

These searches for improved materials of construction of the cell itself as well as a survey of various 4V actives at various Surface Areas or grain sizes was accomplished though 13 experimental sets which yielded 13 internal Reports. A formal experimental agreement was generated and agreed to by Rutgers ESRG PI Dr. Aurelien Du Pasquier and Altairnano PI

Timothy M. Spitler. These experimental set were small cell count designs usually 4 to 6 cells. Various material or cathode actives or construction and assembly techniques would be examined on a head to head basis in a non-mutivarient design. Basically, old school fast paced industrial research.

Once we improved the basic cell design and materials of construction, found the right 4V active and adjusted it's SA to allow very high rate charging and discharging, a matching of the rate performance of the nLTO anode, and found the right electrolyte we intended to do long term cycle life testing and 6 month calendar life studies that would yield sufficient rate of decay data that a good Arrhenius type extrapolation could be made as to the life in years of the power cell.

Ragonne testing of experimental cells at up to 100C rate charges and discharges provided sufficient vision to allow adjustment of the 4V active grain size to allow balanced cell rate performance. That is the anode and cathode charge and discharge rates matched. We demonstrated our ability to produce whatever 4V active we desired to test at any SA required to balance performance. The NCM class of 4V actives were the best materials found. They unlike lithium cobaltate (another layered structure type active) allow good rate performance and cycling performance at -40degC.

As diagnostic tools we relied heavily on Electrochemical Impedance Scans, conducted between 0.01 Hz and 10,000 Hz. at an amplitude of 20mv), Cyclic voltammograms, and differential capacity plots. These tools were adequate to isolate problems and focus our efforts in narrow areas.

Though large improvements in the cell materials or construction were made we never did locate the tough and rugged protective coating system for the current collectors that allowed months worth of cycling at high temperatures. The Acheson product we settled on was EB-815 which did allow 60degC cycling for some weeks without corrosion of the current collector it eventually allow for steadily increasing ohmic or electronic resistance. This problem and the solution was not included in our original scope of activities and was a bit of a surprise to the research team in the degree of difficulty of a solution.

Publications:

The results of this work were presented at the ECS conference held in Phoenix, Arizona in May of 2008.

Internet Sites: None

Networks Fostered:

The collaboration of Rutgers Energy Storage Research Group and Altairnao was fostered and supported. We will continue to work with this outstanding University Research Group.

Technologies:

The process technology used to produce the 14-materials, for testing in cell, was patented by Altairnano previous to this grant. Broad claims included in that patent covered these 14-materials. We had never made these 14 materials by that patented method before. This work provided important processing knowledge and also provided the kind of continued work that is important for future litigation. In producing these materials we had to develop the relationship between work done in milling and the resultant Surface Area of the shards of the cathode actives. We now understand the "cost of communication" and are capable of setting the milling energy input and producing the targeted grain size of any of the materials developed. The production of the final product (a spherical aggregate) requires knowledge of the relationship between thermal treatment temperature, contact time and the resultant SA-BET of the sintered product. This knowledge was developed by this work. We have recipes for these 14 materials.

Inventions:

Data Bases:

Data was produced and is in the form of internal reports and Research Analytical Reports (which contain recipes for production of the materials under study). Additionally a small collection of 2-inch by 3-inch by ¼-inch thick prismatic cells were produced. The bicells are 2.4v with ~30ma charge capacity.

The Objective I, Task II activities were reported in the form a narrative by Matthew Stewart. This Word.doc is available by request. The report is titled "*NARRATIVE OF OBJECTIVE I TASK II PROGRESS*" and is 10 pages in length.

FINAL REPORT – Objective # 2

Project Title**:** Design, Synthesis, and Characterization of Nanosensors for Chemical, Biological, and Radiological Agents

Project PI: Michael Coleman (replaced Robert Marganski)

Teaming Member: Western Michigan University

Executive Summary:

A collaborative research program between Western Michigan University (WMU) and Altair Nanotechnologies, Inc. (Altair) focused on homeland security applications. Sensitive and selective nanosensors for the detection of chemical, biological, and radiological toxins based on the concept of nanoparticlemonomer(or polymer)-nanomolecule-receptor (NMNR or NNNR) were investigated. The primary mode of detection for these sensors is change in fluorescence which is amplified by signal transduction. Arrays of these sensors arelaid on suitable substrates and then integrated into a handheld device driven by a PDA for ease of portability and detection of target toxins. The sensing mechanism(s) extend to include photoacoustic signals in addition to optical signals because the generation of multiple signals when a target toxin is bound to the detector molecule will minimize false positive and false negative signals**.**

Comparison of Goals/ Objectives Met with Planned:

The overall objectives of the research to achieve nanoparticlemonomer(or polymer)-nanomolecule-receptors is divided into three main areas of study:

1. Synthesis of receptor molecules that undergo conformational/electronic changes when exposed to toxic agents,

2. Integration of the receptor molecules into a nanomatrix which translates the receptor molecule's state into a usable signal. Nanomatrix material and methods include self-assembly, nanopolymer design, and use of nanoparticles to anchor nanomatrix materials while at the same time acting as optical devices (photonics) to modify absorption and intensity of signals from the receptor molecule,

3. Construction of a working sensor device built using these receptor molecules and nanomatrix assemblies.

The specific objectives of the research to achieve NNNRs are given below.

1. **Receptor molecules/NNR efficacies:** Synthesis and characterization of receptor molecules for chemical and radiological toxins and assembling them on nanomatrices to form an ordered layer of receptor molecules for sensing and destruction. Investigation of the efficacies of various NNRs to selectively interact with the target chemical and radiological toxins and generate light, electrical, and mechanical signals.

Accomplishment:
Several new potential sensor molecules were synthesized, characterized (IR, Elementary analysis) and tested with nerve gas analog molecules such as Dimethyl methylphosphonate [DMMP] and Diethyl chlorophosphate [DCP] in methanol and acetonitrile medium. Also these complexes were deposited on clean quartz plates and separately exposed to hydrochloric [HCl], ammonia [NH_3], DMMP and DCP vapor to understand the sensitivity and recovery efficiency from emission change with time.

2. **Nanomatrix-nanopolymer-receptor (NNR) composites: Nanopolymer, Nanoparicles and Self-assembly:** Novel synthetic routes to and characterization of robust nanomatrices which will form the foundations for the building of nanomolecular layers of receptors for chemical, biological, and radiological agents. Spontaneous and stimulated self-assembling properties of the nanomatrices to obtain nanomatrix arrays that can detect the target toxins by luminescence (light signal), generation of current (electrical signal), and nanomechanics through deflection of cantilevers (mechanical signal).

Design, synthesis, and characterization of nanoscale polymers that form the interface between the nanomatrices and the receptor molecules for amplification of light, electrical, and mechanical signals. NNR composites generated by attaching various nanopolymers to a nanomatrix, such that nanoparticle receptor molecules can then be attached to the nanomatrix through the nanopolymer linkage. Characterization of NNNR.

Accomplishment:

We attempted to extend our coating technology to encompass patterned depositions of ordered arrays. The mylar sheets that we have been using were exposed to an UV-ozone treatment through a mask. The UV-ozone treatment consists of a two lamp exposure, one at 254 nm and one at 180 nm, the shorter wavelength lamp forming ozone in close proximity to the surface. This treatment has in the past made the substrate hydrophilic enough that particles do deposit quite well. Once so activated the substrates were dipped following our established protocol of 5-15 ml/min in a 15 solution of 40 nm silica particles. SEM micrographs demonstrate that we are not forming the coatings that we have in the past using quartz and silicon but there is some degree of ordering. We have begun to examine the polymer sheets that we have been using and need to change our choice of substrates. These sheets are pulled along the two transverse directions in order to align and strengthen the films. This stretching results in a fairly uneven surface in comparison to the one we have been using on the solid substrates. Additionally for the activation process to be effective the surface must be much more hydrophobic than the current material that we have. We are searching for a replacement material for this coating as this appears to be the best way to move forward on this front.

3. **Sensor devices: Signal amplification and processing:** The NNRs and NNR composites will be self-assembled to obtain sensor devices that signal the detection of chemical, radiological, and

biological toxins by the generation of light, electrical, and mechanical signals that have been appropriately filtered, amplified and processed. Characterization and optimization of the generation and amplification of light, electrical, and mechanical signals by the nanomatrix arrays (photonics).

Accomplishment:
We have been developed the test apparatus necessary to evaluate the arranged samples in a situation similar to that which they will see in service. To that end we have modified our Fluorolog-3 spectrofluorimeter to allow for exposure to these samples to analyte gases. In order to make these in-situ measurements we have placed the solid sample holder inside a quartz chamber fitted with feed-through for flowing gases. An air stream is then fed through a bubbler containing the analyte which we are testing. By adjusting the temperature and concentration of the solution through which we are bubbling we are able to control the gas composition which the sample sees. This addition to our sampling chamber has allowed us to begin to monitor the solid state reaction that is proceeding during the exposure to acid, base, water, and nerve gas analog.

The handheld prototype sensor has been rearranged and reprogrammed using the RabbitCore RCM3100 control module. Using one of the 6 digital input/output ports we have taken control of a stepper motor which we are using to drive the sled containing the sample plate. Potentially this will give us the possibility to move the plate to any x,y position and check the spectrum although currently we are only using a single stepper motor. To speed processing and focus our effort we have been limiting the number of pixels which is transmitted to 10. By examining the spectrum of the NNR which we are analyzing we can pick these 10 pixels such that we have a background signal as well as enough pixels to monitor a change in the shape of the spectrum in response to a chemical signal. As a proof of concept we are using two dyes printed onto a quartz plate. The prototype sensor moves the plate from one position to the other taking spectra continuously. Spectra are then compared to a reference spectra taken prior to exposure. We are currently working on the algorithm which will determine what the device has been exposed to.

Discussion of Accomplishments:

Receptor molecules/NNR efficacies

SETUP USED TO EXPOSE EMMISIVE COMPLEXS TO ANALOG VAPORS.

Over the course of this grant we have proceeded through several iterations on the exposure chamber for analyzing the compounds produced and how they respond to target molecules. Our most recent exposure station now uses a gas manifold to supply the test molecules to the exposure chamber. This setup enables the use of multiple analytes and allows for dilution of the analytes before and during an exposure. The charged air stream is passed through a quartz sample chamber where the samples are placed. Introduction of the quartz chamber has dropped the intensities roughly 20%, however there remains an adequate signal for monitoring the response of the sensor compound to the analyte. The gas leaving the exposure chamber can be split off and tested in a GC-MS to verify the concentration of the analytes in the gas stream.

SENSOR DEVELOPMENT:

A number of potential sensor molecules were synthesized, characterized (IR, Elementary analysis) and tested with nerve gas analog molecules such as Dimethyl methylphosphonate [DMMP] and Diethyl chlorophosphate [DCP] in methanol and acetonitrile medium. Also these complexes were deposited on clean quartz plates and separately exposed to hydrochloric [HCl], ammonia [NH_3], DMMP and DCP vapor to understand the sensitivity and recovery efficiency from emission change with time.

1.Fluoresceinamine complex

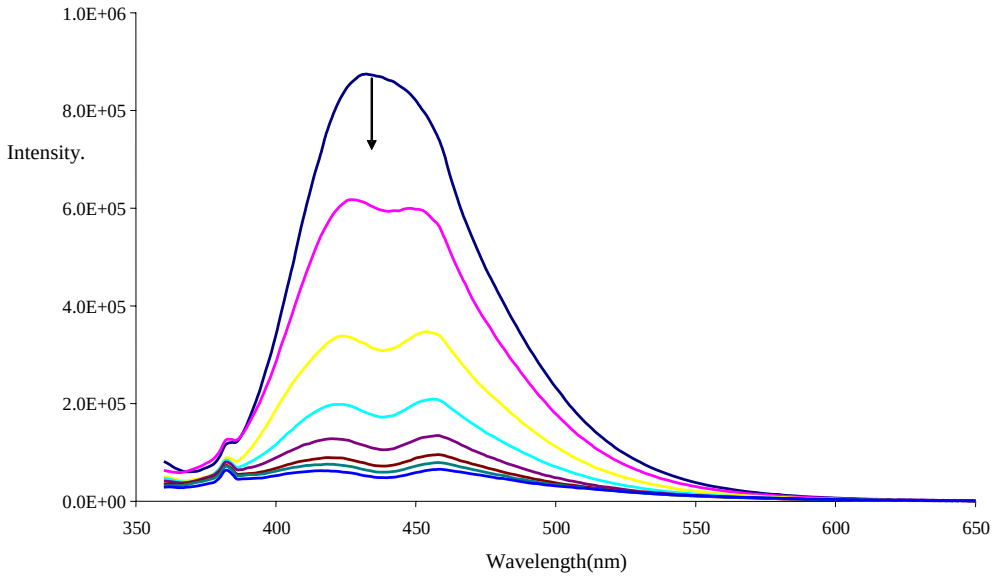

Figure 1: Emission quenching of Fluoresceinamine complex with different concentrations of DCP.[$1*10^{-5}$ to 10^{-3} M DCP] in acetonitrile.

When this molecule is exposed to 1*10-5 M DCP in acetonitrile [Fig 1], the single emission peak at 436nm splits into two peaks(428 & 452nm). In higher concentrations of DCP it continues quenching. This molecule is even more sensitive to HCl. In the presence of very low concentration of HCl it losses it's emission almost completely as seen in figure 2.

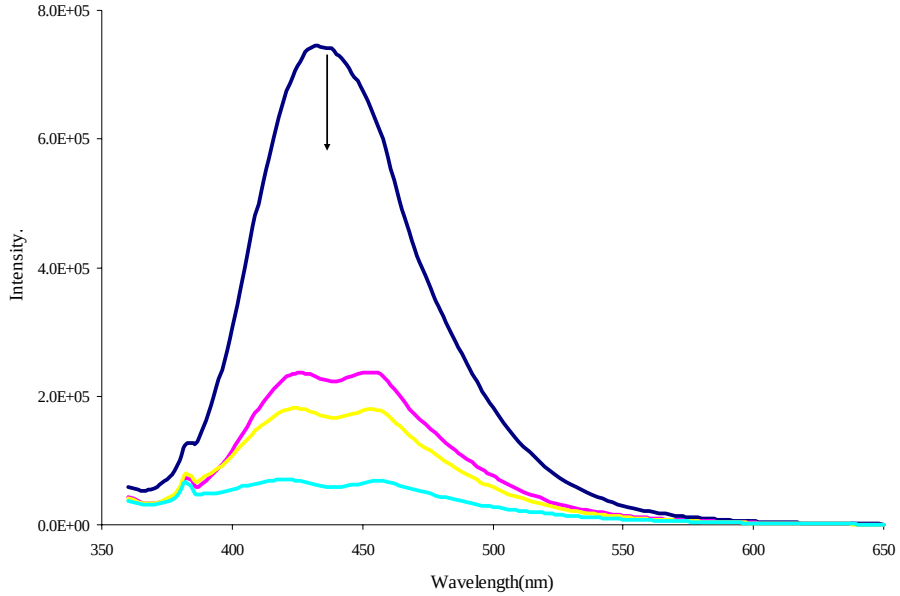

Figure2: Emission quenching of Fluoresceinamine complex with different concentrations of HCl [$1*10^{-5}$ to $1*10^{-4}$] in acetonitrile

2. Europium-thenoyltrifluoroacetone (Eu_TTFA) complex

Principal emission band for this complex corresponding to the $5D^0$ to $7F^2$ transition at 615 nm, figure 3. In the presence of DMMP the emission intensity increases proportional to the DMMP concentration, figure 4. Although this complex is highly emissive, TTFA is weekly bound to europium and in the presence of water vapor it losses it's emission by replacement of TTFA with water. We can increase the stability of this complex by attaching another ligand like 1,10-Othophenanthroline.(OP) Even in the presence of all the four ligands, compound is still not stable to survive in the presence of water, acid or base vapor.

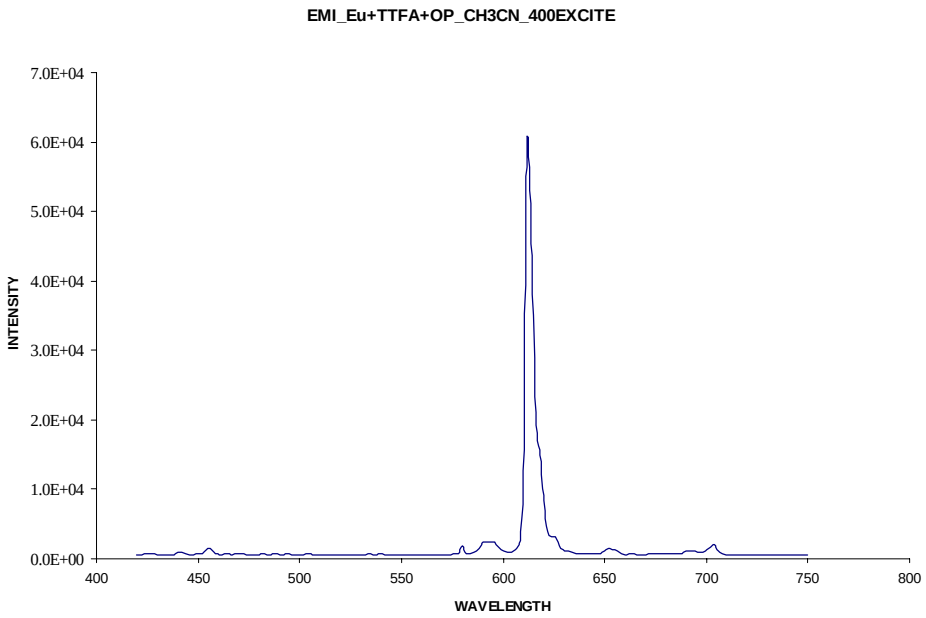

Figure: 3 Emission of Eu_TTFA_OP complex in Acetonitrile

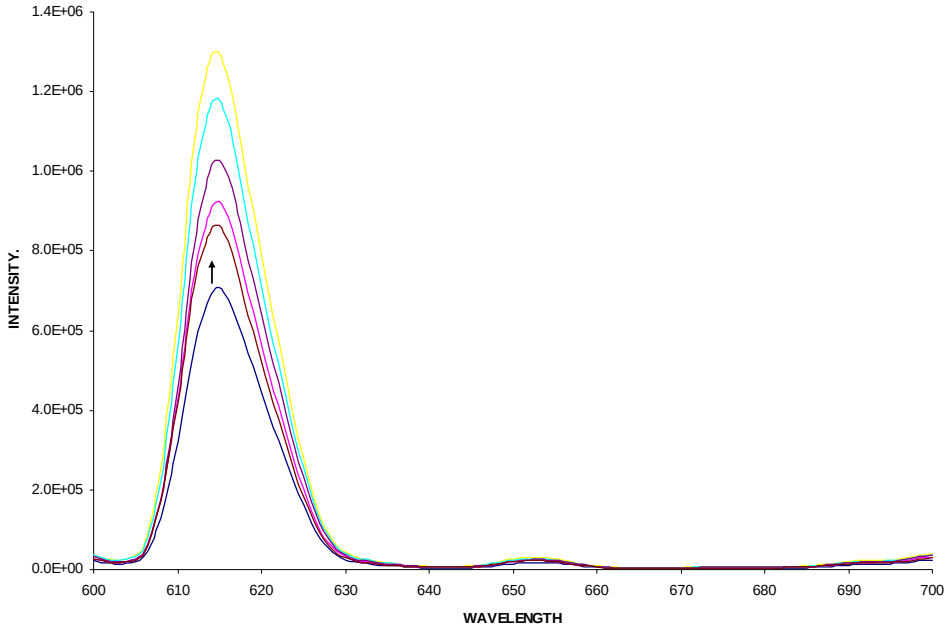

Figure: 4 Emission enhancement of Eu_TTFA complex in ethanol with DMMP($1*10^{-5}$ to $1*10^{-3}$M DMMP).

3. Europium_ 1,10-Phenanthroline complex:

This complex was synthesized, purified and tested with acid, base, DMMP and DCP in both solvent and vapor phase. Because of the very high stability, there was no significant change of the emission with any of above compounds.

4.Euripium 1,10-phenanthroline-5,6-dione complex

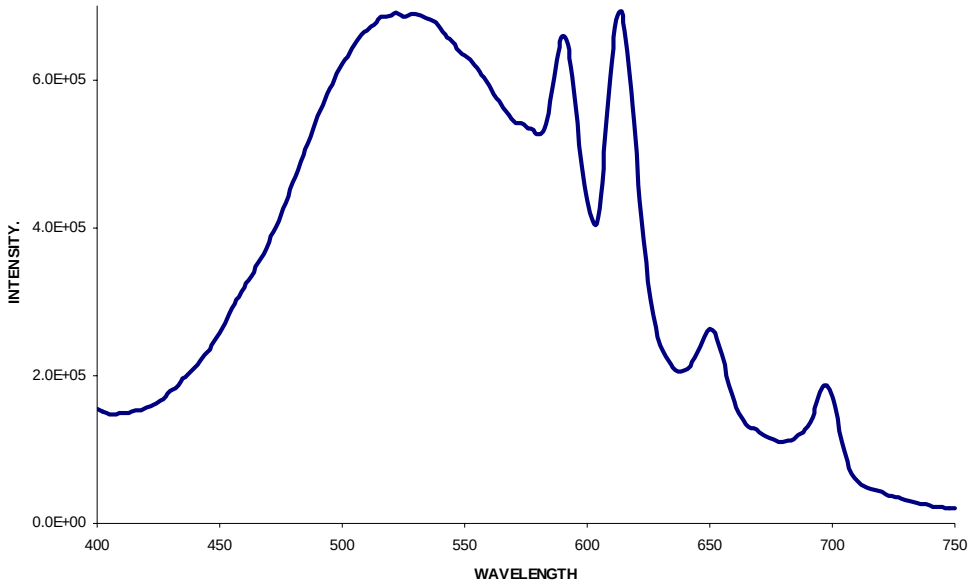

Figure: 5 Emission of Europium_Orthophenanthroline-5,6-dione complex in methanol(325 nm excitation.)

Figure 5 demonstrates the spectra of Eu OP-dione in methanol with the broad peak at 530 nm attributed to the orthophenanthroline-5,6-dione ligand emission and peak at 613 nm is the major $5D^0$ to $7F^2$ energy transfer from ligand to europium metal centre. In the presence of protons (H^+) this complex shows a sudden change in emission and then it has very weak response to hydrochloric acid in methanol medium, figure 6. In the presence of dilute base the major peak for the europium metal centre emission at 613 nm splits into two peaks. Figure 7 demonstrates a quenching as the concentration is further increased. This compound shows a good selectivity for different organophosphates. When exposed to DMMP there is a decrease in the intensity from the ligand but no metal center decrease, however when the compound is exposed to DCP there is a drop in both metal center and ligand emissions, figures 8 and 9.

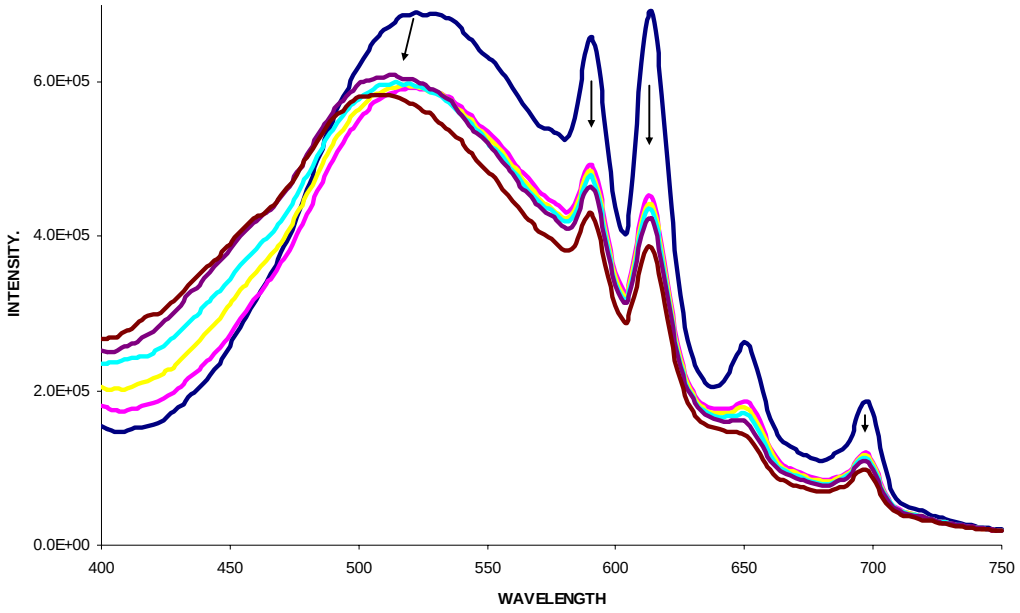

Figure: 6 Emission quenching of Europuim_OP-5,6-dione complex with HCl.[$1*10^{-5}$M to $1*10^{-3}$M].

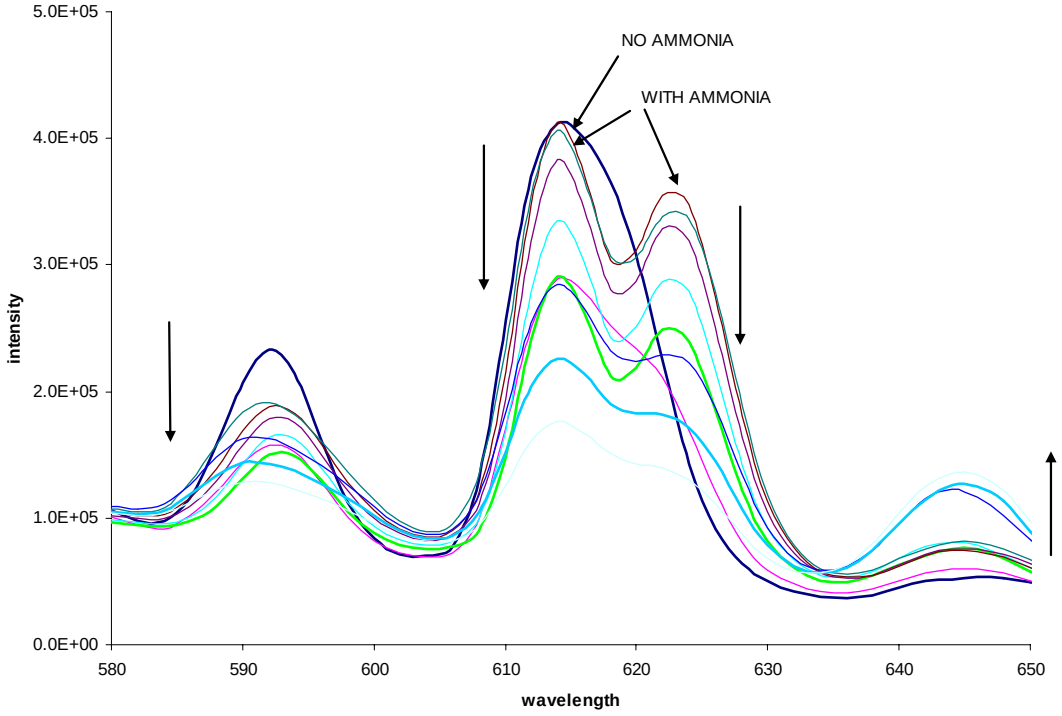

Figure: 7 Emission quenching of Europuim_Orthophenanthroline-5,6-dione complex with Ammonia[$1*10^{-5}$ M to $1*10^{-3}$ M ammonia]

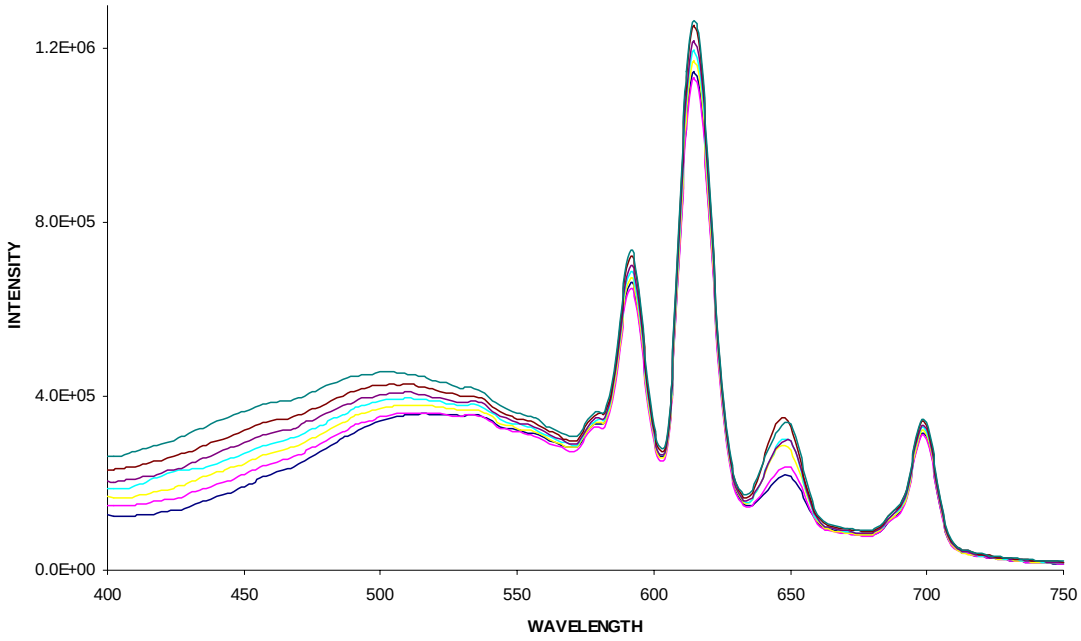

Figure: 8 Emission of Europuim_ Orthophenanthroline-5,6-dione complex with Dimethyl methylphosphonate (DMMP).

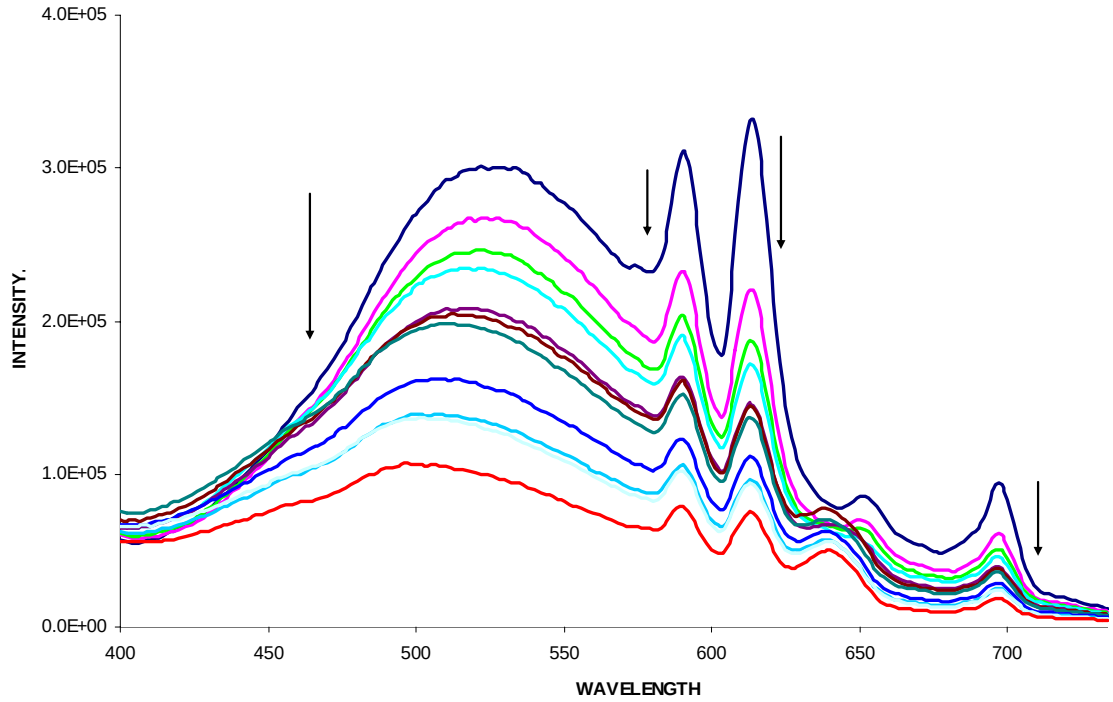

Figure: 9 Emission of Europium_Orthophenanthroline-5,6-dione complex with Diethyl chlorophosphate (DCP).

Solution testing of this complex was followed by solid state testing of the emission with analyte gas flow in air. For the solid state emission testing several drops of the suspended complex were dried on a quartz plate and placed in the fluorescence flow cell, fig 10. After 15 minutes of air flow to ensure the compound was stable, the analyte was added to the flow stream. Spectra were recorded every minute during an exposure. After the response of the compound was noted the analyte was removed from the process stream and the recovery of the compound was observed. Upon exposure to HCl vapor the response is similar to the solution behavior where there is a marked drop in the intensity of the 613 nm peak, fig 11. Figure 12 demonstrates that as the chamber is flushed with dry air the intensity slowly recovers back to the initial intensity. This compound responds to ammonia rapidly also quenching the emission, figure 13. The recovery of the compound is much more rapid than with HCl, returning to full intensity in ~3 minutes, figure 14. In the presence of $1*10^{-5}$ M DMMP there is no change in the emission. When we increased the concentration from 1*10-5 to $1*10^{-3}$ M emission of the complex enhances weakly, figure 15. As with previous experiments, the complex recovers it's emission completely within less than 3 minutes figure 16. The response of the complex to DCCP is very rapid and shows a large increase in the emission, figure 17. Once the dry air is supplied to the chamber the emission returns to the initial state within 20 minutes, showing the selectivity that we have been looking for figure 18.

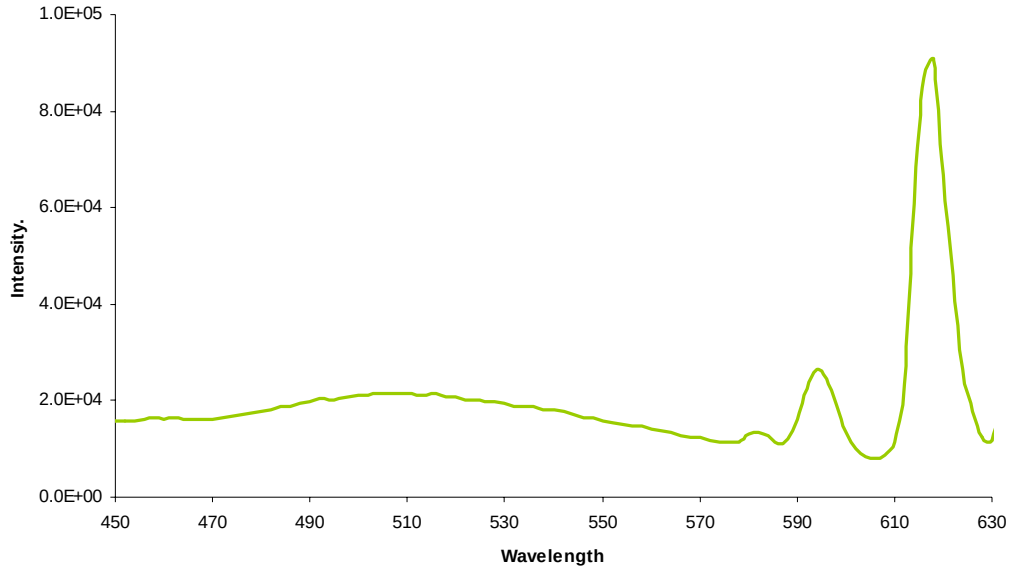

Figure: 10 Emission of Europuim_1,10-Orthophenanthroline-5,6-dione complex on quartz (325 nm excitation.)

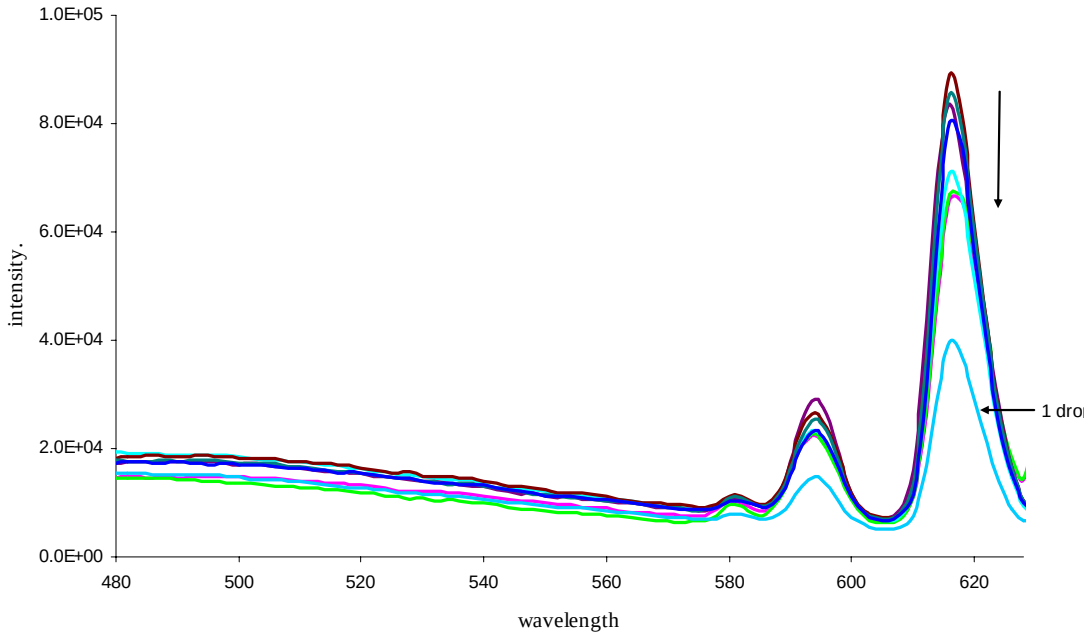

Figure: 11 Emission changes of Europuim_Orthophenanthroline-5,6-dione complex on quartz (325 nm excitation.) with HCl vapor.

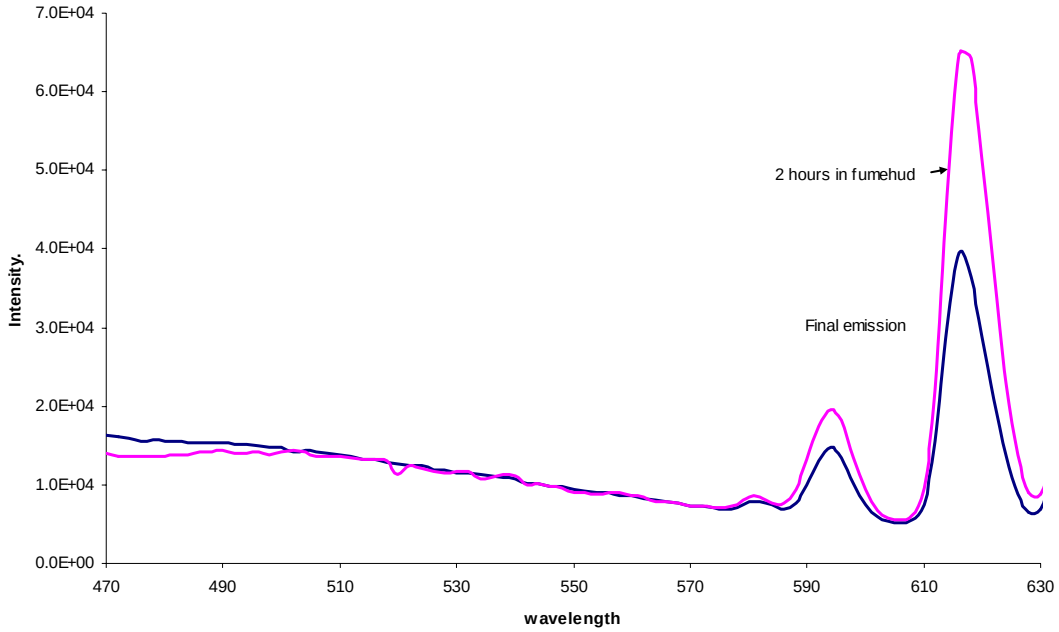

Figure: 12 Emission recovery of Europuim_Orthophenanthroline-5,6-dione complex on quartz(325 nm excitation.) after HCl treatment.

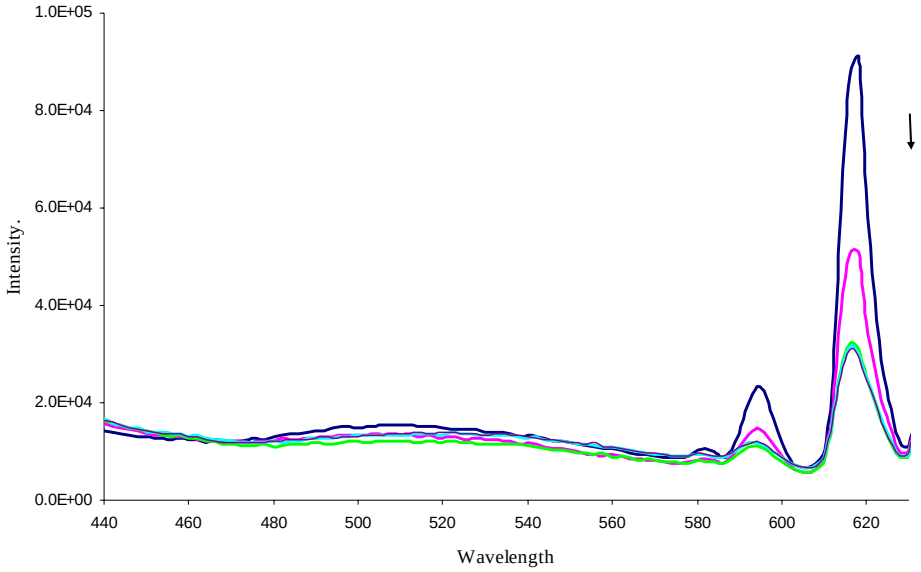

Figure: 13 Emission changes of Europuim_Orthophenanthroline-5,6-dione complex on quartz (325 nm excitation.) with Ammonia vapor.

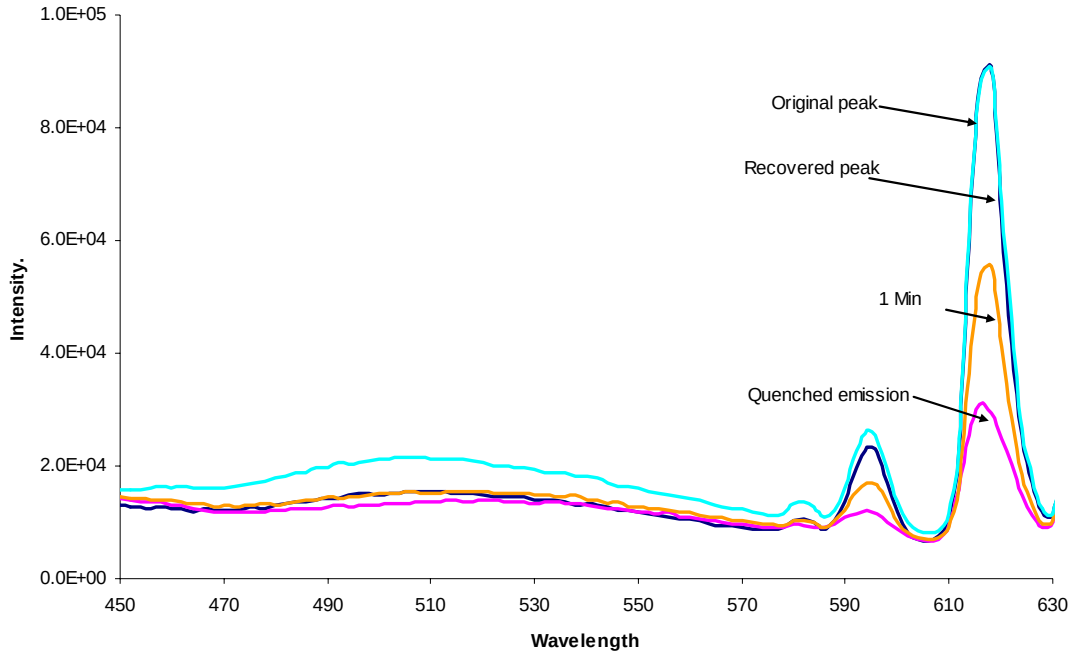

Figure: 14 Emission recovery of Europuim_Orthophenanthroline-5,6-dione complex on quartz (325 nm excitation.) after Ammonia treatment.

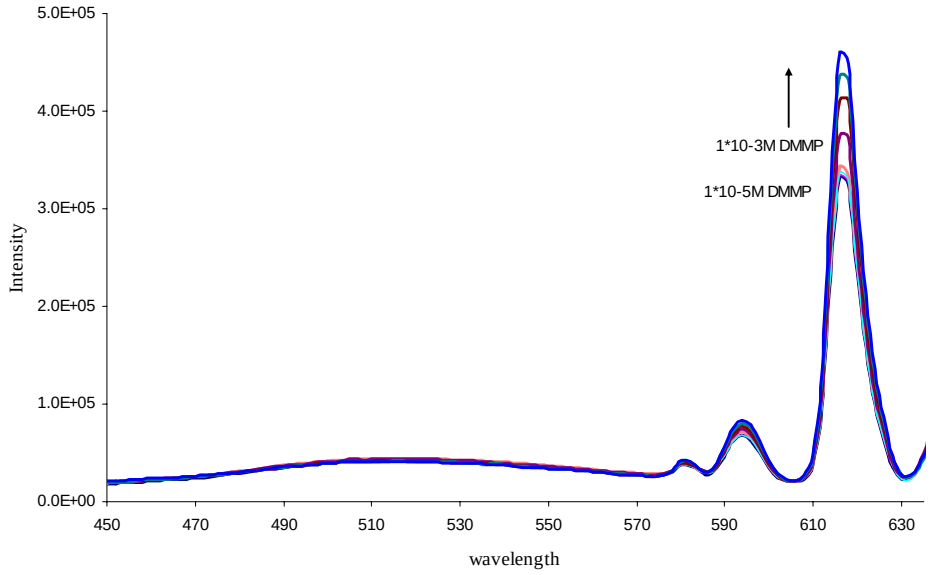

Figure: 15 Emission changes of Europuim_Orthophenanthroline-5,6-dione complex with DMMP vapor.

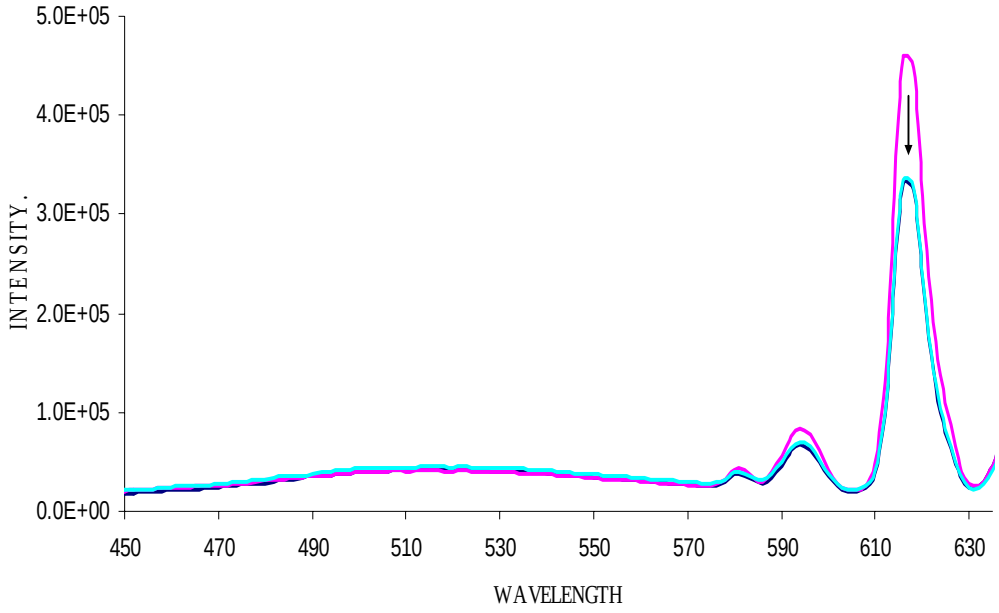

Figure: 16 Emission recovery of Europuim_Orthophenanthroline-5,6-dione 325 nm excitation.) after DMMP treatment.

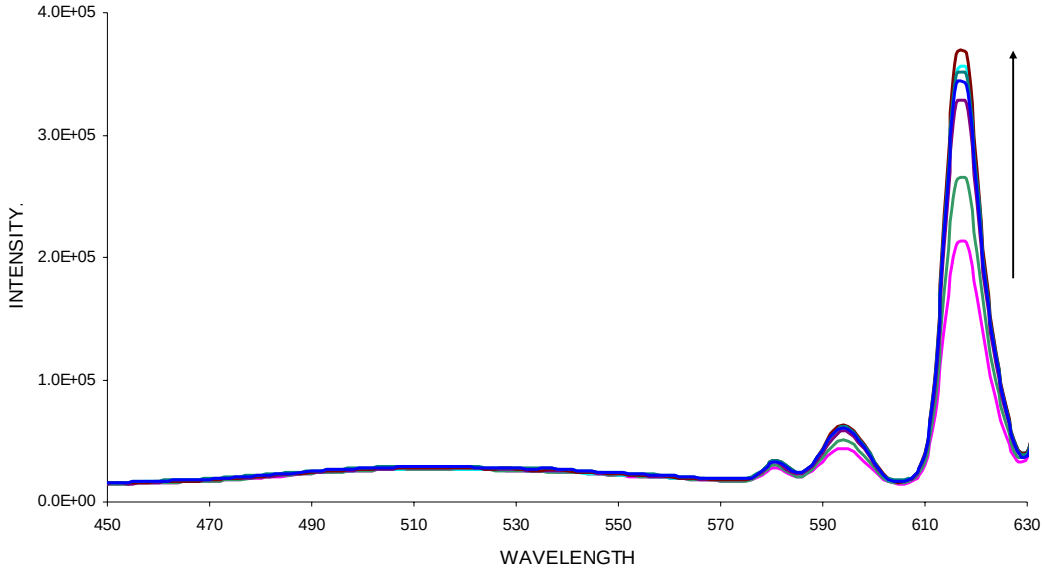

Figure: 17 Emission changes of Europuim_Orthophenanthroline-5,6-dione complex on quartz(325 nm excitation.) with DCP vapor.

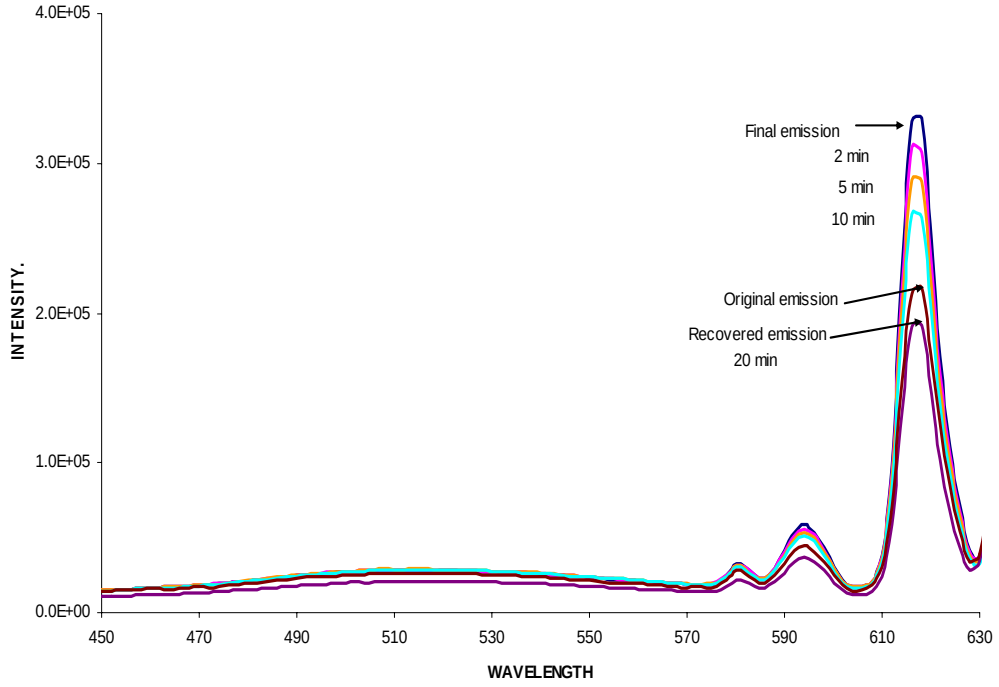

Figure: 18 Emission recovery of Europuim_Orthophenanthroline-5,6-dione complex on quartz(325 nm excitation.) after DCP treatment.

5. Eu $(Otf)_3$ complex

Triflate ligand

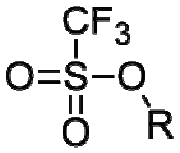

Triflate, more formally known as trifluoromethanesulfonate, is a functional group with the formula CF_3SO_3-. This is an extremely stable polyatomic ion and triflate is an excellent leaving group. This ligand makes a stable complex with lanthanides making it appropriate for use in the environment. Additionally triflate being a good leaving group makes it possible to achieve a significant change in emission at fairly low target molecule concentrations. The interaction of this ligand with acids, bases are reversible and the interaction with nerve gas analogs are partially reversible, allowing the complex to be recharged and reused. For all the experiments we used only one quartz plate with emissive complex and even after full recovery, complex on quartz plate was fluxed with compressed air for 15 minutes prior to the next chemical expose, figure 19.

In the presence of acetonitrile vapor, emission intensity of the complex temporarily decreases and after 10minute with compressed air it fully recovered back to it's original emission figure 20. In the presence of hydrochloric acid vapor, quenching is observed because of temporary replacement of ligands by chloride ions and protonation effect figure 21. It takes 12 minutes to recovered back to the original emission with compressed air. Upon exposure to DCP vapor for 8 minutes, figure 22, there was a rapid quenching of the emission intensity. But recovery from DCP is significantly slow compare to the other vapors and even after 12 hours it recovers only half of it's original emission.

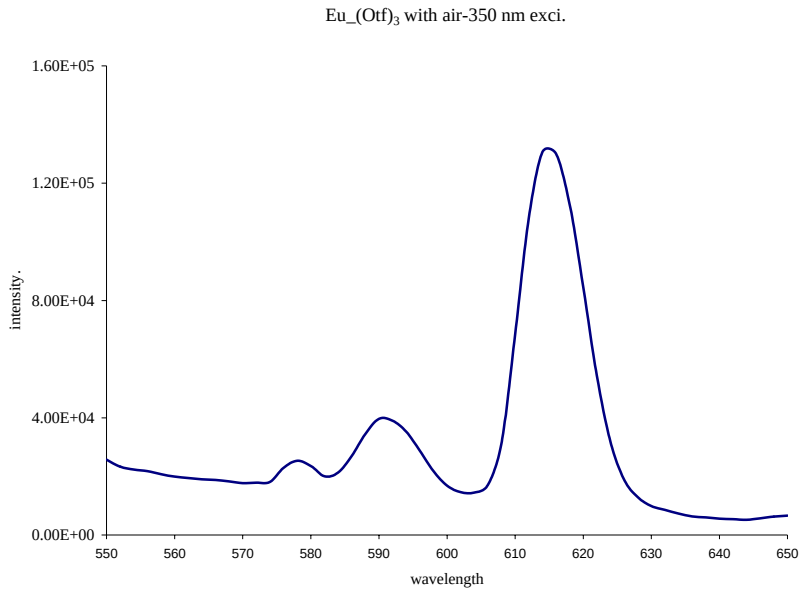

Fig 19: Emission of $Eu(Otf)_3$ complex at 350nm excitation on quartz
Solid phase emission spectra of $Eu(Otf)_3$ complex with compressed air

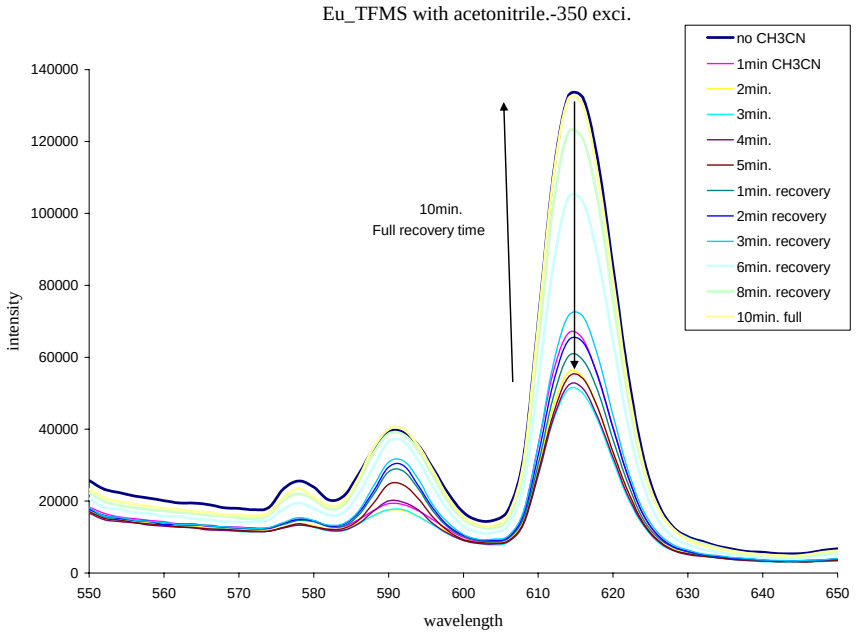

Fig 20: Emission spectra of $Eu(Otf)_3$ complex with acetonitrile (5min.) and recovery of the emission for 10 minutes.

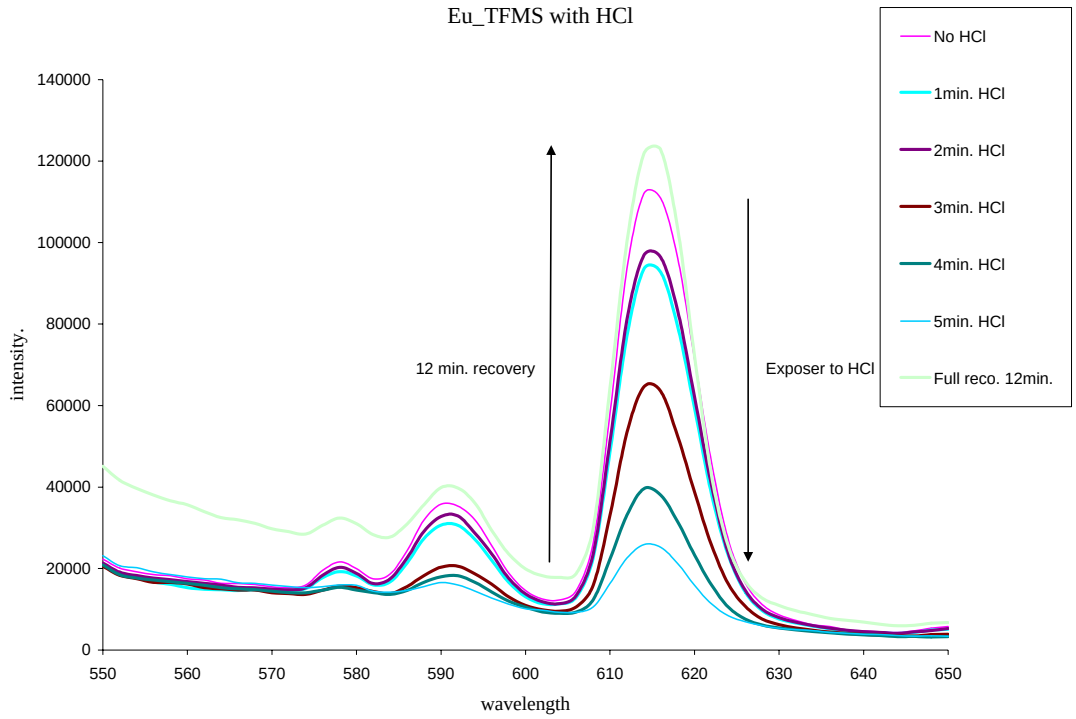

Fig 21: Emission spectra of $Eu(Otf)_3$ complex with Hydrochloric vapor (5min.) and recovery of the emission for 10 minutes.

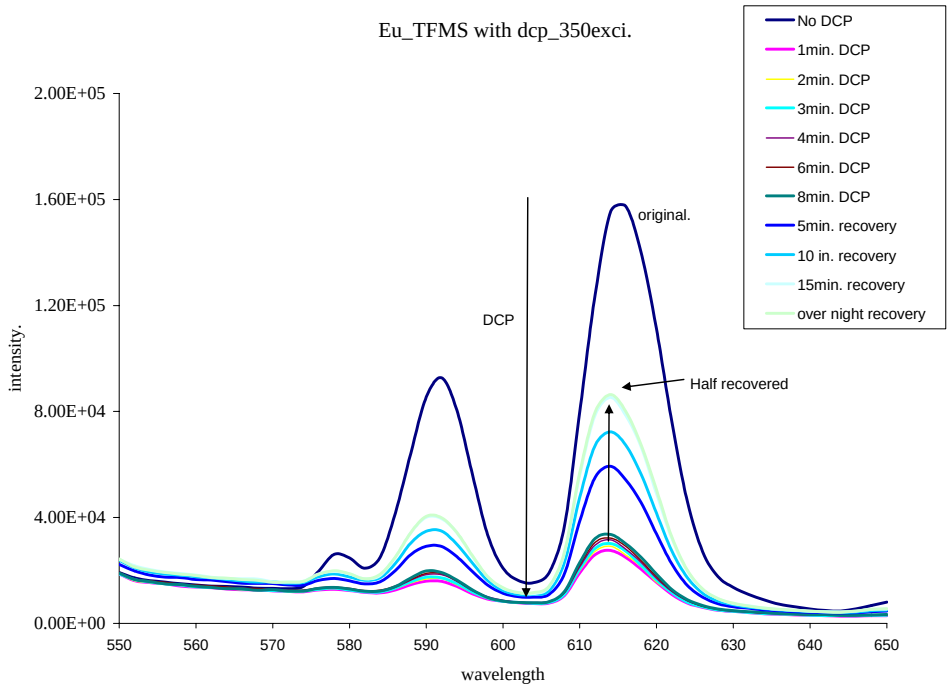

Fig 22: Emission spectra of $Eu(Otf)_3$ complex with DCP vapor (8min.) and recovery of the emission .

6. Polymeric ligand complexes

To minimize the fault positive signals from competitive molecules like acids, bases and other chemicals in the environment we can go with polymeric ligand complexes.

For example:

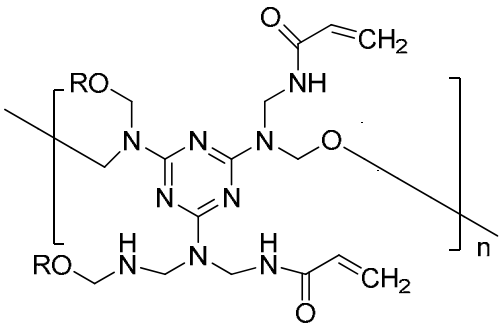

This particular ligand can react with lanthanide metal ions to make stable and fluorescent complex.

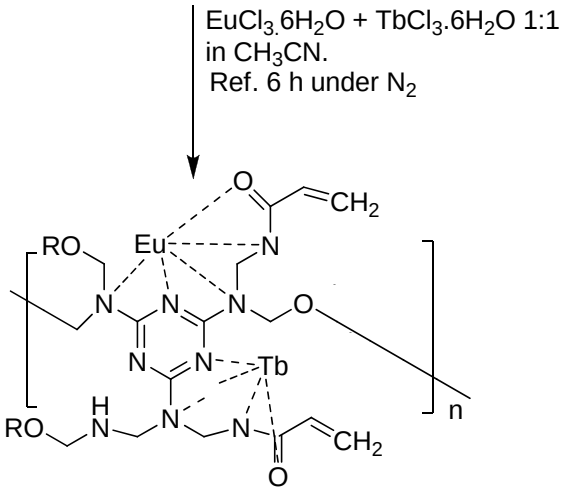

Not only does this ligand react with multiple metal ions, it also can absorb and transfer energy to excited states of both metal ions at the same time resulting in multiple emission bands corresponding to both europium and terbium complexes, figure 23. These emission bands are active in both solvents and solid state, figure 24.

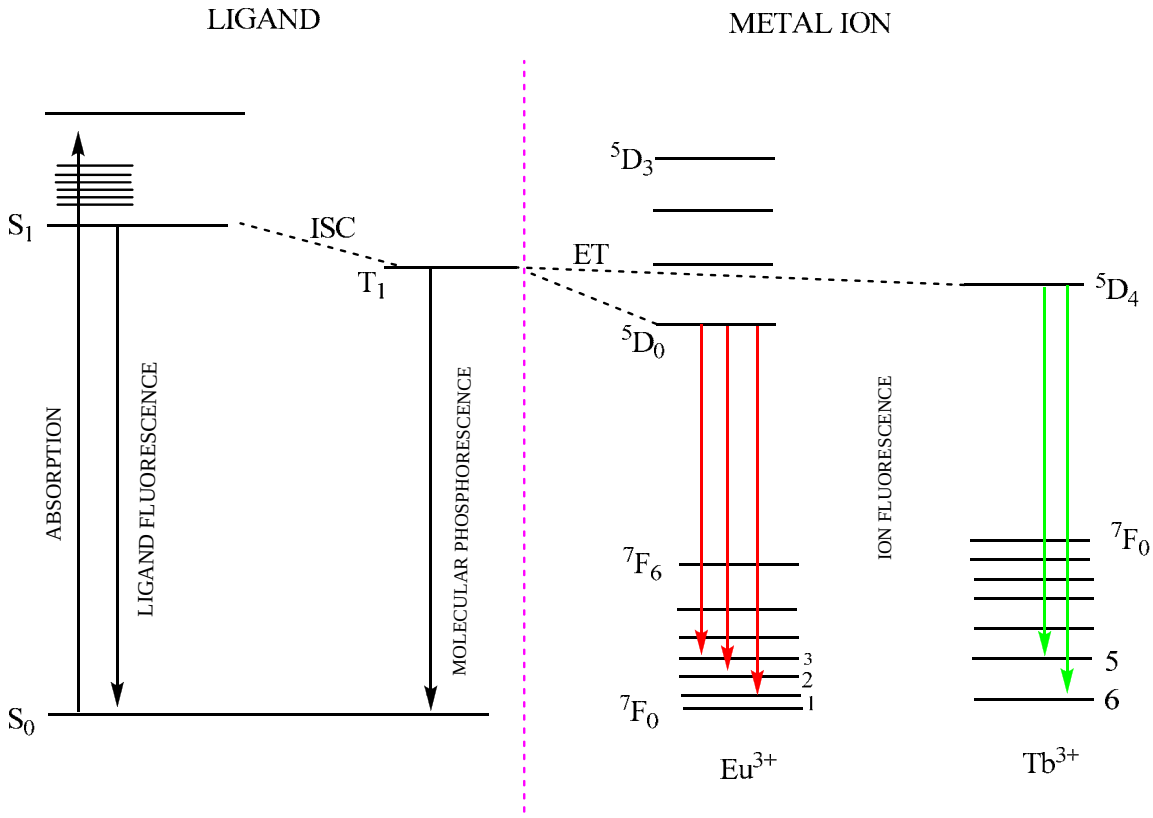

Figure 23. Polymalamine Lignad to metal energy transfer

There are few important reasons to select Eu and Tb over other lanthanides like Sm, Gd and Dy.

- Lanthanide metal ions like Sm, Gd and Dy has significantly lower energy gap between ground and excited states(emits in near IR region). This low gap results more efficient non radiative decay through solvent or ligand vibrations resulting low quantum yield and broad peaks.
- Europium and terbium complexes have high stability constants and lower dissociation constants.
- Broad range of ligands(very simple to complex) have shown to greatly enhance the europium and terbium emission upon complexsation due to favorable energy transfer from the exited ligands triplet state to the emissive levels of the metal ion.

When the complex on quartz is exposed to dry and compressed air, emission enhances due to drying of coordinated water from metal center reducing energy transfer to emission quenchers like water, see figure 25. Figure 26 demonstrates chloride ions(Cl^-), from hydrochloric acid, displacing water and shows emission quenching mainly through vibronic electron transfer. This quenching is not permanent and emission can be regenerated with compressed air. This Eu:Tb polymelamine complex doesn't respond to base, as can be seen in figure 27. There is no emission enhancement or quenching. This complex responds to diethylchlorophosphate nerve gas stimulants by enhancing it's emission for Terbium metal center and quenching it's emission for

Europium metal center, figure 28. This is a very important feature as it distinguishes the response of acids from nerve gases which is always a source of interference s and gives same change similar to nerve gases.

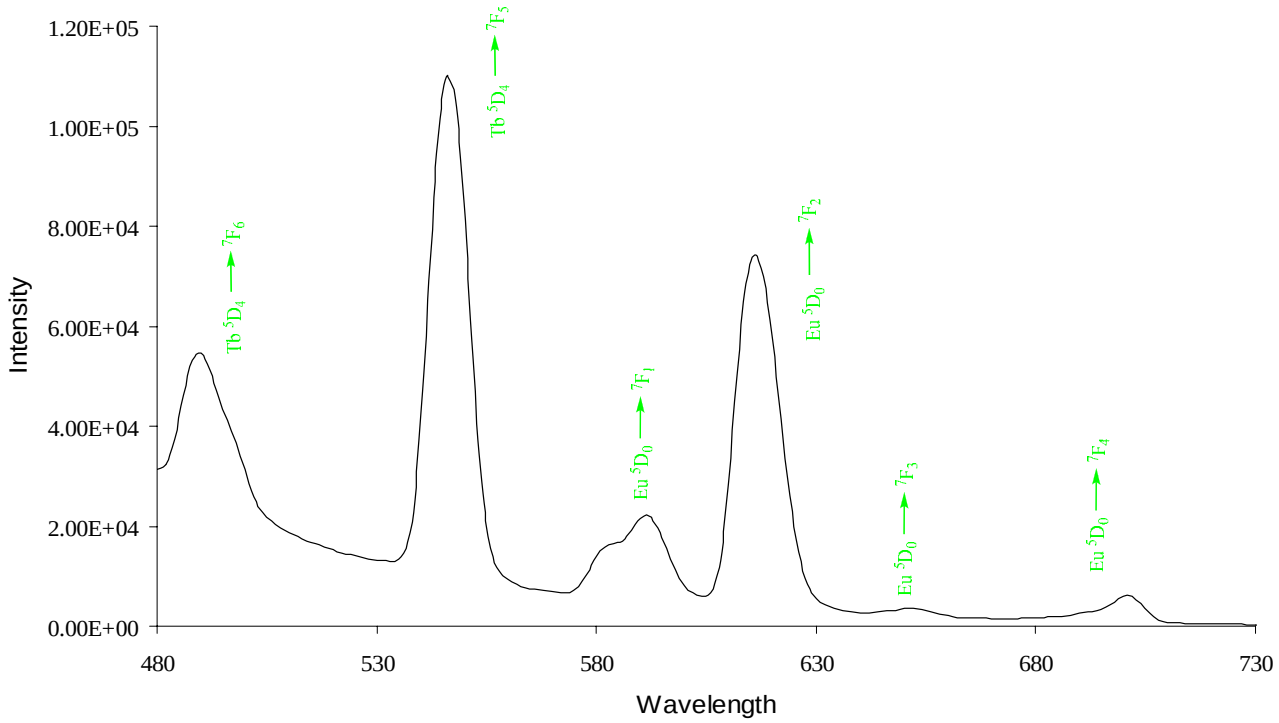

Figure 24. Emission of Eu:Tb 1:1 polymelamine complex emission on quartz

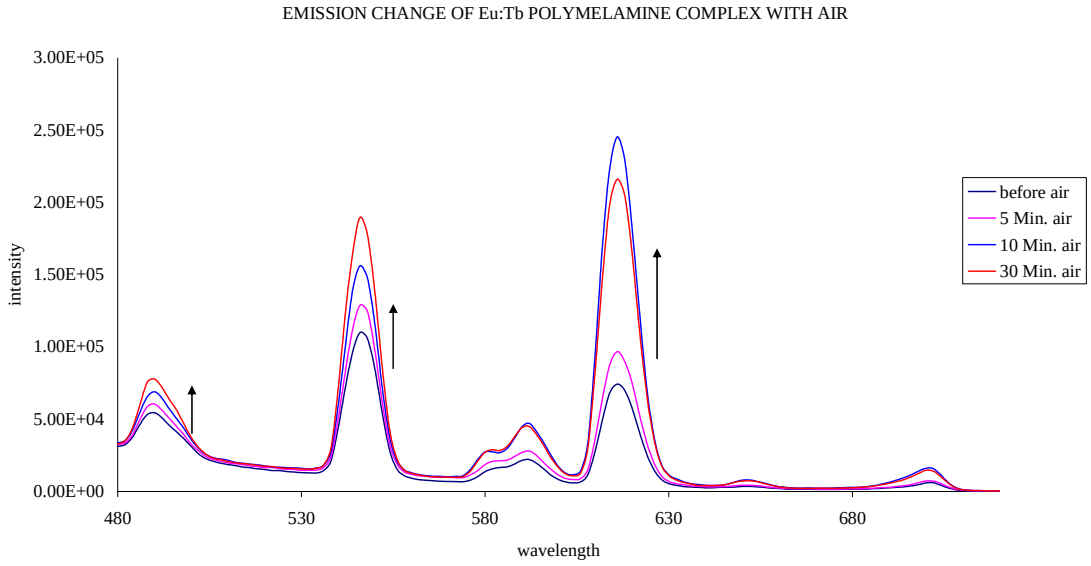

Figure 25. EXPOSE TO AIR
Emission of Eu:Tb 1:1 polymelamine complex emission on quartz

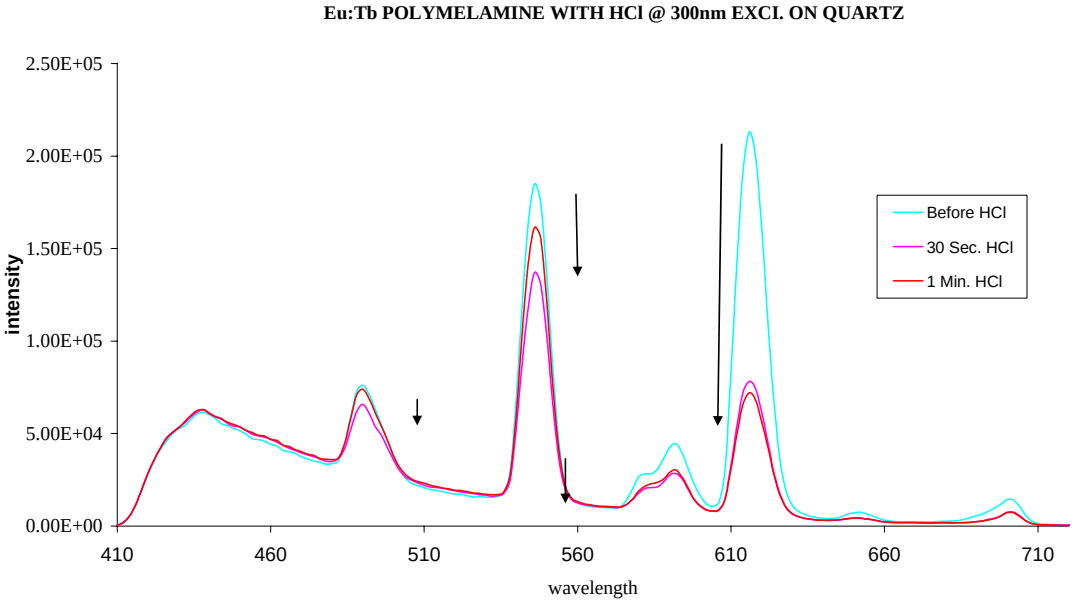

Figure 26. HCl exposure

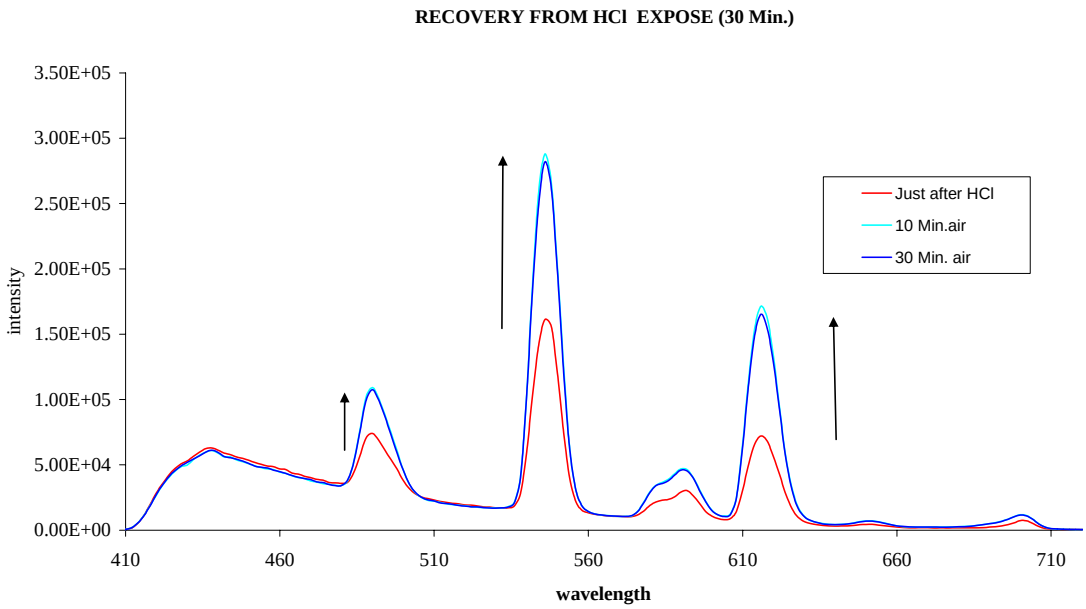

Figure 27. HCl recovery

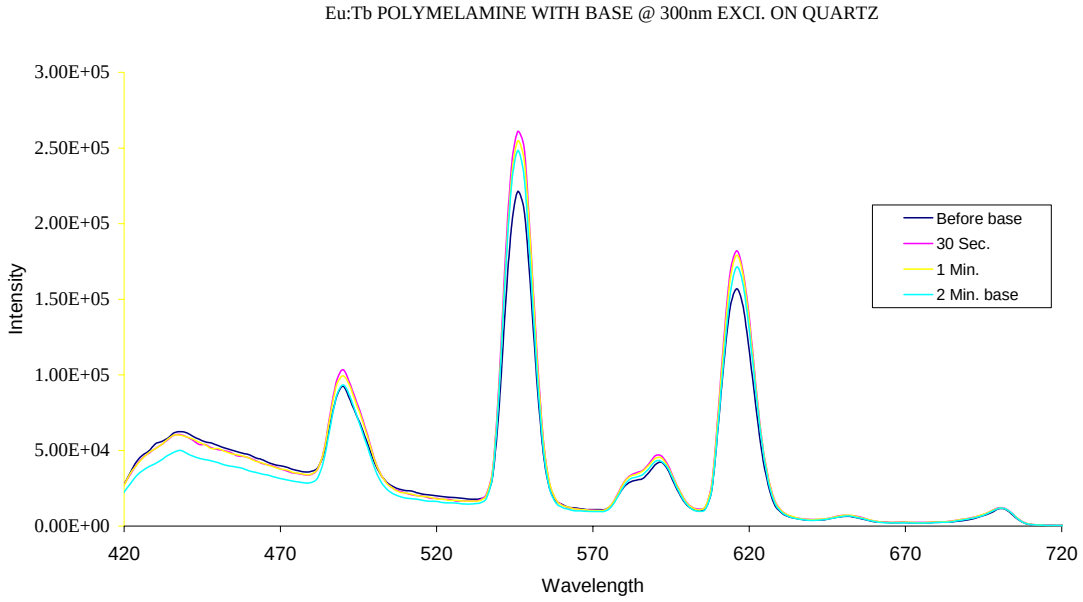

Figure 28 exposure to base

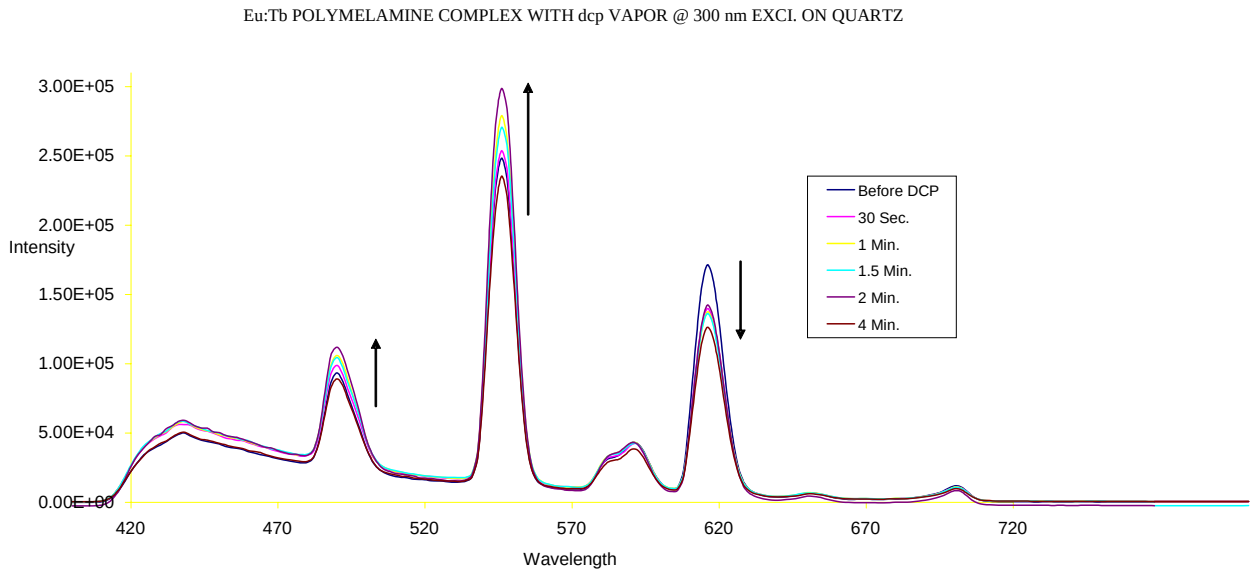

Figure 28 DCP exposure

Nanomatrix-nanopolymer-receptor (NNR) composites: Nanopolymer, Nanoparicles and Self-assembly

Ordered arrays of spherical particles

We have been attempting to extend our coating technology to encompass patterned depositions of ordered arrays. The mylar sheets that we have been using were exposed to an UV-ozone treatment through a mask. The UV-ozone treatment consists of a two lamp exposure, one at 254 nm and one at 180 nm, the shorter wavelength lamp forming ozone in close proximity to the surface. This treatment has in the past made the substrate hydrophilic enough that particles do deposit quite well. Once so activated the substrates were dipped following our established protocol of 5-15 ml/min in a 15 solution of 40 nm silica particles. Figure 29 demonstrates that we are not forming the coatings that we have in the past using quartz and silicon but there is some degree of ordering. We have begun to examine the polymer sheets that we have been using and need to change our choice of substrates. These sheets are pulled along the two transverse directions I order to align and strengthen the films. This results in a fairly uneven surface in comparison to the one we have been using on the solid substrates. Additionally for the activation process to be effective the surface must be much more hydrophobic than the current material that we have. We are searching for a replacement material for this coating as this appears to be the best way to move forward on this front.

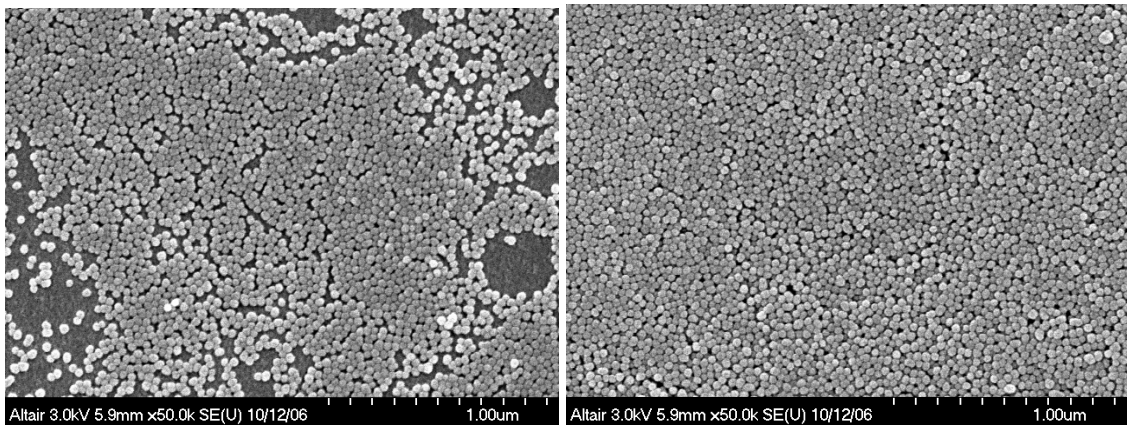

Figure 29. Silica spheres

Silver nanoparticulate – plasmon resonance fluorescent enhancement.

We have been working on enhancing the fluorescent signal from our substrates by coordinating the dye material with a plasmonic resonance structure. Silver and gold are both known to produce these fields but silver is closer to the excitation wavelength that we are using for the europium and ruthenium complexes. The width of the absorption peak as well as the wavelength at which it occurs is dependent on the size and morphology of the particles that are formed. Tailoring the dimensions will allow us to shift this absorption peak to a wavelength that we can use in the device.

To form these silver particles we began by adding 1 ml of 0.1 N $AgNO_3$ to 100 ml of DI water. Once the solution was heated to boiling 1 ml of a 1% solution of sodium citrate was added. Over the course of several minutes the solution became dark black and by the next day the

majority of the silver had precipitated out as large particulate. In order to better control the particle size the sodium citrate solution was dripped into the silver nitrate solution at a rate of 0.85 ml/h and was maintained for 1 hour. The solution became slightly yellow after the hour and after an additional hour of mixing the solution had completely clouded and had a yellow/green coloration. Once cooled, the solution was diluted and an UV-Vis spectrum was recorded, see Figure 30. The absorption peak has a maximum at roughly 440 nm but the peak is quite broad which would suggest a mix in particle size. Scanning electron micrographs of the dried solution showed that in addition to having particles from ~5 nm to 60 nm there were also long fibers present as shown in Figure 31. Using a backscatter filter during the imaging we determined that these fibers were also silver. Based on these results we are now working on better control of the particle growth by changing temperature as well concentration.

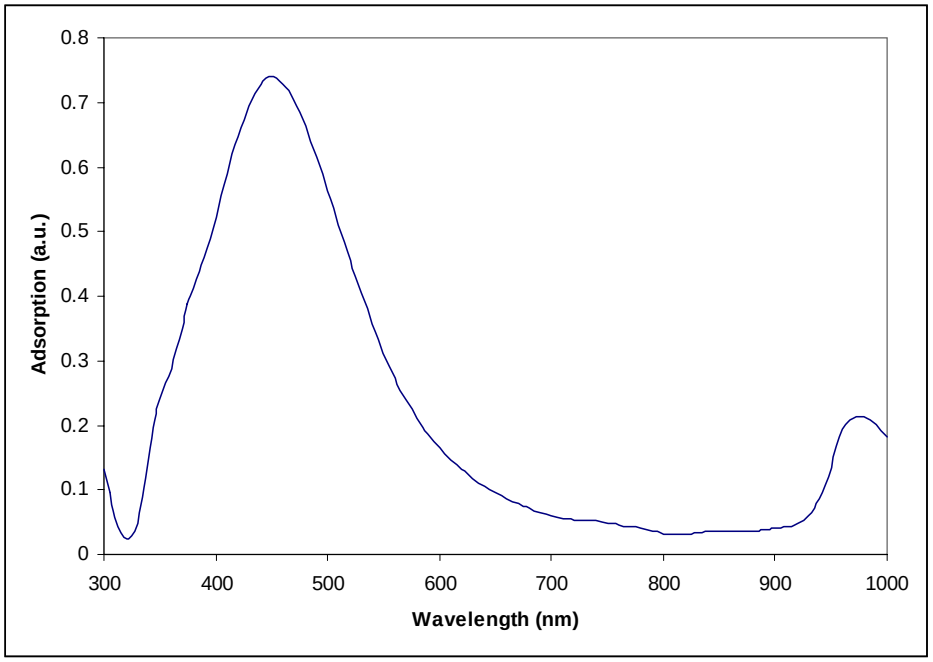

Figure 30:. UV-Vis absorption spectra of silver nanoparticles

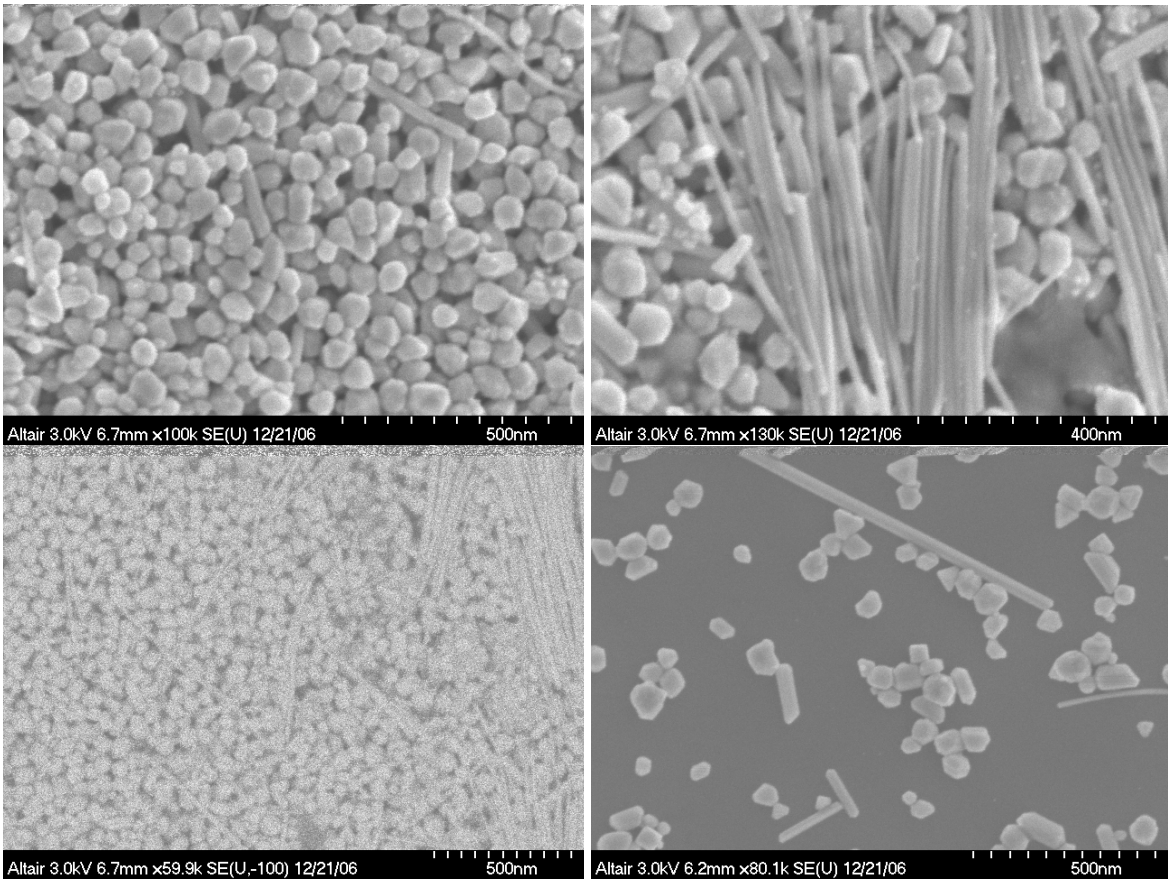

Figure 31. SEM images of the silver nanoparticles. Demonstration of particle size and dispersion. A and b are secondary electron images on carbon tape. Image c is a backscatter image demonstrating that the fibers are made of the same material as the particulate. Image d is a lower concentration dispersion on a silicon chip.

Sensor devices: Signal amplification and processing
Prototype sensor hardware development

We have been working to optimize the signal that we can acquire off of a quartz substrate. Through several iterations we found that placing the receiving fiber directly above the illuminated spot yielded the highest signal and at the same time allowed us to lower the amount of backscattered light that reached the detector. In order to optimize the signal collected the width of the spot created by the illumination fiber was matched to the width of the spot that was collected by the receiving fiber. Using figure 32 we developed the following equations which yield the ratio of the distances that we need to maintain to optimize the signal.

$L2/L1 = \cos 25$
$L3/L1 = \sin 25$
$L1 = L2/0.906 = L3/0.42$

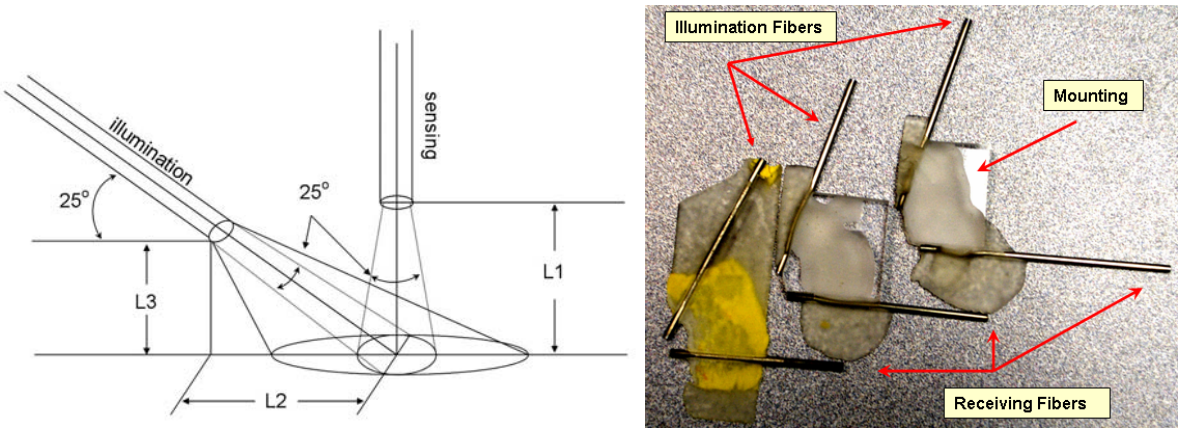

Figure 32. Fiber alignment diagram and several probes with different values of L1.

Using the above equations we mounted the fibers setting L1 = 0.5 cm. Using a europium phenanthraline complex we acquired a spectrum using a 100 ms integration time and the standard 380 nm illumination. Figure 33 demonstrates the quality of the signal that we were able to achieve using this configuration. The peaks that located at 380 nm and 760 nm are due to the incident illumination being scattered back into the detector, and can be used to scale the fluorescent signal.

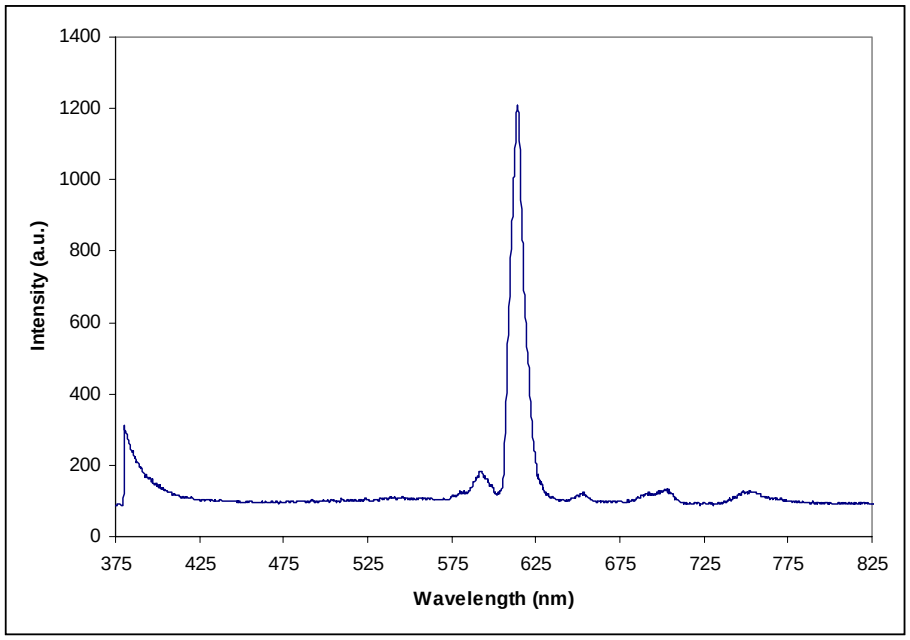

Figure 33. Europium phenathraline benzoylate on quartz substrate. Receiving probe is positioned 0.5 cm above the slide. Spectrum was collected in 100 ms using 380 nm excitation source. Peaks at 390 and 780 represent illumination background.

Based on the results from the first probe a chamber was built which utilized this same design. In order to accommodate the translation hardware it was necessary to move the receiving fiber to 1 cm while keeping the ratios equal. The chamber was fit with a solenoid to move the sampling platform under the probe to one of two positions thus monitoring two dye complexes in the same gas stream. By increasing the probe distance above the sample it was necessary to increase the integration time to 3 seconds to get a comparable signal. The increased integration time also increased the amount of illumination background light that made it into the detector, but currently there is no overlap with the fluorescent peaks and thus is not considered detrimental at this time.

During this stage we felt it was necessary to explore the possibility of using a total internal reflectance setup to acquire the fluorescent signal. Using this arrangement the illumination fiber is butted up directly along the side of a glass or quartz plate. The receiving fiber is then placed similarly but at a right angle with respect to the illumination fiber. For this test the same 1 inch square quartz plate with the europium benzoylate phanathreline coating on one side was used. Again it was necessary to increase the integration time to 3 seconds to achieve an adequate signal. Figure 34 demonstrates the quality of the signal that can be collected. Illumination background is most likely unavoidable, but like above there is no overlap with the peaks above so this can be a viable technique. The area of illumination is limited to a thickness of roughly 200 nm which would allow us to use an extremely thin layer of dye and therefore increase the sensitivity. Coating both sides of the plate would allow us to increase the signal as well. We are concerned with attaching multiple plates to the spectrometer and with how to integrate the new hardware, but the increase in sensitivity might make this a requirement.

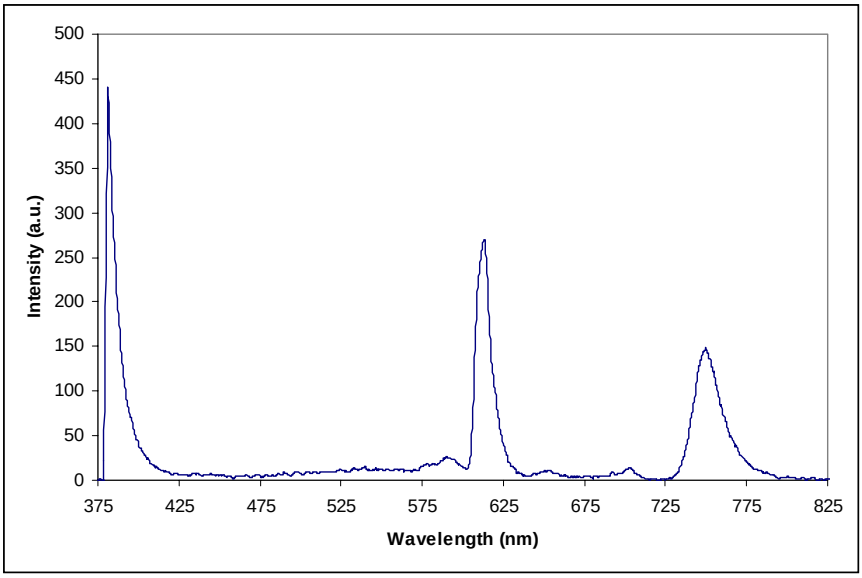

Figure 34. Europium phenathraline benzoylate on quartz slide in sample chamber. Integration time 3 seconds, excitation wavelength 380 nm.

In the early portion of this work we were using a Palm Lifedrive to control the spectral acquisition of the USB2000 spectrometer, however there are several concerns about the device that have caused us to begin looking to other controllers. At this point the major problem concerns the use of the solenoid to translate the stage. With only one digital output from the Lifedrive it is not possible to control a stepper motor or similar drive system while also controlling the spectrometer. Additionally the Lifedrive unit consumes a relatively large amount of power, is bulky and due to the conventional hard drive is not as rugged as we would like. As an alternative we have begun working with a RabbitCore RCM3100 control module. This control module has 54 digital I/O lines 6 of which can be used for serial communication. The controller is 1.65 X 1.85 X 0.5 inches and runs off of a 3 V power supply. A stepper motor controlled stage can now be attached and accurately placed below the probe mount (See Figures 35 and 36).

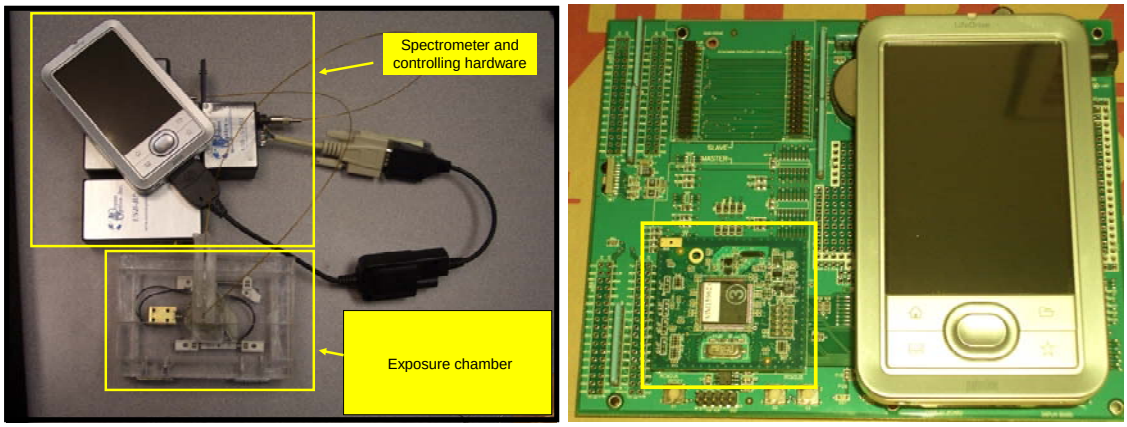

Figure 35. Second generation prototype with grazing incidence probe and solenoid translation system. New RabbitCore controller in relation to the Lifedrive controller.

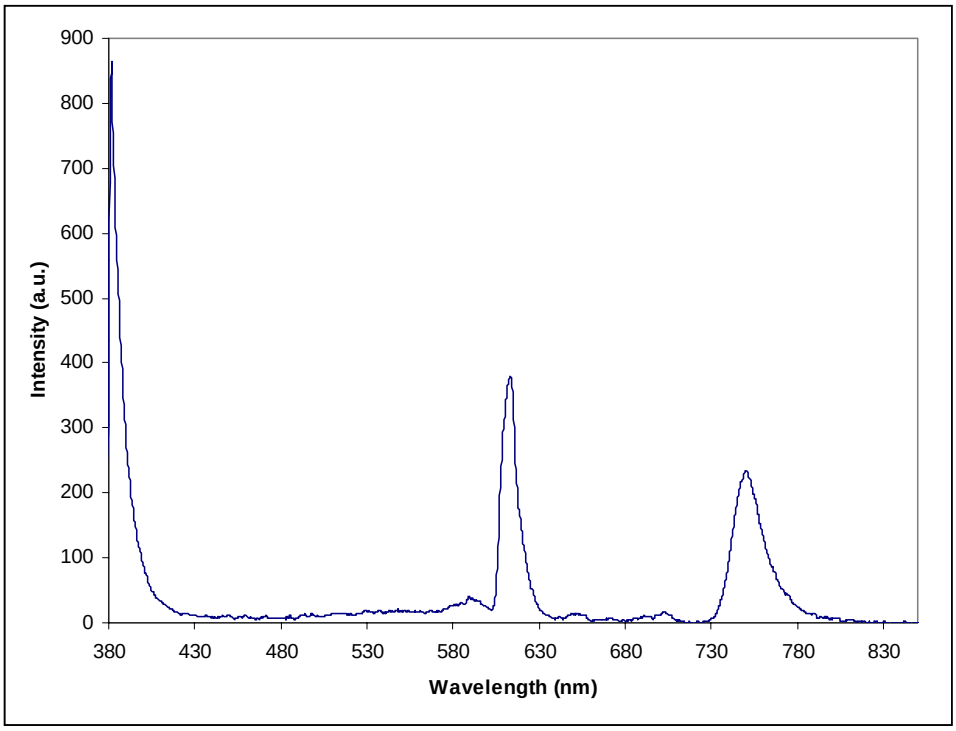

Figure 36. 1 inch square quartz slide with europium phenathreline benzoylate. Integration time 3 seconds. Sample collected using total internal reflectance design.

This has led to the latest revision, with a stepper motor control and smaller chamber. We have successfully coated 2 complexes on differing positions on the slide. The probe can be driven back and forth between the two complexes and both can be monitored in a very short time. Using two of the complexes from our library we have used this system to differentiate between a nerve gas analog and HCl, one of our main interference compounds. Figure 37 demonstrates the response of these two complexes to two analytes and the direction of the response. By comparing the two spectral responses it is possible to register the nerve gas analog and distinguish it from the acid.

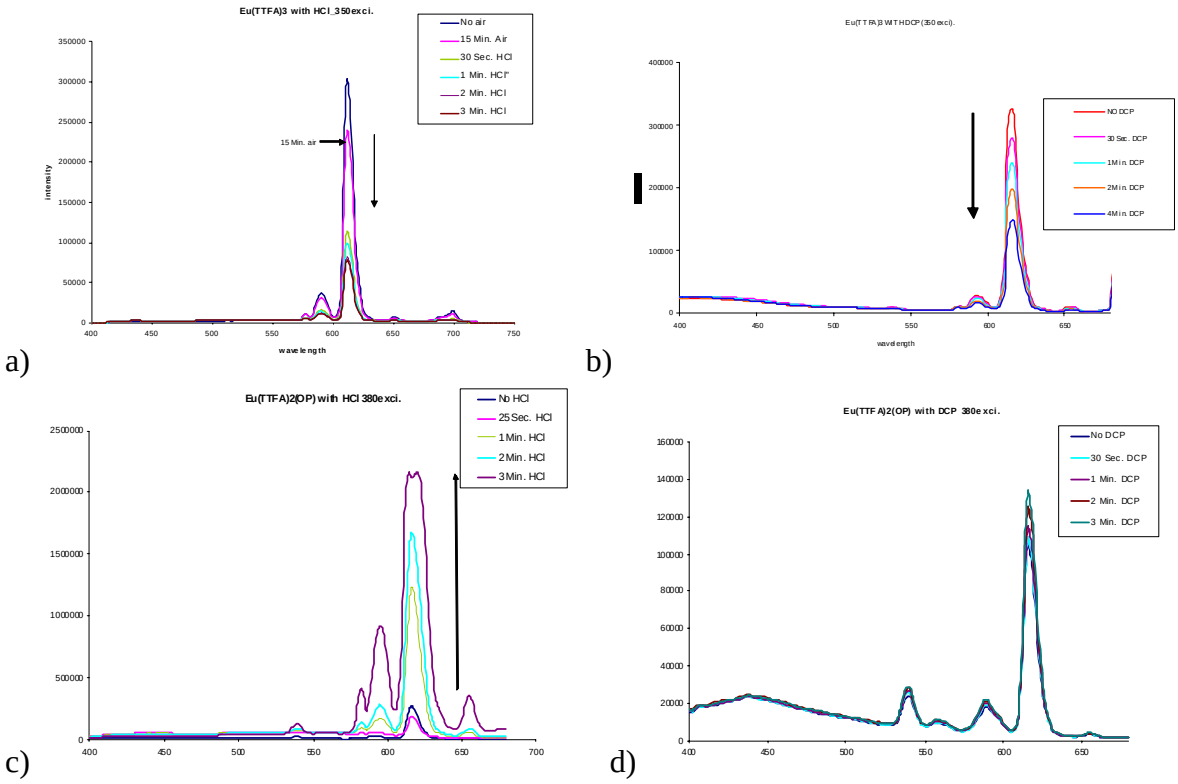

Figure 37. The response of $Eu(TTFA)_3$ and $Eu(OP)_2TTFA$ to two analytes, a)HCl:$Eu(TTFA)_3$ yields a decrease in intensity b)DCP:$Eu(TTFA)_3$ yields a decrease in intensity c)HCl:$Eu(OP)_2TTFA$ yields an increase in intensity d)DCP:$Eu(OP)_2TTFA$ yields no change.

Radiation Detection

We have been working on developing a detector to obtain a response to ionizing radiation and incorporate this into our sensor platform. Based on the semiconductor properties and our current laboratory and scale up capabilities we are attempting to fabricate low temperature diamonds. Diamonds are high band gap semiconductors which can be doped into p-type functionality for detector elements. Our laboratory is equipped with a high density large area plasma enhanced chemical vapor deposition chamber. This apparatus is capable of coating relatively large thicknesses of material in a shorter time and at a lower temperature than thermal CVD units. Using the Buchanan diamond phase diagram for a starting point we have examined several gas compositions in the attempt to form these coatings. The literature has shown primarily microwave CVD processes using water vapor and hydrogen to selectively etch away the non diamond phases. We have examined the combination of several gases to achieve similar stoichiometry in the process chamber. Primarily we have been using combinations of ethanol, methanol, carbon monoxide, oxygen and argon. By controlling the deposition parameters we are able to produce smooth featureless coatings, such as figure 38a. We can also increase the etch rate placing sparse coatings along the way. We also reach a point where the phases being deposited switch. To date we have not confirmed the presence of diamond in any of these coatings. From x-ray diffraction results it does appear that we have an intermediate phase present which adds to the idea that we are on the correct path. Surface treatment and precursor conditions make a large difference in the morphology and chemistry of the coating formed. As we move forward we might have to use a

heated stage to achieve a diamond coating.

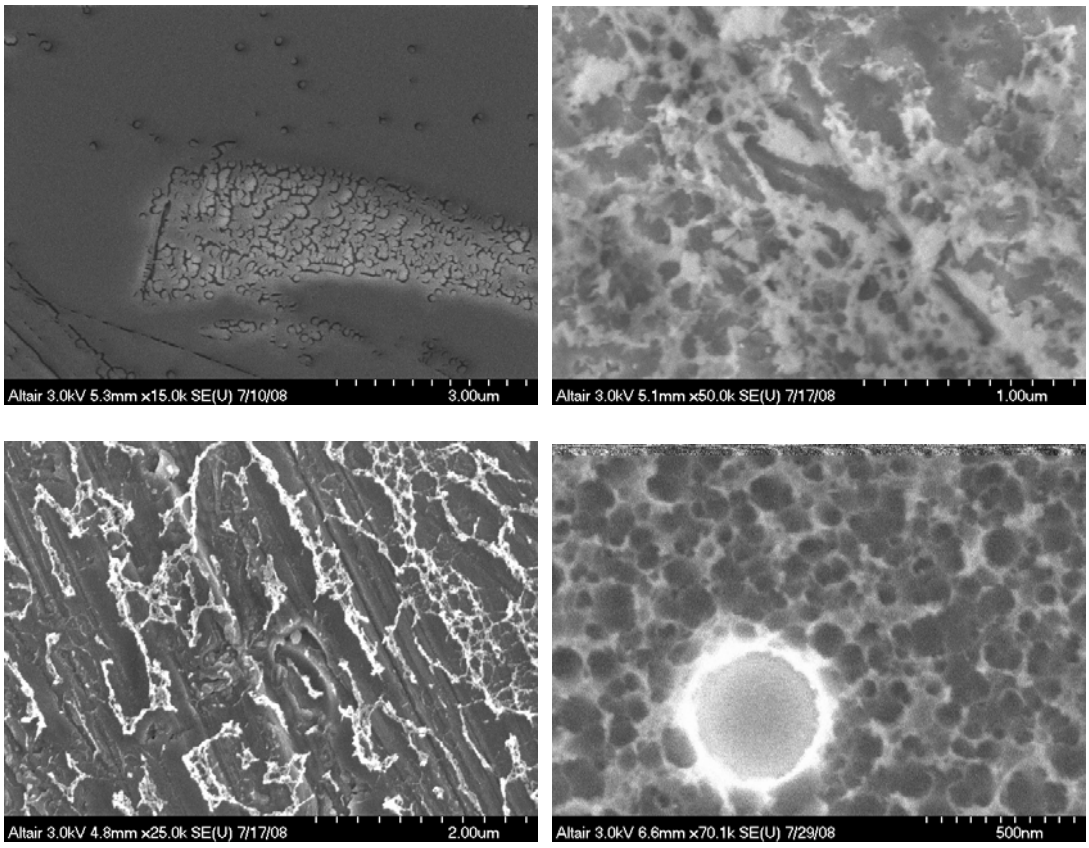

Figure 38. 4 etch rates using various gas concentrations and power levels.

Publications:

Internet Sites: None

Networks Fostered:

Strong collaboration was fostered between academia and the private sector with this portion of the grant. Western Michigan Univerity and Altair shared individual areas of expertise and collaborated on the analysis and interpretation of experimental results.

Technologies: None

Inventions: None

Data Bases: None

FINAL REPORT -Objective #3

Project Title: Development, Testing, and Demonstration of a High Rate Low Temperature Lithium Ion Battery

Project PI: Veselin Manev, Ph.D.

Teaming Member: None

Executive Summary:

Primary goals included development of a negative electrode, a positive electrode and selection of electrolyte for low temperature & high charge/discharge rate The experimental results conducted confirm that the low temperature performance of the nano-LTO negative electrode developed by Altairnano shows very good performance. The contribution of the nano-LTO electrode to the overall cell impedance at lower temperatures is negligible. The cell impedance and the rate capability at lower temperatures are controlled by the positive electrode and in particular by the positive electrode/electrolyte interface resistance. As the interface impedance is controlled by the nature and morphology of the electrode material a study for a better positive electrode material was performed. As displayed in Table 1 the cells with optimized design show 96% capacity retention at 1C charge/discharge rate and -30°C and respectively 84% capacity retention at 1C charge/discharge rate and -40°C.

Summary of capacity retention of nano-LTO based cell with optimized design during continuous cycling at extremely low temperatures		
	Temperature	
Charge/Discharge rate	-30°C	-40°C
0.5C charge & 0.5C discharge	98%	93%
1C charge & 1C discharge	96%	84%
2C charge & 2C discharge	88%	71%

Summary of capacity retention of optimized cell at -30°C and -40°C during continuous cycling test at 0.5C, 1C and 2C charge & discharge rate.

EXPERIMENTAL

Electrode materials

Negative electrode material $Li_4Ti_5O_{12}$ (LTO) was prepared according to Altairnano nano proprietary technology. Preliminary tests of materials with specific surface area (BET) in the range of 10 to 80 m^2/g have shown that the electrodes with specific surface area between 40 and 50 m^2/g have the lowest cell impedance. Because the rate capability of the cell at low temperature is controlled in particular by cell impedance, LTO material with BET between 40 and 50 m^2/g was selected as a baseline negative material for this study.

On the other hand the preliminary EIS cell measurements have shown that the cell impedance in the range of -30°C to -40°Cis is controlled by the positive electrode material and in particular by its interface resistance. Thus a large variety of materials have been tested that include: $LiMn_2O_4$ (LMO) from TODA, LICO, Nippon Denko and Erachem, $LiCoO_2$ (LCO) from LICO and Electro Energy and $LiNi_{1/3}Co_{1/3}Mn_{1/3}O_2$ (LNCMO) from LICO and TODA. In addition part of these materials were processed in order to modify their physical properties and to decrease their interface impedance.

Electrode preparation

Electrode compositions for both electrodes were selected based on the strong lithium ion battery expertise of the Altairnano battery team, taking into account the large variety of electrode materials with different size, morphology, density, porosity and electronic conductivity. For electrochemical testing of both positive and negative electrode materials Altairnano selected an electrode composition that

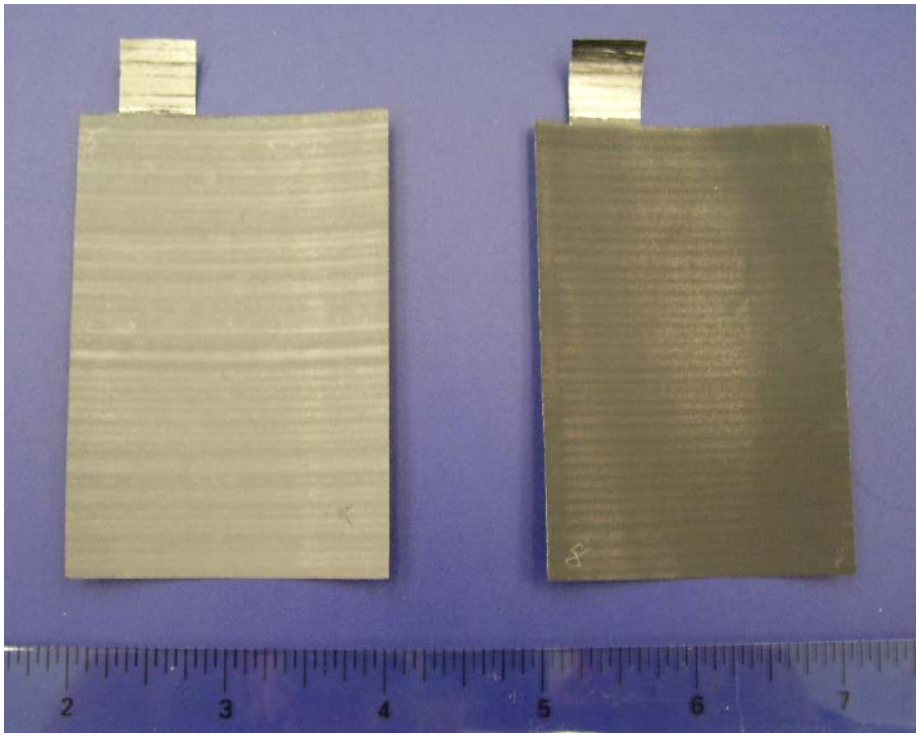

Fig. 1. Test electrodes: nano-$Li_4Ti_5O_{12}$ negative electrode (left) and positive electrode (right)

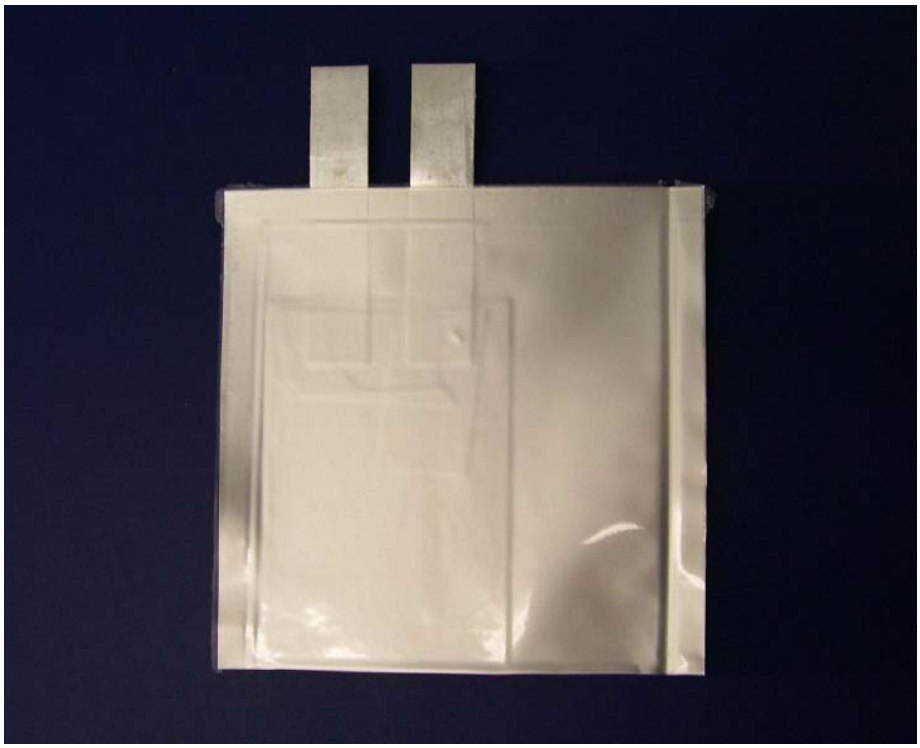

Fig. 2 Electrochemical test cell

included 75% active material, 10% PVDV binder and 15% conductive carbon additives. This composition gives a stable electrode performance regardless of the particle size, BET and morphology of the electrode materials. However after the electrode material selection each electrode (positive & negative) composition was separately optimized in order to obtained maximum low temperature performance.

The negative and positive electrodes (Fig. 1) are the same size (2 by 3 inches) and both use Al foil as a current collector. After a preliminary screening test a 30 g/m2 coat weight was selected for the negative electrode, while the coat weight of the positive electrode was calculated based on the specific capacity of the positive material in order to keep the cell negative electrode limited with a negative electrode/positive electrode capacity ratio of about 1/1.25. As a result a coat weight of 60 g/m^2 was used for $LiMn_2O_4$ electrodes and 45 g/m^2 for $LiCoO_2$ and $LiNi_{1/3}Co_{1/3}Mn_{1/3}O_2$ electrodes.

Test cells

We designed and used a soft pack cell (Fig. 2) for material selection and electrode optimization This cell has the advantage that all the cell components and cell technology used are exactly the same as in full size cells. Thus all the data obtained in a lab cell configuration can be easily scaled up and the expected full size cell performance can be simply predicted by multiplying a factor reflecting electrode active area ratio. Each cell consists of one negative and one positive electrode, both coated on one side of a 20 micron Al current collector and separated by a standard

polypropylene separator Cellgard 2400. 1.2 M $LiPF_6$ in EC:EMC = 1:3 ratio was used as a baseline electrolyte.

Fig 3. Climatic chamber & thermostat with temperature range from -80°C to +120°C

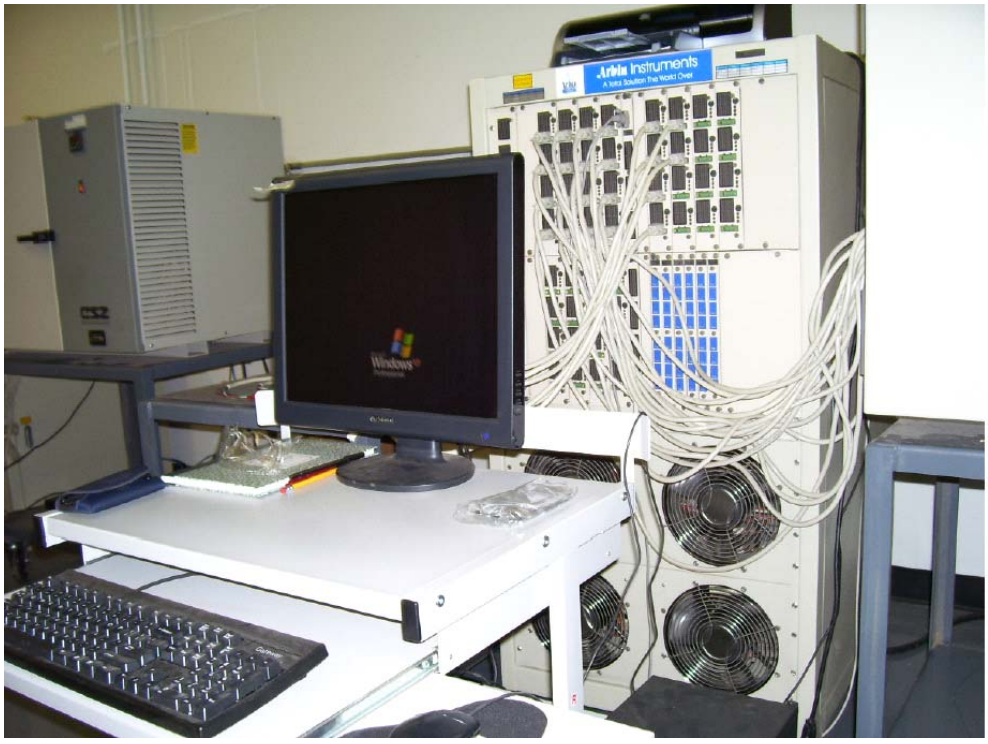

Fig. 4. 48 channels Arbin BT2000 computer controlled electrochemical cells testing system

Electrochemical characterization.

After cell activation with electrolyte, the cell was placed in a climatic chamberwashere the cell is kept at thermostatic condition (Fig. 3). The temperature range of the climatic chamber is from -80^{o}C to +120^{o}C. However, the typical measurements related to the current project were performed in the temperature range -50^{o}C to +80^{o}C. Although the performance at -50^{o}C was out of the scope of this project, some measurements were performed and reported at -50^{o}C because of significant hysteresis effects in the electrolyte conductivity in temperature range below -30^{o}C.

All general electrochemical characterization of the cells were performed with the 48 channel electrochemical cell testing system Arbin BT2000 (Fig. 4) This instrument measures charge and discharge capacity & energy, cycle live, cycling efficiency, charge & discharge rate capability and cell pulse power performance.

Electrochemical impedance EIS measurements were performed with a Solartron frequency response analyzer SI-1260 combined with electrochemical interface SI-1287 (Fig. 5). This instrument separates impedance contributions from electrolyte conductivity, electrodes/electrolyte interface resistance, and diffusion-controlled processes. Using a Li reference electrode it may separate the positive electrode contribution in cell impedance from the negative electrode contribution. Previous data obtained by the Altairnano lithium ion batteries team shows that lithium ion transport across the electrodes/electrolyte interface has the determining effect on the cell performance at extremely low temperatures, thus special attention was paid to evaluation and improvement in electrodes/electrolyte interface impedance.

Fig. 5 EIS measurements are performed with Solartron frequency response analyzer with electrochemical interface

RESULTS

Selection of negative electrode material

As the charge/discharge rate capability of the electrodes directly correlated with their impedance, our first step in development of high rate & low temperature negative nano $Li_4Ti_5O_{12}$ electrode was selection of negative electrode material with lowest specific impedance. Altairnano previous results showed that the high frequency part of the EIS impedance curve is controlled by interface impedance of the positive electrode, while the lower frequency part is controlled by the impedance of the negative electrode (Fig.6, left). We have used this previous finding as a screening test to optimize the specific surface area (BET) of the LTO negative electrode material. LTO samples with BET between 15 m^2/g and 80 m^2/g have been prepared and tested. As was shown on Fig 6,

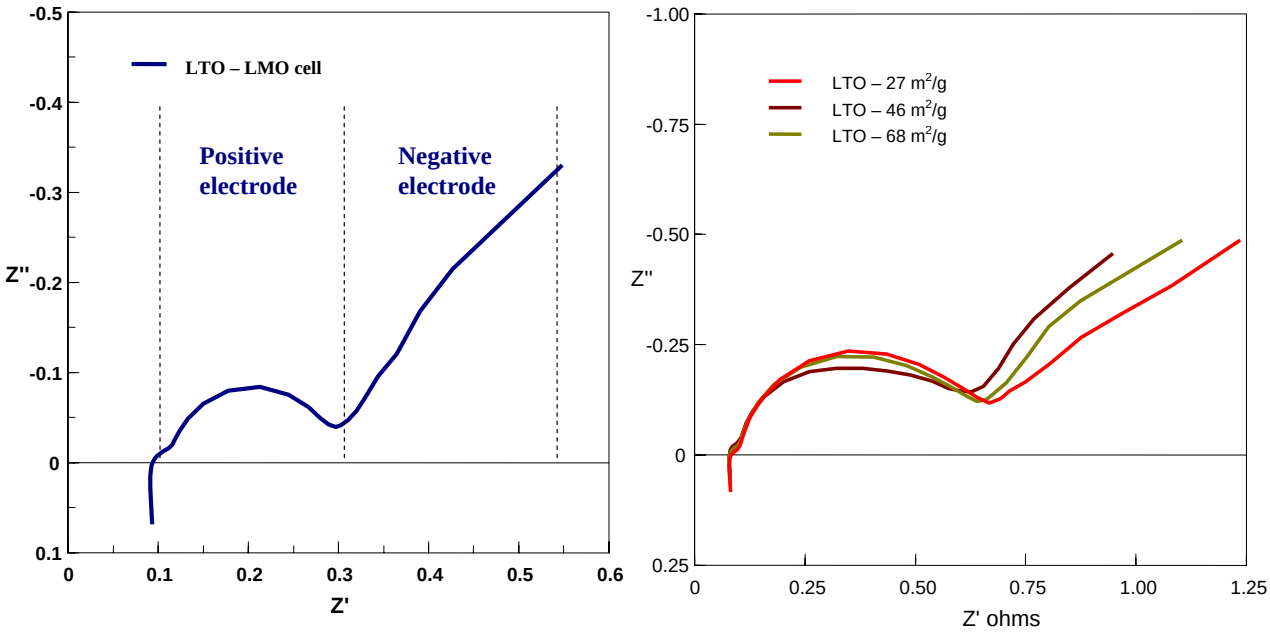

Fig. 6 EIS impedance of LTO-LMO cell, showing the contribution of each electrode (left) and cell impedance as a function of LTO surface area BET (right)

right, the LTO sample with SSA in the range of 40 – 50 m^2/have the lowest impedance. Thus LTO with specific surface area 45±5 m^2/g was selected for the low temperature tests. The morphology of the material with BET 45±5 m^2/g used as a baseline anode material in this study is shown in Fig 7 (left). As displayed the nano crystallites are organized in large spherical particles with mean particle size of about 12 microns. Part of this material was additionally processed using new soft (Vortec) milling technology in order to decrease the mean particle size about three times from 12 microns mean particle size to about 4 microns without affecting significantly the morphology of the crystallites. The SEM picture of the sample after this micronizing step is shown in Fig 7 (right) and the particle size distribution corresponding to it in Fig. 8.

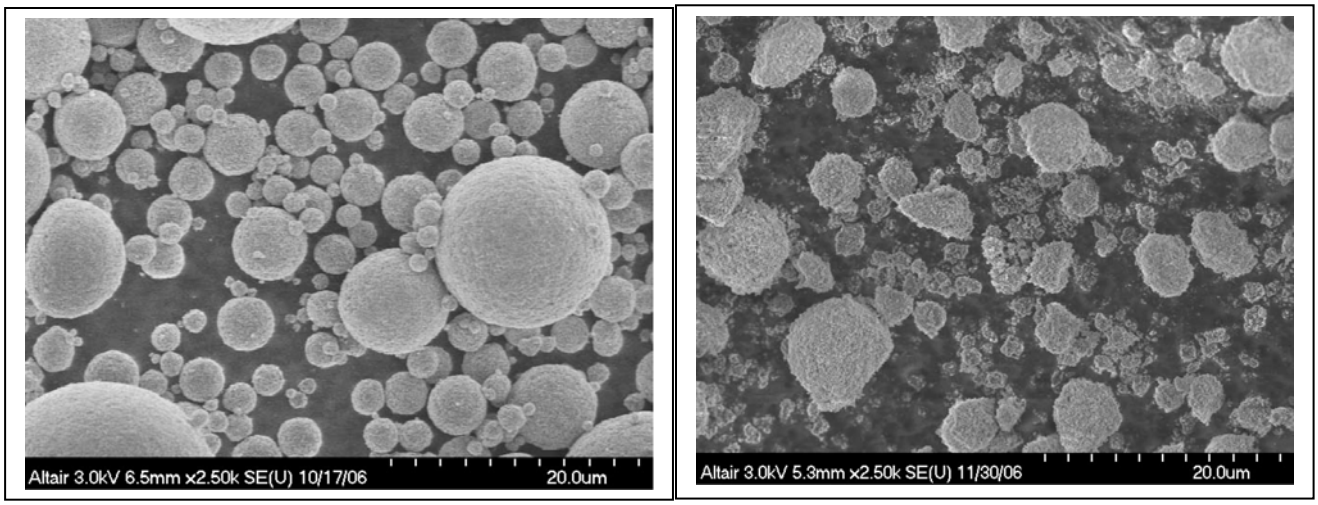

Fig. 7 SEM photographs showing the morphology of baseline negative electrode material with BET 45±5 m^2/g (left) and after micronizing it using Vortec soft milling process (right)

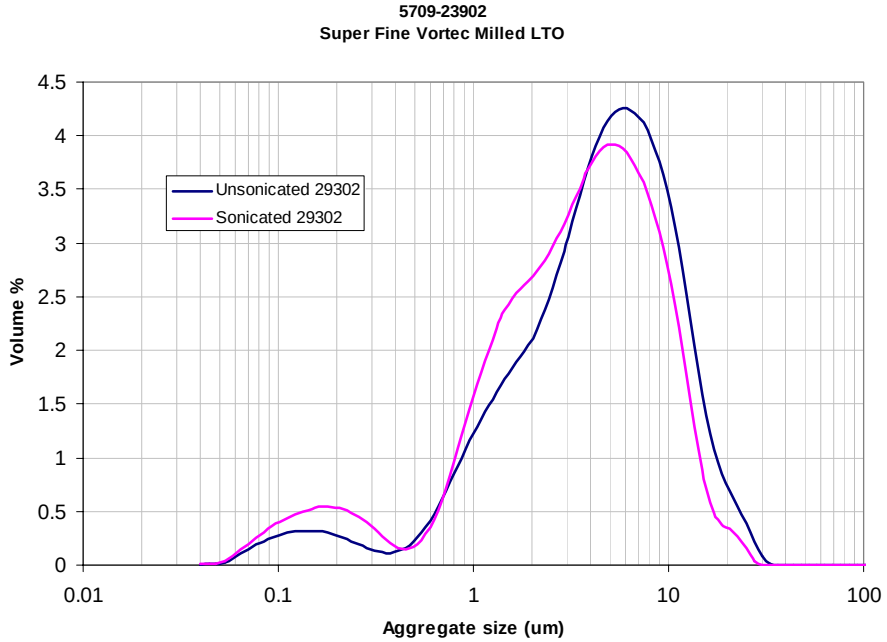

Fig. 8 Particle size distribution of the nano-$Li_4Ti_5O_{12}$ electrode after the micronization (Blue) and after additional sonication (red).

Selection of positive electrode material

As mentioned earlier a large variety of materials have been tested as received that include: $LiMn_2O_4$ (LMO) from TODA, LICO, Nippon Denko and Erachem, $LiCoO_2$ (LCO) from LICO and Electro Energy and $LiNi_{1/3}Co_{1/3}Mn_{1/3}O_2$ (LNCMO) from LICO and TODA. After

preliminary screening tests of all these materials as received, only $LiMn_2O_4$ (LMO) from LICO and LMO Nippon Denko showed relatively low impedance and relatively good charge/discharge rate capability at -40oC. Thus these two materials were selected for additional processing in order to meet the project objectives. However, during the additional tests the LMO from LICO showed significant drawbacks such as: large variation in capacity, increase in impedance with time and large self-discharge rate. As a result, the Al doped $LiMn_2O_4$ (LMO) from Nippon Denko (Figs 9 & 10) was selected as baseline positive electrode material for this study.

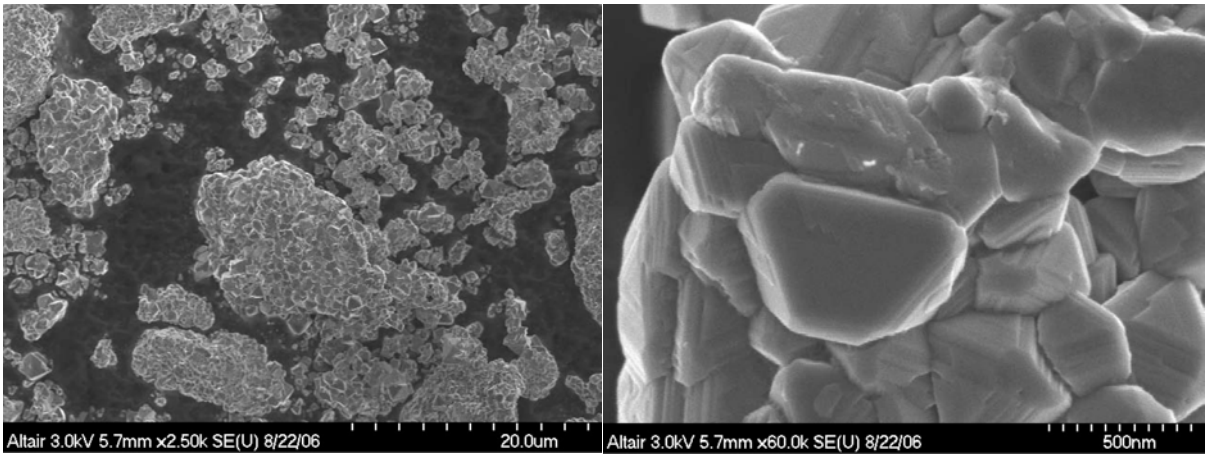

Fig. 9 SEM pictures showing morphology of baseline $LiMn_2O_4$ (LMO) positive electrode material as received from Nippon Denko.

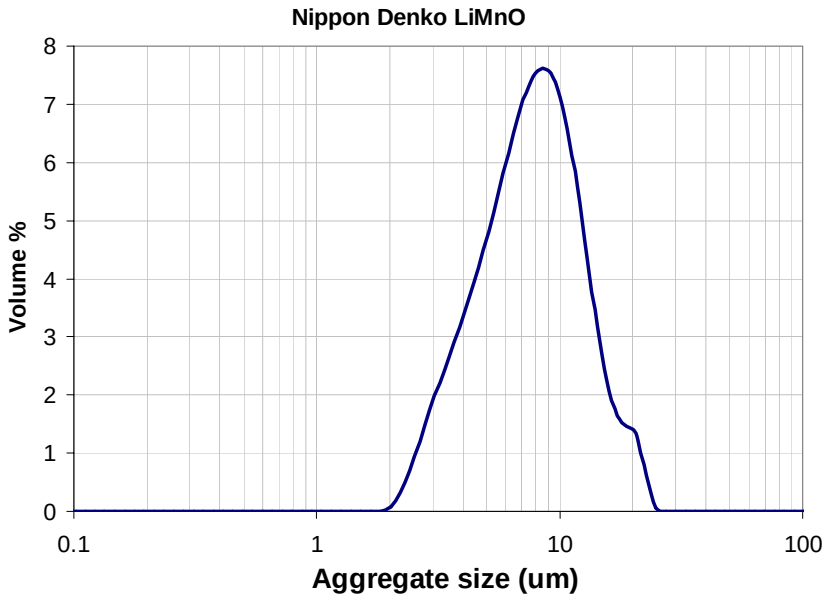

Fig. 10 Particle size distribution of baseline $LiMn_2O_4$ (LMO)

After detailed analysis of physio-chemical properties of the other positive electrode materials and appropriate electrochemical screening tests, two of them were selected as alternative positive electrode materials: $LiNi_{1/3}Co_{1/3}Mn_{1/3}O_2$ (LNCMO) from TODA and $LiCoO_2$ (LCO) from Electro Energy.

The $LiNi_{1/3}Co_{1/3}Mn_{1/3}O_2$ (LNCMO) from TODA was in particular used as model electrode in order to confirm that the large semi circle observed in the EIS curves is controlled by electrolyte/electrode interface of the positive electrode. If the semi-circle corresponds to the interface impedance of the positive electrode, then the increase in the positive electrode & electrolyte interface area (positive electrode BET) will cause an adequate decrease in diameter of this semi-circle and respectively a decrease in cell impedance. We processed this material using the soft milling procedure in order to increase the specific surface area (BET) from 0.45 m^2/g to 3.85 m^2/g. The requirement for soft milling is important in order to preserve good cycle life of the material. This means that the milling procedure needs to separate crystallites in the material aggregates with out causing cracks in the crystallite that later will cause a decrease in cycle life.

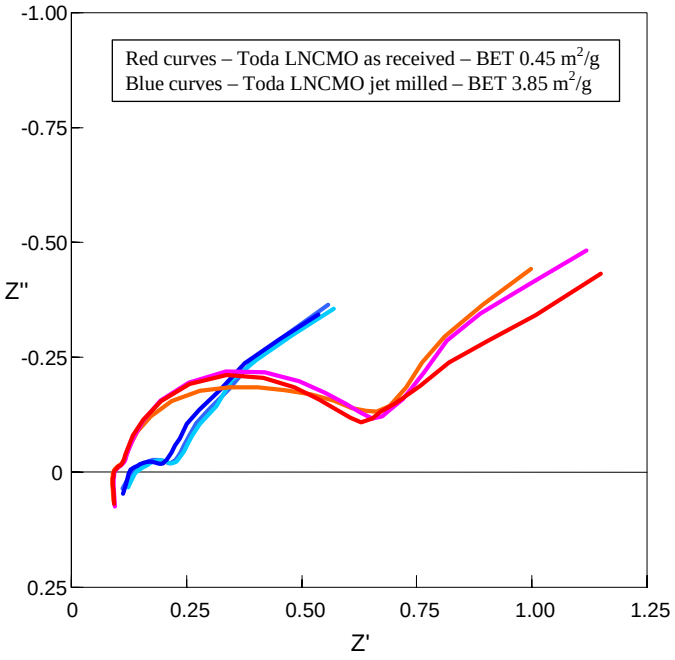

Fig. 11 EIS impedance of Toda LNCMO as received (red) and after increase in BET from 0.45 to 3.85 m^2/g

As illustrated in Fig 11, the increase in BET of the positive electrode material by a factor of 8 decreased the diameter of the semi-circle by about a factor of 8. This proves that this part of the impedance belongs to the positive electrode material and also supports our previous finding that this is positive electrode/interface impedance. To prove that the soft milling process does not cause cracks or other crystallite defects that may significantly reduce the cycle live of the material we ran a cycle life test. As illustrated in Fig. 12 the cell with soft milled LNCMO shows outstanding cycle performance, showing 98% capacity retention after more than 1200 cycles.

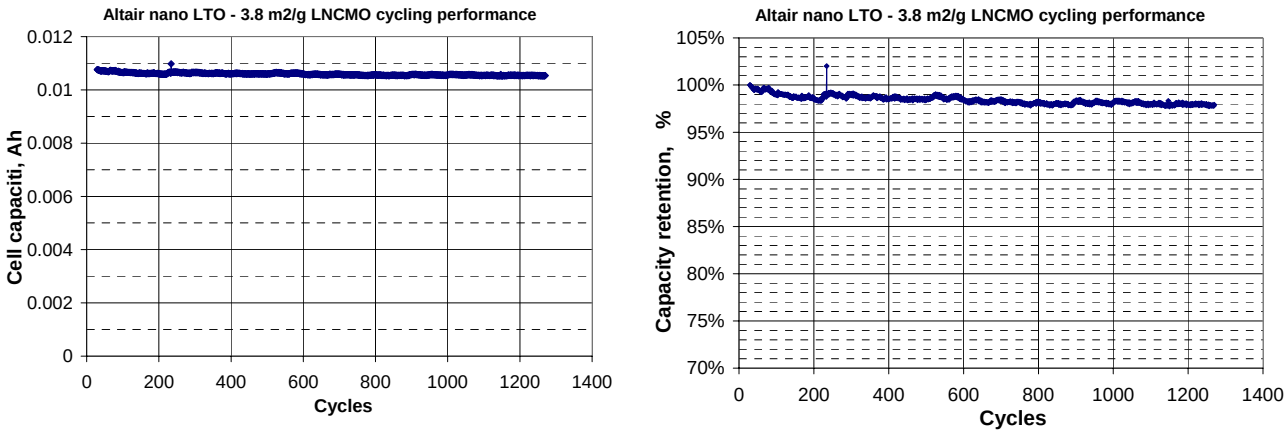

Fig. 12 Cycling performance of LNCMO with BET 3.8 m^2/g

The EIS impedance data at lower temperatures confirms the importance of using positive electrode materials with higher BET area. Fig . 13 shows the EIS impedance data of nano-LTO – LMO cell at 25^{o}C (black), 0^{o}C (red), -20^{o}C (blue) and -40^{o}C (green). As displayed even for material with relatively lower interface impedance (semicircle) at room temperature (black curve) with decrease in temperature the contribution of the interface impedance (semicircle) increase and -40^{o}C have a dominant contribution.

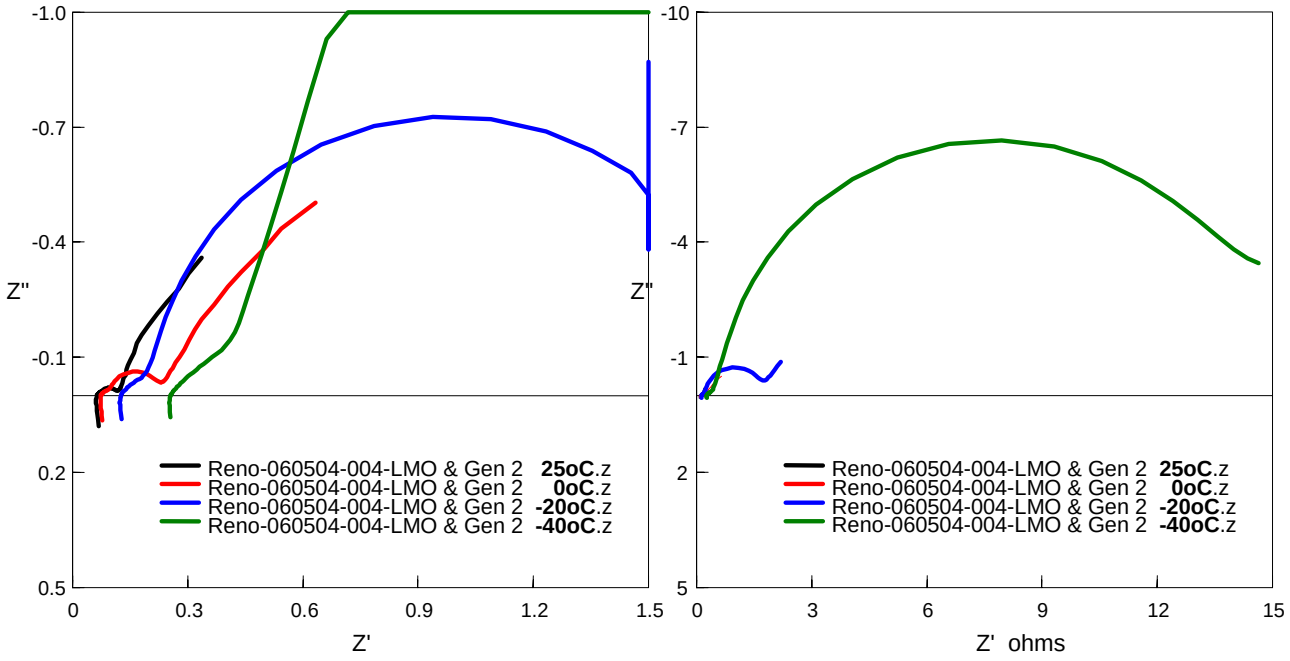

Fig. 13 EIS impedance of nano LTO–LMO cell at 25^{o}C, 0^{o}C, -20^{o}C and -40^{o}C

Thus it can be concluded from Fig 13 that the interface impedance of the positive electrode is controlling the cell impedance at -40^{o}C. Decreasing it by an increase in positive electrode interface area (BET) with the electrolyte can be one of the main tools in improving rate capability

at lower temperature. Based on this these results the baseline LMO from Nippon Denko and the LCO from EE will be also subjected to the soft milling procedure in order to increase their BET surface area in the range between 3 and 5 m^2/g.

Electrolyte selection

Two families of electrolytes were used for this study. The first family is a typical lithium ion battery electrolyte: 1.2 M $LiPF_6$ in EC:EMC = 1:3 ratio. The second family is an Altairnano multi component proprietary electrolyte that will be referred to as Gen 2 electrolyte.

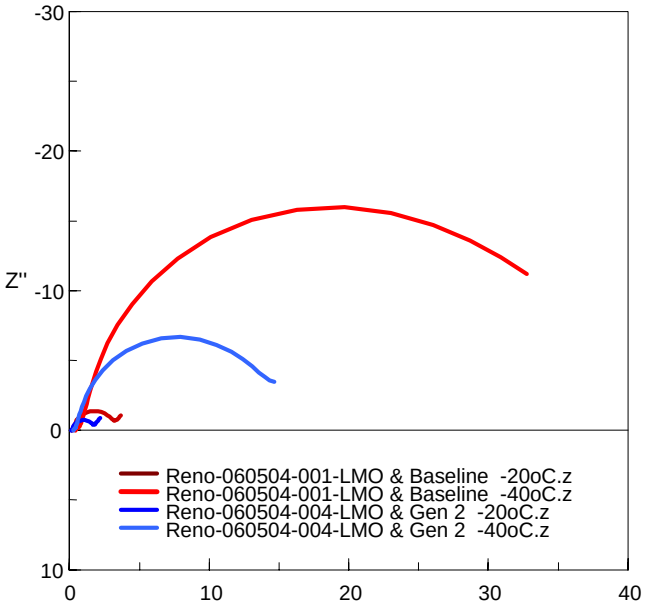

Fig. 14 EIS impedance of LMO-LTO cells with baseline (red) and Gen 2 (blue) at -20°C and -40°C

Fig 14 compares the EIS impedance of cells with the two types of electrolyte at -20°C and -40°C, suggesting that the electrolyte nature also affects the positive electrode/electrolyte interface impedance. As displayed cell with Gen. 2 electrolyte has more than 2 times lower electrolyte/positive electrode impedance than cell with baseline electrolyte. Thus the right selection of the electrolyte solution and its additives was the other tool used for improvement of -40°C performance.

In addition to these electrolytes, the AN based electrolyte developed for this project with a composition 60%AN + 40% 3MPN as a solvent and 1M LiTFSI + 0.5M LiBF4 as a salt was used. This electrolyte will be referred to as AN based electrolyte.

Results with non-optimized electrodes

Capacity retention of test cells using baseline nano-LTO electrode and LMO Nippon Denko as received at -30°C and -40°C is shown in Fig. 15 and Fig 16. As displayed in Fig 15 capacity

retention at -30°C of cells with Gen 2 electrolyte and at 1C rate is 84% and at 2C rate is 75%. As shown in Fig. 16 capacity retention of the lab test cells at 1C charge and discharge rate & -40°C is 68%.

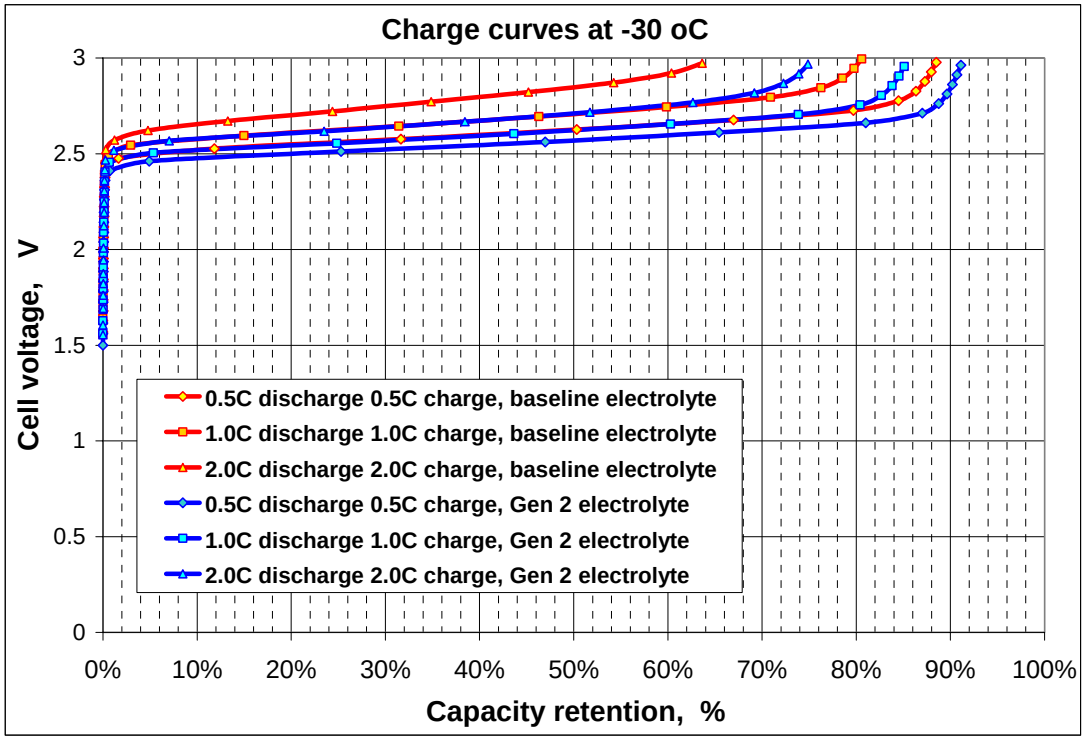

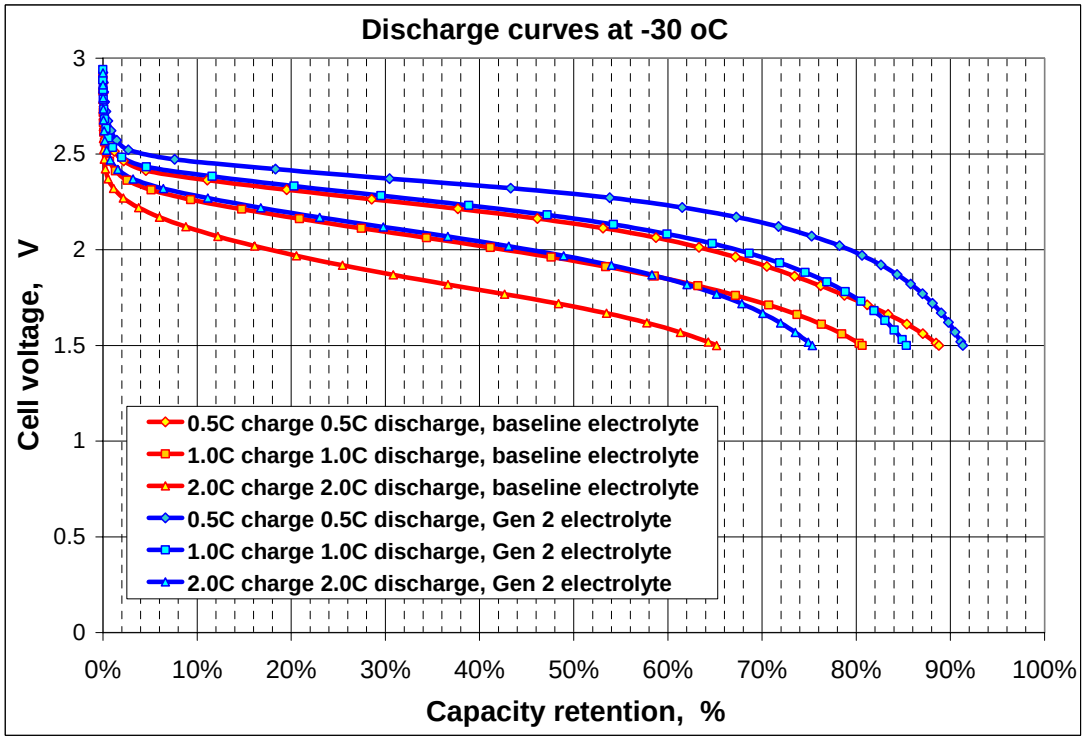

Fig. 15 Nano-LTO & LMO charge discharge curves at -30°C with baseline and Gen 2 electrolytes.

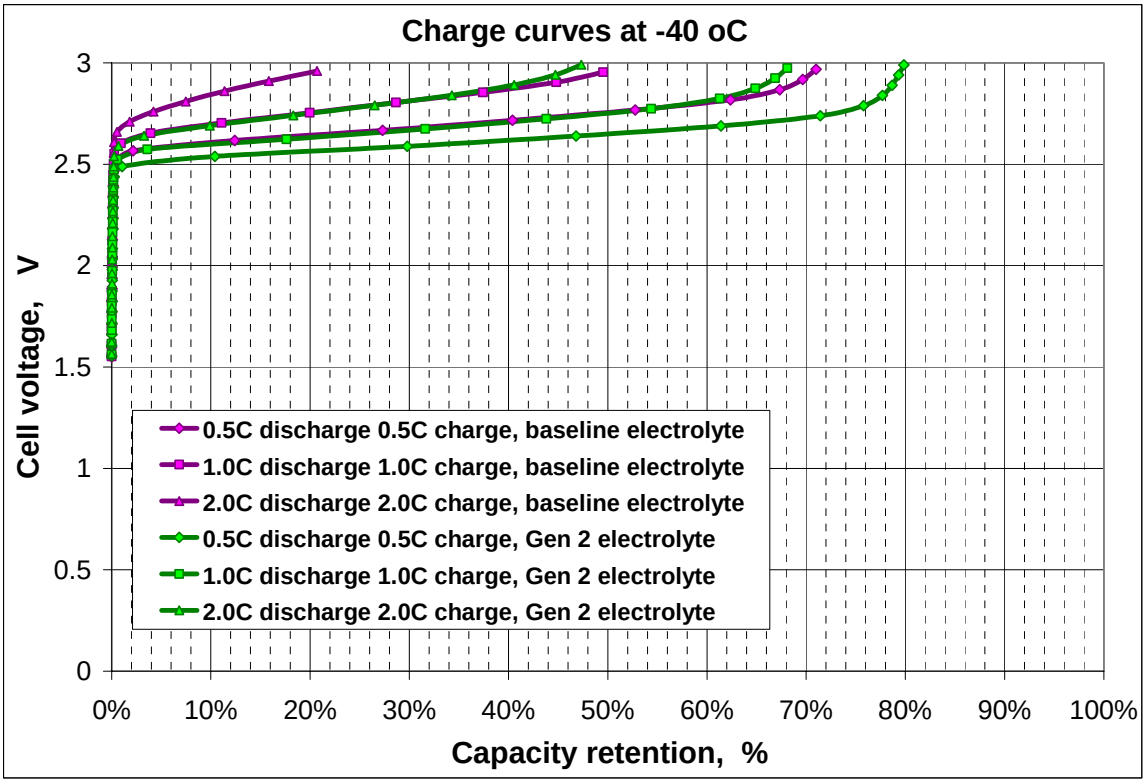

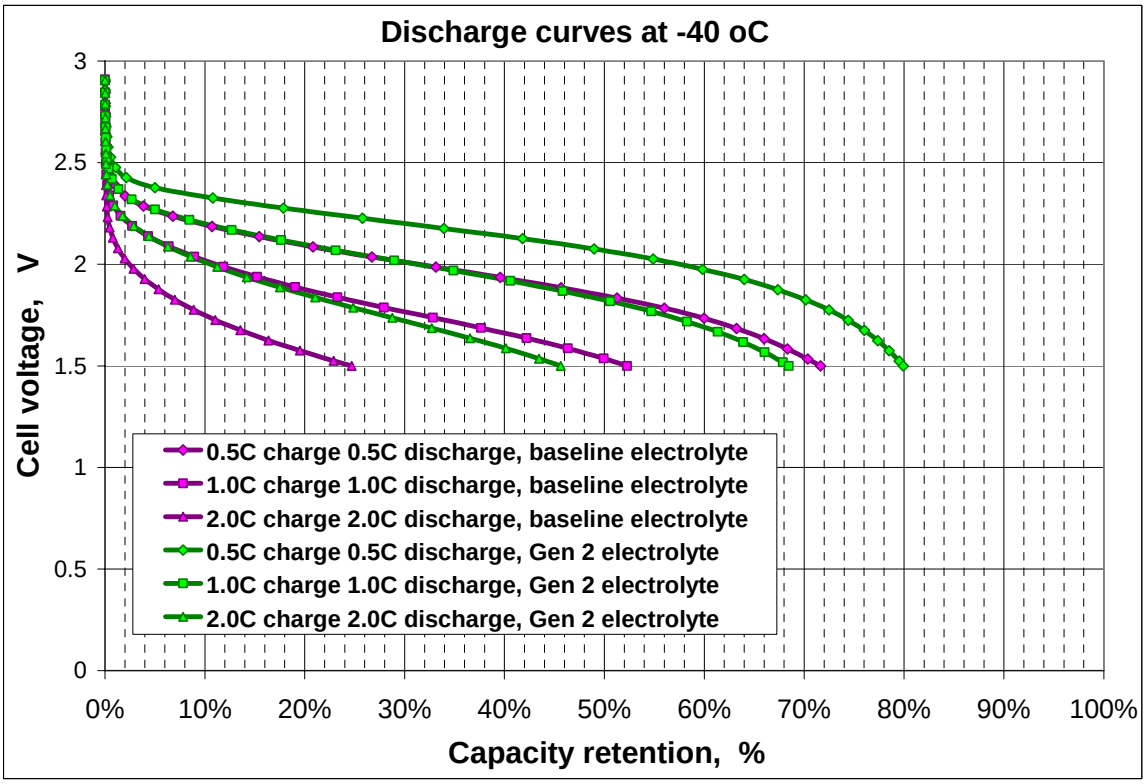

Fig. 16 Nano-LTO & LMO charge discharge curves at -40^{o}C with baseline and Gen 2 electrolytes.

To evaluate the experimental results shown in Figs 15 and 16 we have to take into account that these results are obtained with small lab cells, where the self-heating effect is negligible because of intensive heat exchange with environment. Our previous experience has shown that there is significant self heating effect in full size (large) cells at high charge/discharge rate cause by Joule heating according to the formula:

$$Q= I^2R$$

High current (high rate) combined with the significant increase in cell impedance R at low temperature (more than one order of magnitude) causes substantial increase in cell internal temperature in comparison with cells at ambient temperature. Typically the heat generated in the full size (large) cell at 1C rate increases the cell temperature at least by 10^{o}C and at 2C by more than 20^{o}C.

There is rule of thumb that large cell performance at low temperature is at least as good as a small single electrode cell at 10^{o}C higher temperature. Thus we may expect that the large full size cell will show -40oC performance at least equivalent to the lab cell performance at -30^{o}C (Fig. 15). Taking into account the results shown in Fig 15, we have to expect that even with current cell configuration and chemistry the large full size cell will show at least 85% capacity retention at 1C & -40^{o}C. On the other hand, we expected significant additional improvement in -40^{o}C performance by increasing positive electrode/electrolyte interface area, improvement in PSD of the negative electrode and optimization of both electrode formulation and density.

All this lead us to the conclusion that to meet project goals we need to optimize the electrodes and cell design.

Optimization of electrodes and cell design

The impedance measurement of the cells in wide range of temperature and variations in the properties of LTO material have shown that the impedance of LTO material with BET 40 m^2/g has the lowest impedance contribution at lower temperature ranges than LTO material with lower or higher specific surface area. More ever, at -40 ^{o}C the impedance contribution of the LTO electrode with 40 m^2/g is so low that the cell impedance is controlled only by impedance of the positive electrode. This is illustrated in Fig17 and Fig.18 where Fig 17 shows the cell impedance at room temperature using LTO with 40 m^2/g as negative electrode. As displayed in Fig 17. the cell impedance at room temperature is nearly equally distributed between the interface impedance of the positive electrode and mass transport controlled impedance of the negative LTO electrode. In contrast, as shown in Fig. 18, at -40oC the charge transfer impedance of the positive electrode becomes so large that the mass transport controlled negative electrode impedance is negligible. As a result the LTO with specific surface area 40 m^2/g and mean particle size about 10 microns is selected as baseline material for this study and the next efforts were concentrated on optimizing the positive electrode material and the electrolyte.

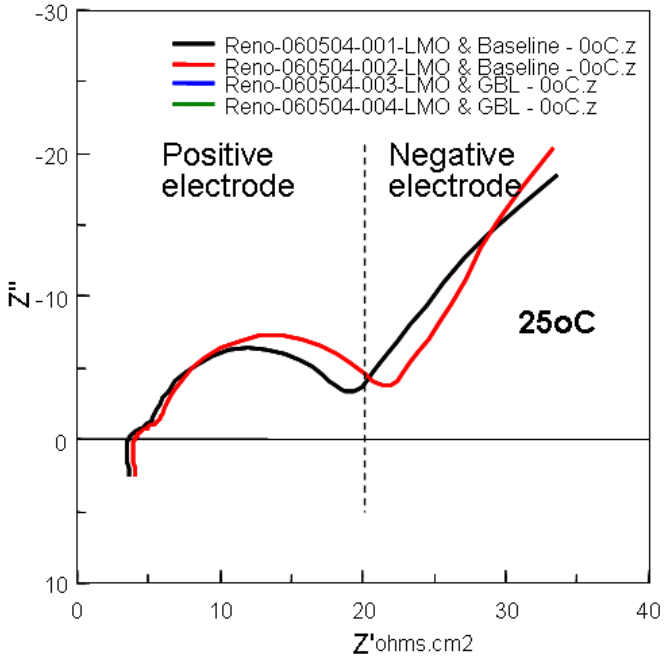

Fig. 17 Cell impedance at 25°C showing that the cell impedance at room temperature is controlled by the equivalent contribution of both positive and negative electrode

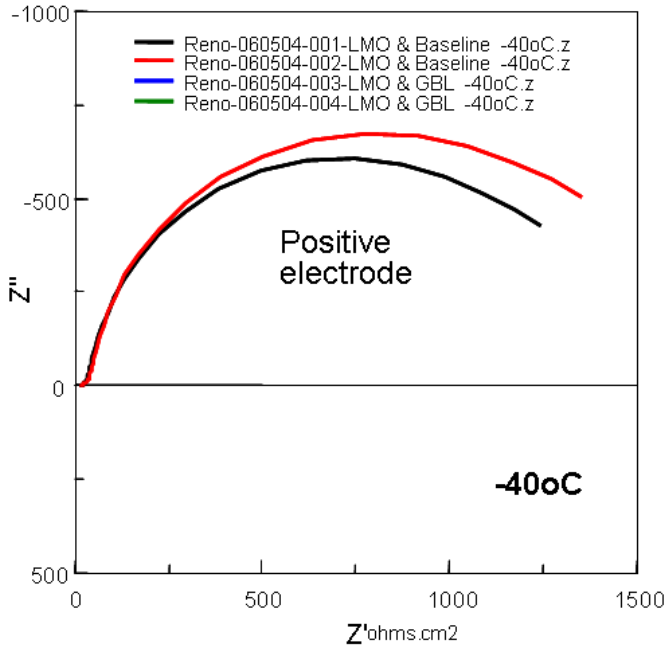

Fig. 18 Cell impedance at -40°C showing that the cell impedance at -40°C is controlled in particular by the positive electrode interface impedance and negative electrode contribution is negligable

As shown in Fig 18 the cell impedance at -40oC is controlled in particular by the interface (charge transfer) impedance of the positive electrode. According to theory the charge transfer resistance depends on electrode nature, interface area and surface properties of the electrode material. Thus development of a positive electrode with suitable nature, morphology and surface properties were our main tools to achieve project goals.

Several additional electrode samples from $LiCoO_2$ (LCO) were prepared for characterization. These included LCO sample from Umicore, Korea, From LICO, Taiwan and Seimi, Japan. All theses samples were sent to Superfine in Israel for suitable change in particle size distribution and morphology. The goal was to increase the specific surface area from typical 0.3-0.4 m^2/g to about 2.0 m^2/g.

As shown in Fig. 19 the micronized LCO sample from Umicore, Korea is a product with highly non-uniform morphology and particle size distribution. This is confirmed from the particle size distribution curve shown in Fig 20. As displayed, micronizing this product leads

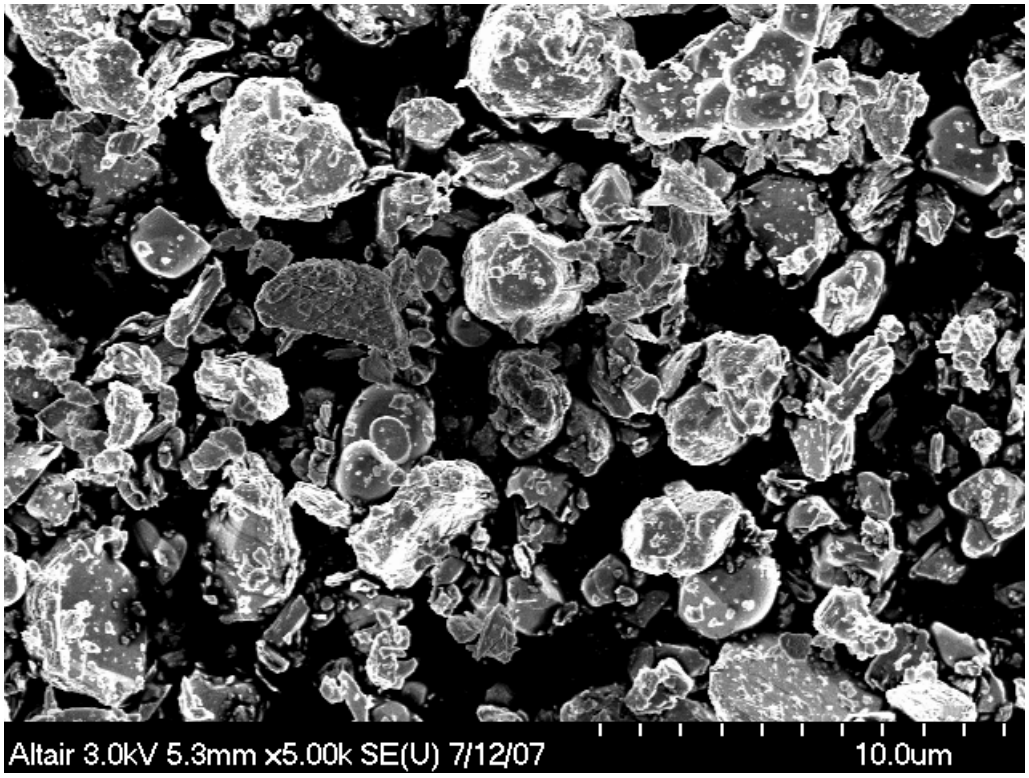

Fig. 19 SEM photograph of LCO from Umicore, Korea micronized to 2.5 microns of mean particle size, showing non-uniform morphology and particle size distribution

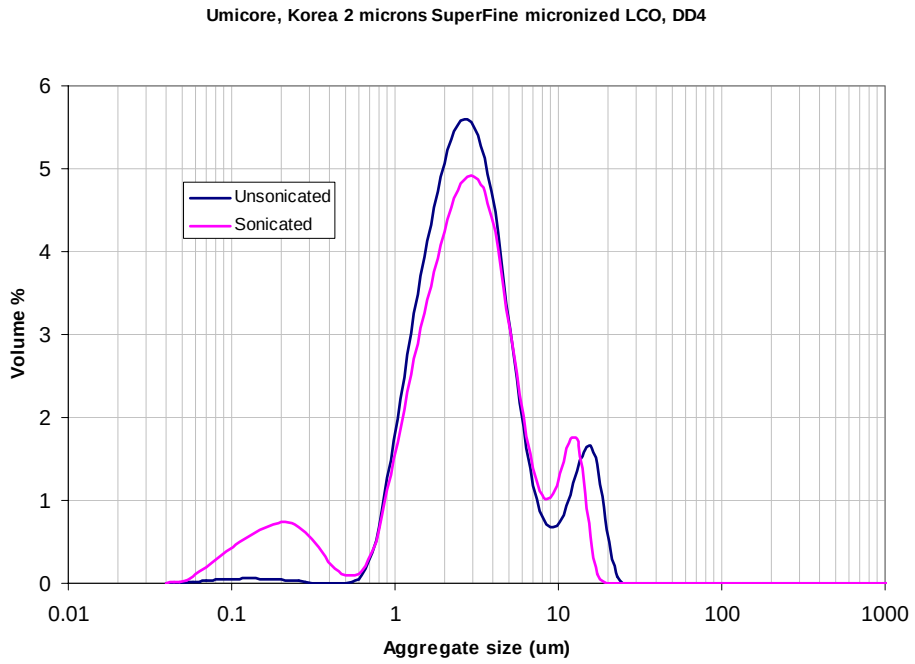

Fig. 20 PSD of LCO from Umicore, Korea micronized to 2.5 microns of mean particle size, showing non-uniform particle size distribution

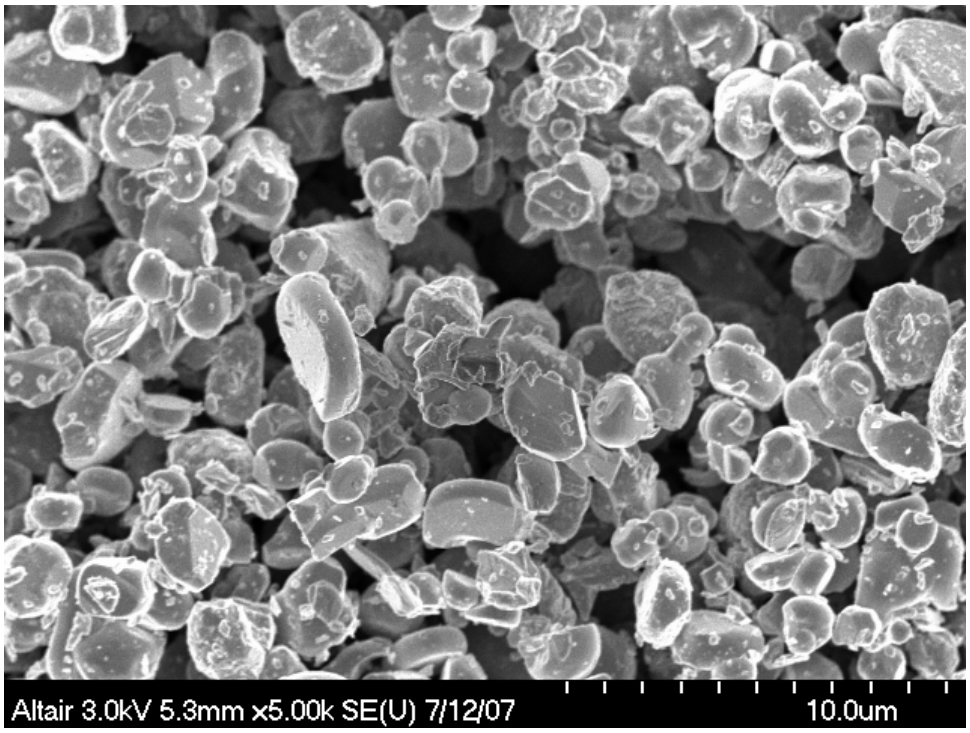

Fig. 21 SEM photograph of LCO from LICO , Taiwan micronized to 2.5 microns mean particle size, showing uniform particle size distribution and particle morphology

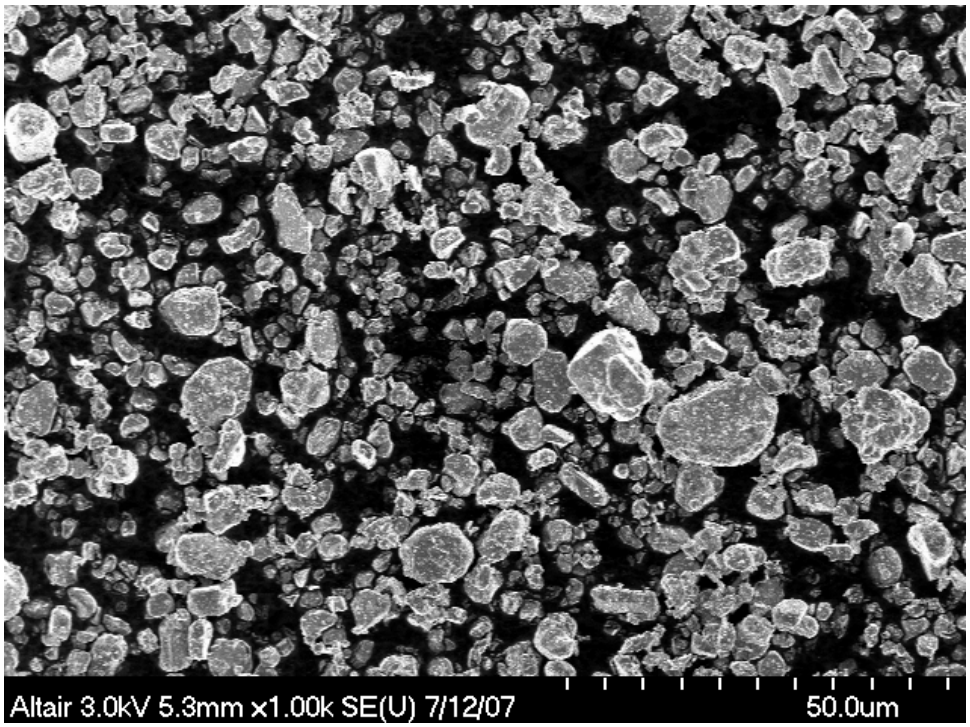

Fig. 22 SEM photograph of LCO from Seimi, Japn micronized to 5 microns mean particle size, showing relatively good particle size distribution and morphology

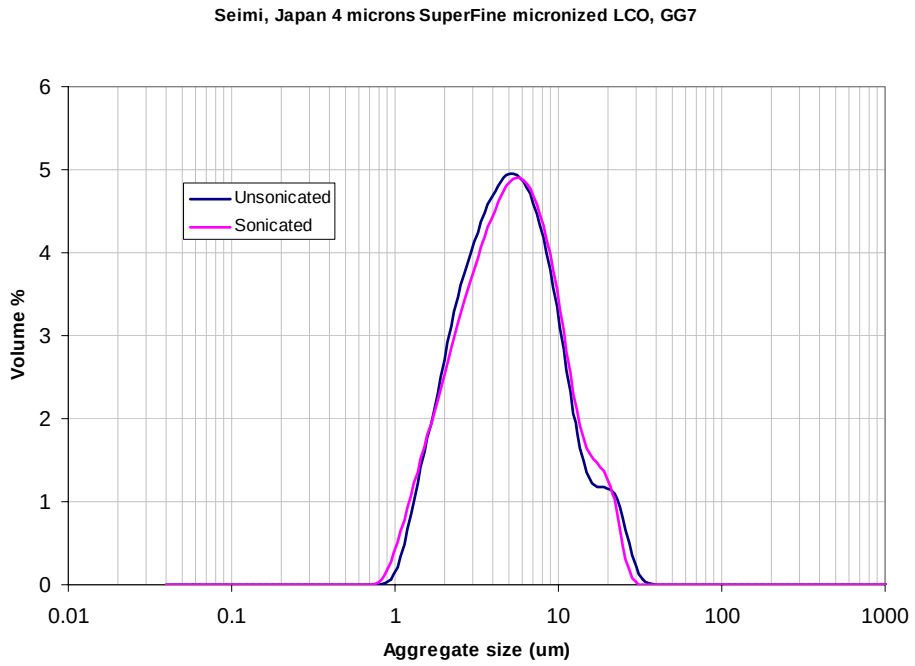

Fig. 23 PSD of LCO from Seimi, Japan micronized to 5 microns mean particle size, showing relatively uniform particle size distribution.

to product with significant amount of fines and large particles. As a result the LCO material from Umicore, Korea was moved out of consideration for additional electrochemical tests.

In contrast the micronized LCO material from LICO Taiwan is a product with highly uniform particle size distribution and particle morphology (Fig. 21). In addition the specific surface area (BET) obtained is 2.06 m^2/g which is very close to the target 2 m^2/g.

The LTO material from Seimi, Japan was micronized to 5 and 2.5 microns mean particle size. The delivered product has relatively uniform particle size distribution and morphology (Fig 22 and Fig.23) and, respectively, specific surface areas of 2.16 m2/g and 4.12 m2/g. These surface areas were very close to target values. As a result the LCO from LICO Taiwan with mean particle size 2.5 microns and specific surface are 2.06 m^2/g and LCO from Seimi, Japan with mean particle size 2.5 and 5 microns and, respectively, specific surface area of 2.16 m2/g and 4.12 m2/g were selected for additional electrochemical tests. However, the comparison between the electrochemical performance of all these materials at lower temperatures showed unambiguously than manganese spinel materials have significantly better performance. Thus LiMn2O4 from Nippon Denko was selected as positive electrode material and micronized to 4.8 m2/g for the final measurement.

On the other hand the AN based electrolyte showed superior performance at low temperature in comparison with the other two electrolyte and thus was also selected for the final cell configuration.

Final results with optimized electrodes and cell design

In the following several figures, the cycling performance and the rate capability of an optimized cell design using positive electrodes as received in the market and modified only by applying additional grinding procedures are displayed.

The final cell configuration includes:

- LTO negative electrode material with BET 45±5 m^2/g with mean particle size of about 4 microns
- LMO positive electrode from Nippon Denko with decreased particle size to about 4 microns and increased BET specific surface area to about 4.8 m^2/g
- AN based electrolyte as described earlier

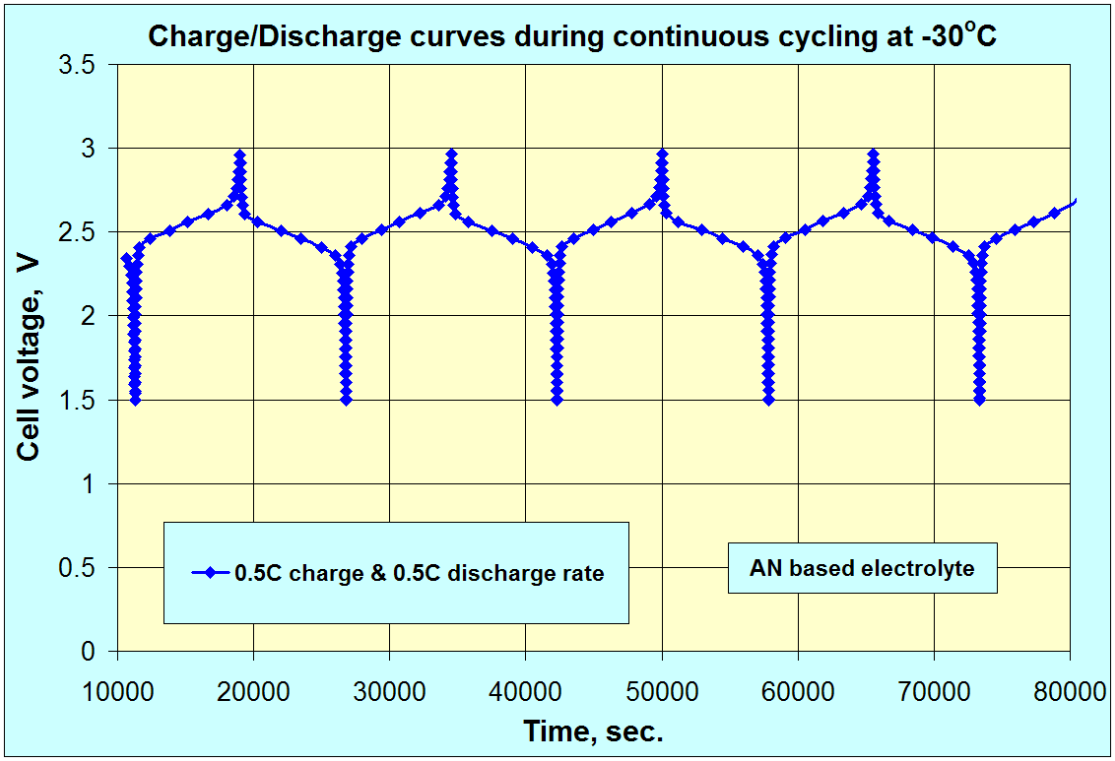

Fig. 24 Cycling performance of optimized cell at -30°C and 0.5C charge & 0.5C discharge rate

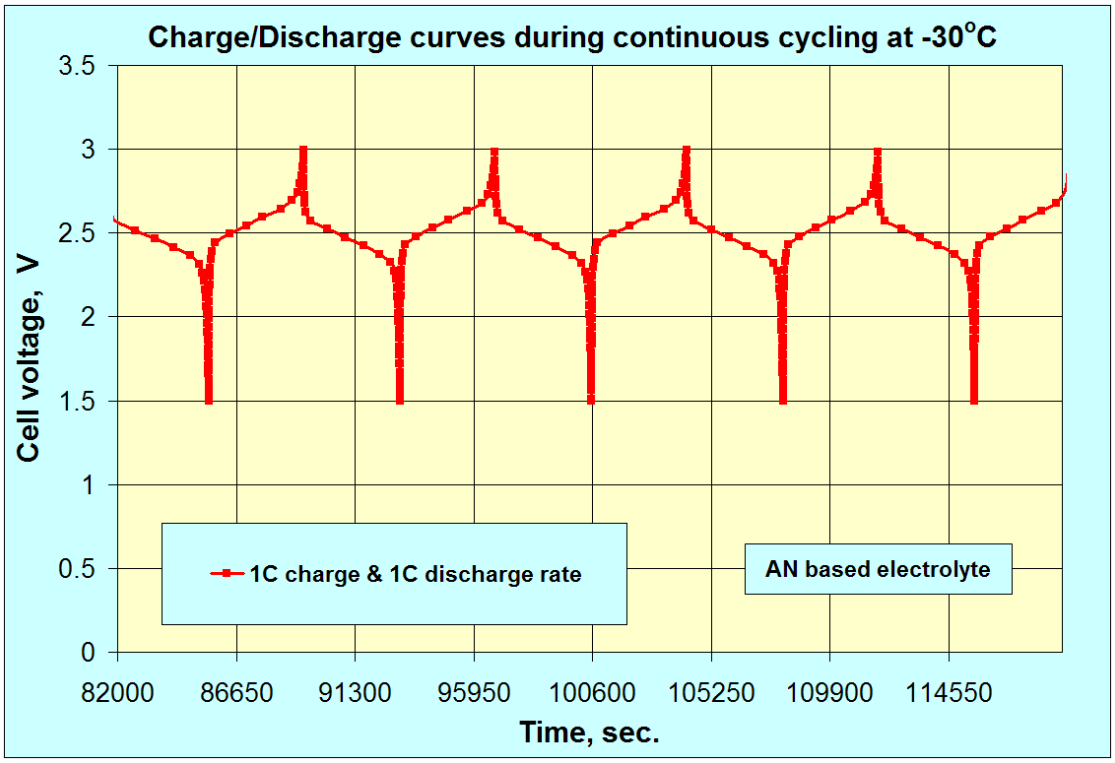

Fig. 25 Cycling performance of optimized cell at -30°C and 1C charge & 1C discharge rate

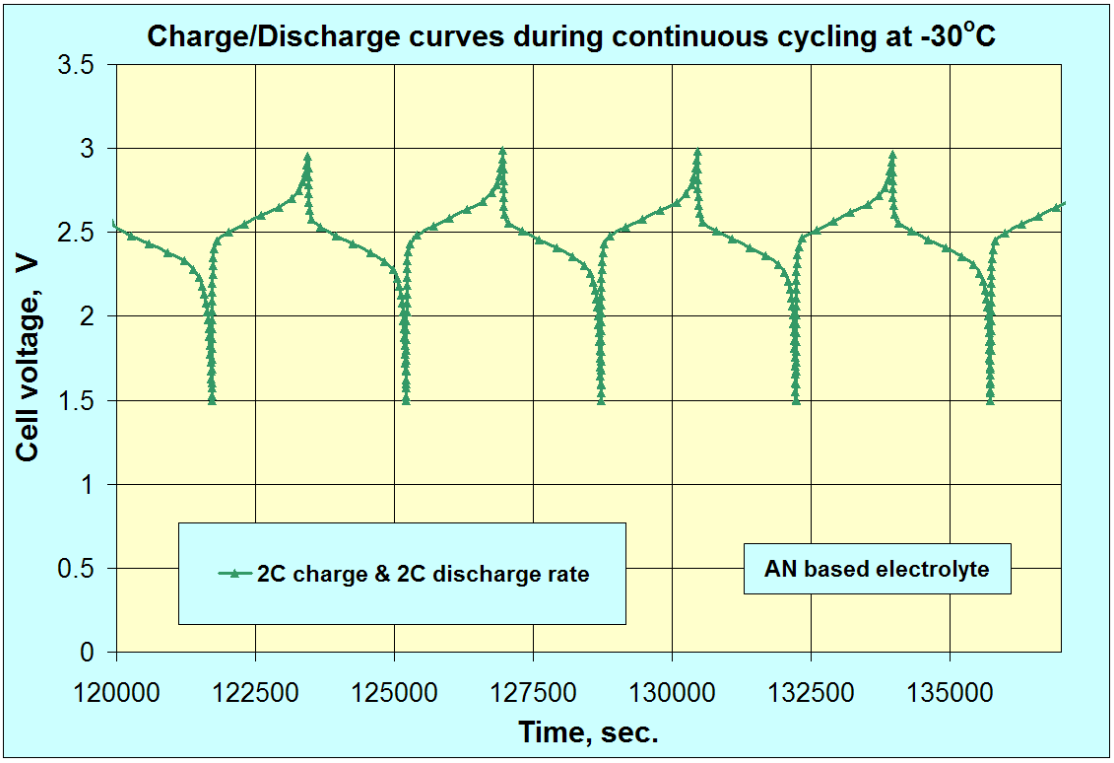

Fig. 26 Cycling performance of optimized cell at -30°C and 2C charge & 2C discharge rate

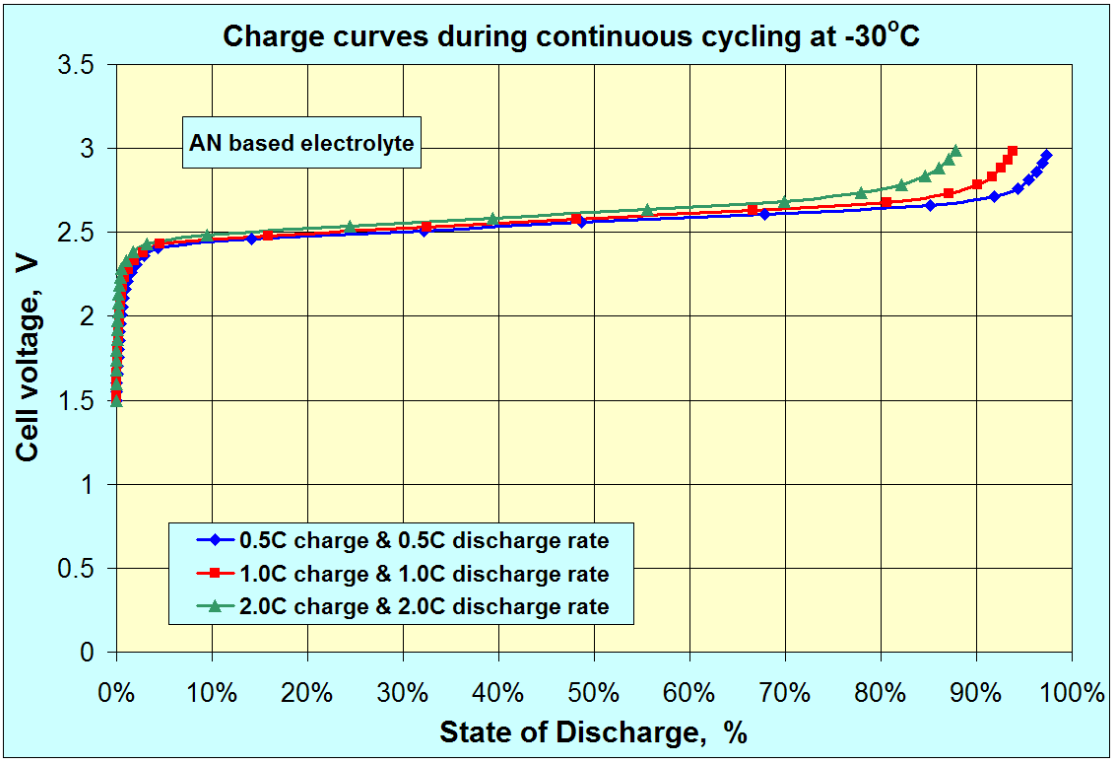

Fig. 27 Capacity retention during the charge process as a part of continuous cycling test of optimized cell at -30°C and at 0.5C , 1C and 2C charge & discharge rate.

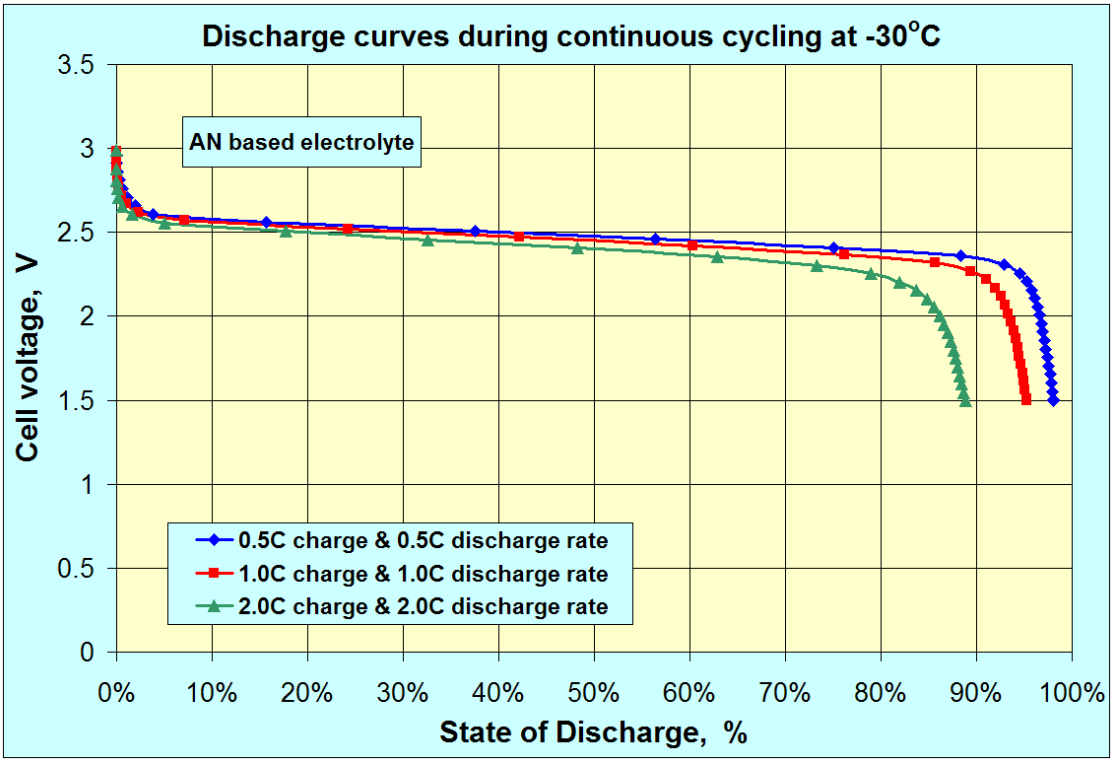

Fig. 28 Capacity retention during the discharge process as a part of continuous cycling test of optimized cell at -30°C and at 0.5C , 1C and 2C charge & discharge rate.

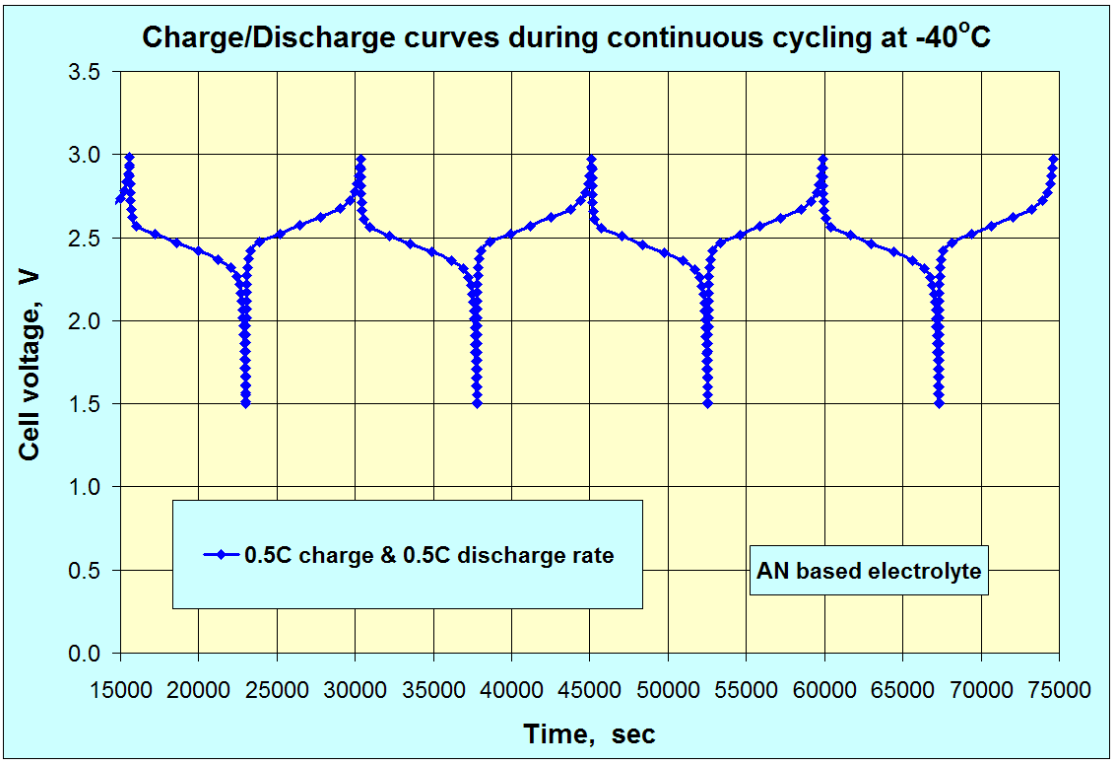

Fig. 29 Cycling performance of optimized cell at -40°C and 0.5C charge & 0.5C discharge rate

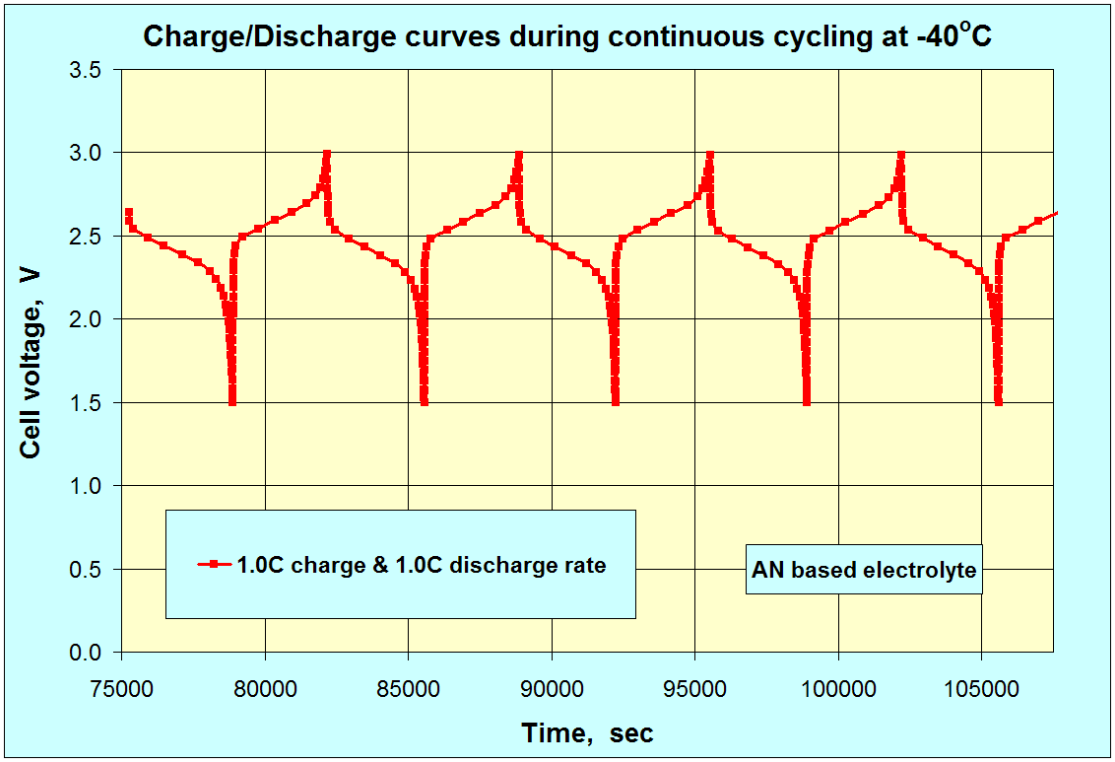

Fig. 30 Cycling performance of optimized cell at -40°C and 1C charge & 1C discharge rate

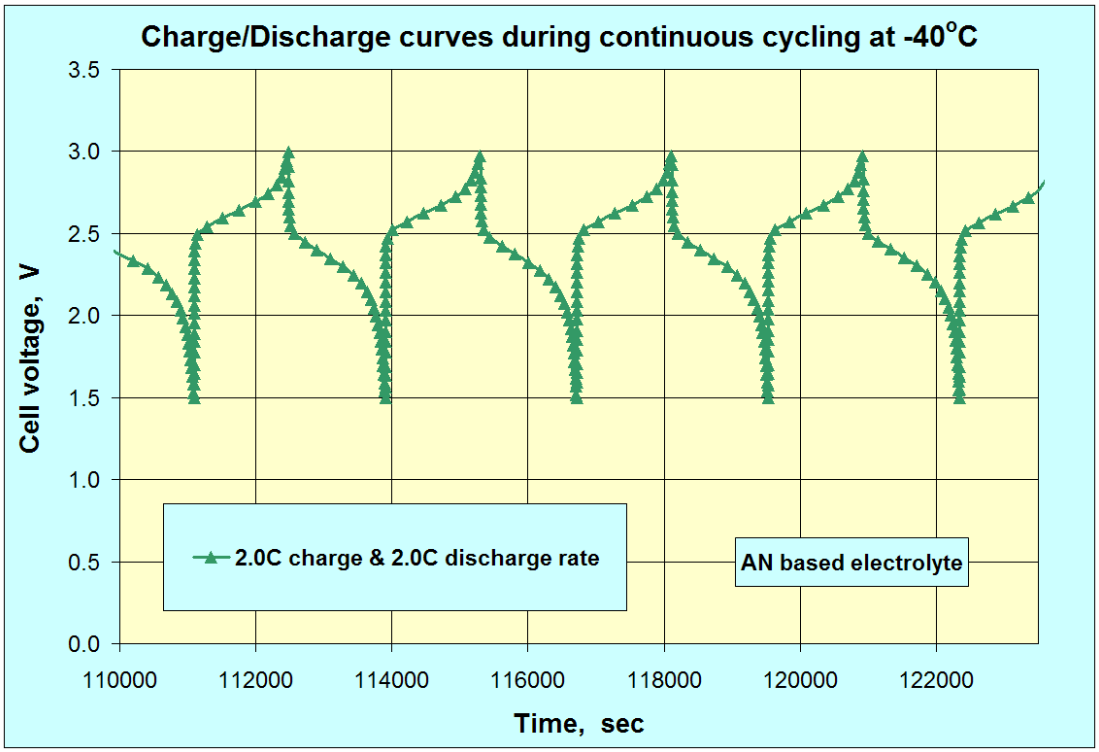

Fig. 31 Cycling performance of optimized cell at -40°C and 2C charge & 2C discharge rate

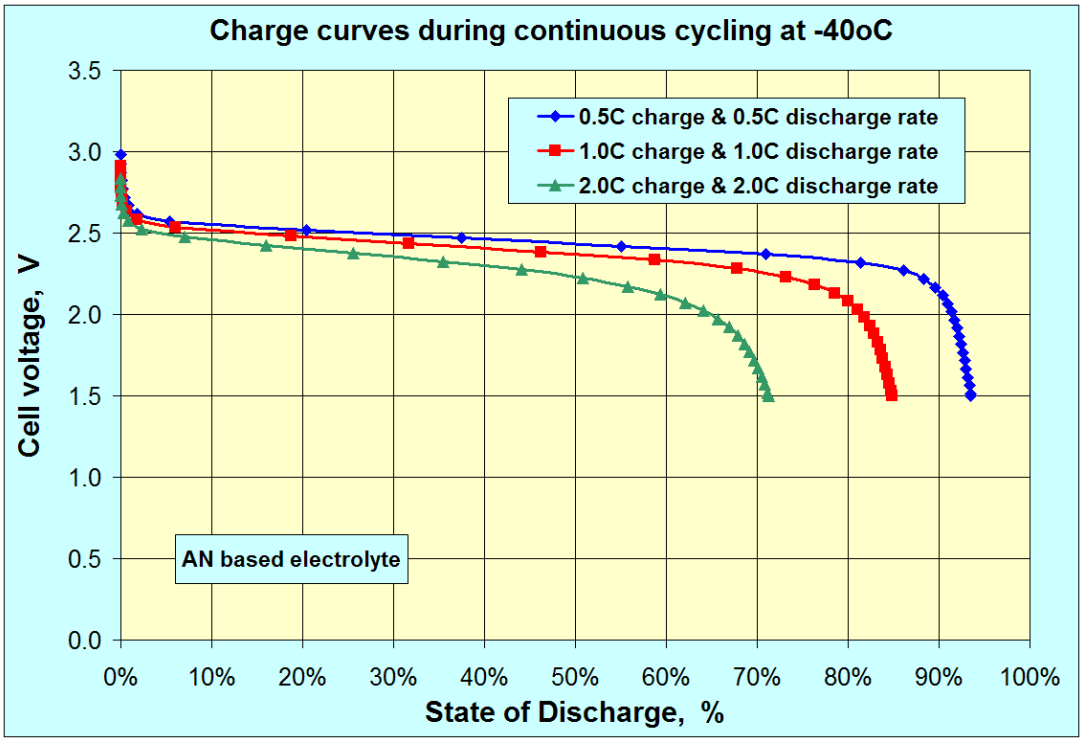

Fig. 32 Capacity retention during the discharge process as a part of continuous cycling test of optimized cell at -40°C and at 0.5C , 1C and 2C charge & discharge rate.

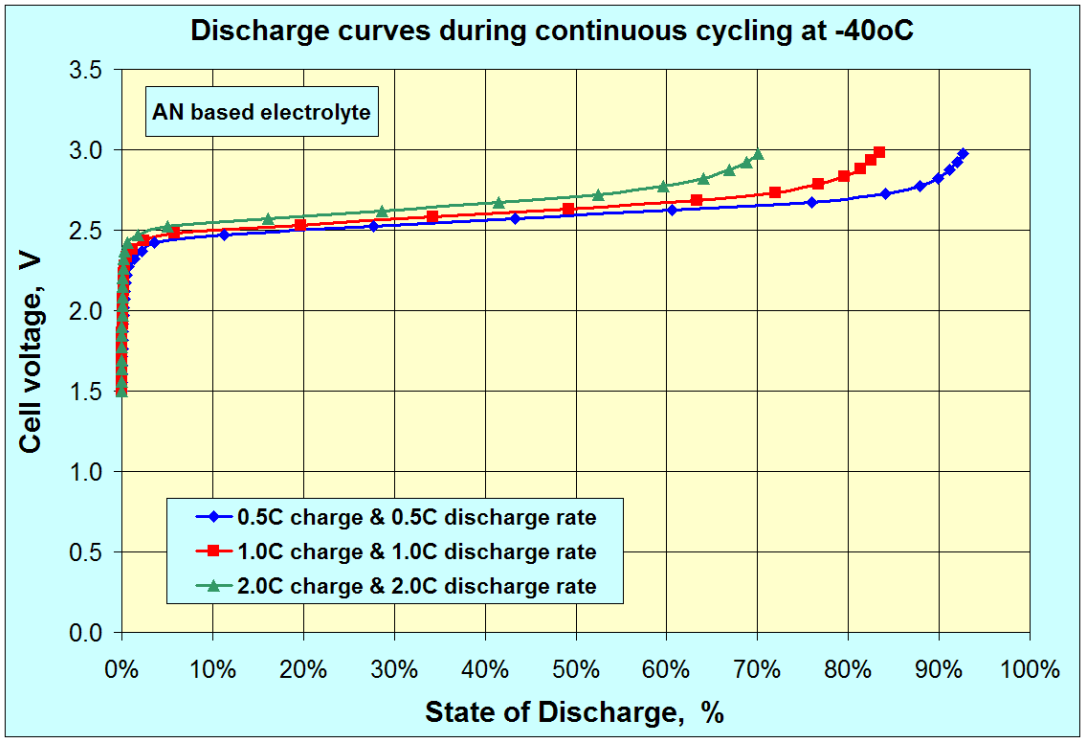

Fig. 33 Capacity retention during the discharge process as a part of continuous cycling test of optimized cell at -40°C and at 0.5C , 1C and 2C charge & discharge rate.

Publications: None

Internet Sites: None

Networks Fostered**:** None

Technologies: None

Inventions: None

Data Bases: None

FINAL REPORT – Objective # 4

Project Title: Interactions of Engineered Nanoparticles with Environmentally and Societally Important Bacteria

Project PI(s): Galen Stucky, Ph.D., Patricia Holden, Ph.D., Andrea Neal Ph.D., Won Hyuk Suh, M.S./Ph.D.

Protected Information: None

Executive Summary:

This research investigated bacterial interactions with engineered nanoparticles. Significantly, this work is aimed at building a foundational base on which to understand the physical parameters of engineered particles that affect bacterial responses. Bacteria constitute the largest biomass on this planet and comprise the most numbers of living organisms. They are ubiquitous in the air, soil, water, and make up the base of all nutrient recycling/ecological recycling and therefore every foodchain. Some species are, or can become, pathogenic and so understanding the effects of human introduced nanoparticles on bacterial responses is critical.

This Objective defined routine physical parameters of four nanoparticles of relatively low known toxicity, i.e., containing metals of low toxicity potential. Surface area, X-ray diffraction patterns, energy dispersive X-ray patterns, and zeta potential were defined for each particle and confirmed to be characteristic for the known chemical formulae. Photocatalytic activity was assayed for the uptake and degradation of rhodamine dye under UV excitation, and two of the four particles were found to be as or more photocatalytic than the control group containing P25 Degussa titanium dioxide.

Bacterial cell interactions with nanoparticles were investigated using liquid cultures and biofilm cultures of the gram negative species *Pseudomonas aeroginosa*. Dose-dependent toxicity studies indicated a reduction in bacterial growth under light and dark conditions for the titanium-containing nanoparticle. Fluorescent methodology quantified live and dead cells and confirmed toxicity for all nanoparticle groups tested, with few exceptions at specific timepoints. Photocatalytic activation of the highest concentration of nanoparticles studied resulted in severely decreased growth. At lower nanoparticle doses, bacterial cultures demonstrated a bimodal growth pattern. Titanium-containing nanoparticles were further investigated and induced a novel bacterial biofilm formation compared to other synthetic nanoparticles of similar chemistry. Biofilms exposed to lanthanum and titanium nanoparticles demonstrated a quantifiable marked surface roughness. Biofilms were also characterized with regards to exopolymer macromolecule deposition. Specifically, protein, carbohydrate, DNA, and pyoverdine concentrations exhibited differences from control cultures under both light and dark conditions, however there was no clear trend noted by either exposure condition (light, dark) or by nanoparticle group.

In summary, these proprietary nanoparticles of low toxicity potential were found to cause changes in the activity of a bacterial species. Growth patterns and the internal molecules produced by this bacteria changed upon incubation with the nanoparticles tested, suggesting that further study is needed to identify and further characterize the cellular interactions of nanoparticles and bacteria found in the environment.

Comparison of Goals/ Objectives Met with Planned:

This objective, organized into biological and physical/chemical tasks, characterizes the physical and chemical structure of the engineered particles and investigates the effects of these nanoparticles on liquid and biofilm bacterial cultures. Overall, all goals were accomplished with regards to scientific investigation of nanoparticle-bacterial interaction, with the exception that the one year of funding allowed for the investigation of only one organism, *Pseudomonas aeroginosa*, and not also *Bacillus subtilis* as planned.

Summary of Project Activities

Biological Tasks:

Task 1: The effect of nanoparticles on aqueous culture growth under light and dark conditions in a concentration-dependent manner was completed. Compared to control cultures, the titanium-containing nanoparticles showed a dose-dependent decrease in bacterial growth under both light and dark condition. Only at the highest concentration did the lanthanum-containing nanoparticle inhibit growth of bacterial cultures.

Task 2: The effect of photocatalytic activation using UV radiation on aqueous culture growth was completed. All culture exposures to UV irradiated nanoparticles at the higher dose (0.5mg/ml) demonstrated a severe decrease in bacterial culture growth throughout the 4 hour UV period as well as the 24 hour period following UV exposure. At lower doses of nanoparticles (0.25mg/ml) under the same irradiating conditions, bacterial cultures demonstrated a short-term dramatic spike in cell number, followed by continued increased growth compared to control cultures. These initial data represent an unexpected bimodal effect on bacteria, and warrants further investigation.

Task 3a: Using concentrations of titanium-containing nanoparticles that demonstrated an inhibitory effect on bacteria in Task 1 and 2, liquid cultures were further investigated to characterize the bacteria-promoted dispersion of nanoparticles. Titanium-containing nanoparticles induced bacterial biofilm formation that was not observed when compared to other synthetic nanoparticles of similar chemistry. Biofilm aggregates were quantified by histogram and displayed a range of micrometer length (0.3 – 5.2 μm) that changed over the time assessed (12 and 18 hours). This task was not pursued further as aggregate quantification using ESEM was costly and conclusions were confounded by decreased image clarity.

Task 3b: Data gathered questioned optical density as a sole measurement of biomass, as aggregate formations make optical density readings unreliable. Fluorescent methodology was

employed to quantify live and dead cells following nanoparticle exposure to bacterial cultures. Thus, accurate measurements of total cell number and cell viability are obtained. With regards to total cell numbers, exposure of cultures to nanoparticles resulted in a significant increase in initial cell numbers compared to controls, with a subsequent (overall) decrease in the total number of cells compared to control in all groups of nanoparticles except lithium-containing particles. Lithium-containing particle exposure resulted in total cell numbers indistinguishable from control culture at the last time studied (12 hr). All groups of nanoparticle exposure resulted in early increased live cell counts (4 and 6 hours), with subsequent decreased live cell counts compared to control culture at 12 hours. The total number of dead cells was significantly raised in all exposure groups at all time points compared to control, except for the yttrium-stabilized zirconia group which was not significantly different from control at 12 hours. Thus, using this methodology, it is conclusive that there is a display of toxicity from exposure to all nanoparticle groups tested, with few exceptions at specific timepoints. It is unknown at this time whether early times displaying increased cell numbers represents a positive response towards growth or a stress response (negative) to nanoparticle exposure.

Task 4: Biofilms exposed to nanoparticles were quantified with regards to growth and cell distribution. Aggregate surface roughness was quantified at concentrations that demonstrated the highest toxic potential. In quantification, a higher calculated variety value indicates a rougher surface. Exposure to nanoparticles resulted in biofilm formation for all groups, as this bacterial species demonstrated an affinity for the aggregate surface. Surfaces available were colonized immediately following inoculation. Notably, exposure to the lanthanum and the titanium-containing particles resulted in the most surface roughness when quantified at 12 hours from control cultures. The significance of this is not understood.

Task 5: Biofilm exposures from Task 4 were further characterized with regards to exopolymer macromolecule deposition. Specifically, protein, carbohydrate, DNA, and pyoverdine concentrations were quantified under light and dark incubation conditions. Pyoverdine was added subsequent to initial studies. Extracellular macromolecule concentrations exhibited differences from control cultures under both light and dark conditions (see report), however there was no clear trend by exposure conditions (light,dark) or by group of nanoparticle. Pyoverdine was investigated as a molecule associated with this bacterial culture's virulence. Excitation of each biofilm was investigated at 365nm. The lithium-containing nanoparticle displayed excitation at 365 under all temperatures (30ºC and 37ºC) and light/dark conditions investigated. However, chemical identity of pyoverdine was not confirmed (i.e., using immunoassay).

Physical/Chemical Tasks:

Task 1: Complete XRD and energy dispersive x-ray (EDX) profiles were generated for engineered nanoparticles. All nanoparticles displayed a characteristic XRD spectrum and correct atomic weight percent ratio.

Task 2: Particle Surface Area was completed for engineered nanoparticles and confirmed Altair known values.

Task 3: Particle Zeta Potential was negative for all engineered nanoparticles.

Task 4: Photocatalytic activity was quantified *in vitro* using the absorption and decomposition of rhodamine 6G dye molecules. Altair engineered particles were compared to Degussa P25; as expected, the titanium and lithium-containing nanoparticles displayed increased photocatalytic ability compared to P25.

Mechanisms of Cell-Particle Interactions: Undetermined to date.

Publications:

Manuscripts: None to date.

Meetings:
SETAC North America 28th Annual Meeting, November 11-15 2007, Milwaukee, Wisconsin (Poster Presentation)
Bio-physicochemical Interactions of Engineered Nanomaterials Workshop, September 9 - 11, 2007, Los Angeles, California (Poster Presentation)
The 2nd International Congress of Nanobiotechnology & Nanomedicine (NANOBIO 2007), June 18-21, 2007 in San Francisco (Oral Presentation)

Internet Sites: None

Networks Fostered:

Strong collaboration was fostered between academia and the private sector with this portion of the grant. UCSB and Altair shared individual areas of expertise and discussed hypotheses as to mechanisms of action to explain data gathered. UCSB invited Altair to present at a special workshop (Biophysicochemical Interactions of Engineered Nanomaterials) presented at UCLA's Center for NanoSystems Institute. Altair connections and support of academic centers were extended as a result, as international relations were promoted with McGill University (Montreal, Canada).

Technologies: None

Inventions: None

Data Bases: None